# Investigation of Flow of Polarizable Particles Between Microelectrodes of Different Shapes Subjected to Nonuniform Electric Fields

**THESIS**

Submitted in partial fulfilment
Of the requirements for the degree of
**DOCTOR OF PHILOSOPHY**

By

**D. Nagendra Prasad**
**ID. No. 2011PHXF0424H**

Under the Supervision of
**Prof. Souri Banerjee**


**BIRLA INSTITUTE OF TECHNOLOGY AND SCIENCE, PILANI, HYDERABAD CAMPUS**
**2018**

**BIRLA INSTITUTE OF TECHNOLOGY AND SCIENCE, PILANI**

# CERTIFICATE

This is to certify that the thesis entitled **"Investigation of Flow of Polarizable Particles between Microelectrodes of Different Shapes Subjected to Nonuniform Electric Fields"** submitted by **D. Nagendra Prasad** ID No **2011PHXF0424H** for the award of Ph. D of the institute embodies original work done by him under my supervision.

Signature of the Supervisor: _____

Name: **Prof. Souri Banerjee**

Designation: **Professor**
Department of Physics
BITS-Pilani Hyderabad Campus.

Date:

## ***Acknowledgements***

*It is a moment of gratification and pride to look back with a sense of contentment at the long travelled path, to be able to recapture some of the fine moments and to be able to thank the infinite number of people, some of whom were with me from the beginning, some who joined me at some stage during the journey, whose rally round kindness, love, and blessings have brought me to this day. I wish to thank each and every one of them with all my heart.*

*Foremost, I am thankful to BITS Pilani for giving me great opportunity to pursue my Doctoral degree. I would like to express my deep sense of gratitude to my Supervisor Prof. Souri Banerjee for the continuous support of my Ph.D. study and research, for his patience, motivation, enthusiasm, and immense knowledge. His valuable guidance helped me in all the time of research and writing of this thesis.*

*Many persons to be thanked who helped me in this Ph.D. journey with their valuable time, suggestions and encouragement. I will start with my doctoral advisory committee (DAC) members, I am thankful to acknowledge Dr. Hari Hara Venkataraman and Prof. Meenakshi Viswanathan for their support and encouragement during this period. I thank Physics department DRC convener Prof. Kannan Ramaswamy for his valuable suggestions and his encouragement. I am thankful to HOD, Physics department, Prof. P K Thiruvikraman, entire Physics department faculty members. Special thanks to Dr. VSN Murthy and Dr. Asraul Haque for which I had a great interaction time and space with them. And special thanks to friendly person Prof. N Rajesh, Chemistry department, BITS Pilani Hyderabad campus for his suggestions and discussion space.*

*I am grateful to former vice-chancellor Prof. Bijendra Nath Jain, vice-chancellor Souvik Bhattacharyya of BITS Pilani, former director Prof. V. S. Rao and present director Prof. G Sundar of BITS Pilani Hyderabad Campus for giving me an opportunity to pursue and to carry out my Doctoral research work in the institute.*

*I would like to express my sincere thanks to Prof. Vidya Rajesh, Associate Dean, Academic Research Division (Ph.D. Programme), BITS Pilani for their continuous support and encouragement during my research work. And I extend my thanks to Mr. Praveen, ARD for his help and information to complete the course formalities in time.*

*I am grateful to CeNSE, IISc, Bengaluru and CEN, IIT-B, Mumbai for utilizing fabrication and characterization facilities to carry out microelectrode devices. I am*

*thankful to INUP (Indian Nano-Users Program) for facilitating familiarization and hands-on workshops.*

*I am thankful to acknowledge Sudarshan, Shukla, Astha, and Samatha for their contribution and help to carry out my Ph.D. thesis. I thank my department friends and non-teaching staff for their support and encouragement throughout my Ph.D. journey. I am thankful to Santosh, Sai, Krishna, Hemanth, Veera, Gangaram, Santhanam, Bharathi, Narsimhulu, Srinivasa Rao, and Satish, who all helped me and supported me in campus throughout my Ph.D. journey.*

*Away from the department, special thanks to my beloved brother Sandeep who encouraged me and helped me to pursue Ph.D. and I am so much indebted to him for his efforts. I would like to extend special thanks to my well-wisher Padmini T, who inspired me and encouraged me in tough times to achieve this final stage with her great support. And I would like to acknowledge my brother Praveen, Dr. Tirupati Rao and my bestie Dhanu for their great help, support and motivation throughout my Ph.D. journey.*

*Last but not least, I convey heartfelt love and deep respect to my parents and sisters for their hope, patience, and support at every stage of my life. I cannot simply thank them enough.*

***(D N Prasad)***

*BITS Pilani*
*May 2018*

## ***Abstract***

*Electro-kinetics, namely AC electro-osmosis (ACEO) and Dielectrophoresis (DEP) have been judiciously utilised to manipulate movement of polarisable particles like DNA suspended in electrolytic solution and placed between electrically fed microelectrodes. Researchers around the globe have tried to fabricate electrodes of different geometries to understand how electric field owing to sharpness of the electrodes has influenced the aforementioned electro-kinetic properties. Presented a development in design of patterned electrodes used to align and trap DNA molecules in and around the electrodes. We have examined the pros and the cons of such geometry of the set of the micro-electrodes and also tried to provide a solution in terms of shape and sharpness of the electrode that would facilitate DNA molecules to bridge between the electrodes for further application of conducting DNA as molecular wire.*

*There has been a huge interest in manipulating polarisable particles like DNA using electrical forces in micro devices as it finds novel applications in lab-on-a-chip technology or in DNA diagnostics. It is well understood that in a suitable condition, DNA molecules suspended in electrolytic solution would develop a strong electric dipole moment and this induced dipole allows trapping and manipulation of the molecule, when placed between two micro-electrodes due to a process known as DEP. In this context it is worth mentioning that the dielectrophoretic motion of DNA molecules requires alternate current (AC) electric field to suppress the electrophoric effect of the molecules' net charge. However, the motion of the DNA molecules and hence their trapping/manipulation possibilities within a set of microelectrodes will also be countered by the flow of the electrolyte known as ACEO. This in turn implies that a balancing of DEP and ACEO should be a promising and non-destructive technique to probe non-contact manipulation/trapping of DNA molecules suspended in an electrolyte solution and placed within electrically fed microelectrodes7. In the text later, the processes ACEO and DEP is discussed.*

# TABLE OF CONTENTS

# List of figures

# List of abbreviations

| | |
|---|---|
| *LOAC* | *Lab on a chip* |
| *μTAS* | *Micro total analytical system* |
| *DNA* | *Deoxyribonucleic acid* |
| *λDNA* | *Phage DNA bacterial* |
| *MEMS* | *Microelctromechanical system* |
| *NEMS* | *Nanoelectromechanical system* |
| *ACEK* | *AC Electrokinetics* |
| *ACEO* | *AC Electroosmosis* |
| *DEP* | *Dielectrophoresis* |
| *EO* | *Electroosmotic* |
| *EP* | *Electrophoresis* |
| *EDL* | *Electrical double layer* |
| *N-S equation* | *Navier-Stokes* |
| *FEM* | *Finite element method* |
| *PDF* | *Partial differential equation* |
| *GUI* | *Graphical user interface* |
| *Re(C-M) factor* | *The real part of Clausius-Mossotti factor* |
| *pDEP & nDEP* | *Positive and negative DEP* |
| *EBL* | *Electron beam lithography* |
| *SEM* | *Scanning electron microscope* |
| *PCB* | *Printed circuit board* |
| *CPE* | *Coplanar parallel electrode* |
| *CTE* | *Coplanar triangular electrode* |
| *rms* | *root mean square* |
| *PMMA* | *Polymethyl methacrylate)* |

# Synopsis

This thesis is based on “Investigation of flow of polarizable particles within microelectrodes of different shapes in inhomogeneous electric fields”. The research work consists of TWO aspects, one is computational study using COMSOL Multiphysics software package and second is experimentation which involved fabrication of microelectrodes and characterization. The thesis architecture is planned for comprising of FOUR chapters in the following order and presenting the description of each chapter briefly.

1) Introduction
2) AC Electrokinetics
3) Numerical Simulation/Multiphysical Modelling
4) Microelectrodes: Fabrication, Characterization and Electrical contacts

**Chapter-I: (Introduction)**

It provides complete information about the chosen problem of research. It has a historical approach to the problem of study by means of literature review and motivation of the research problem. The main objective of this chapter is to understand the process of manipulation or trapping of polarizable molecules like DNA using various (rectangular and triangular) configuration of microelectrodes subjected to electric fields. We will also address the electrokinetic effects. We propose the idea of trapping/manipulation of polarizable molecules like DNA using triangular microelectrodes geometry.

**Chapter-II: (AC-Electrokinetics)**

It presents the complete background study of physics that govern the research problem. The objective of this chapter is addressing the process of manipulation/trapping of polarizable molecules like DNA under electrokinetic effects subjected to AC electric fields. The physics of electrokinetic phenomena namely AC-Electroosmosis (ACEO) and Dielectrophoresis (DEP) are discussed in detail along with their governing equations which would help determine the force exerted by the polarizable molecules that are being suspended in electrolyte solution (KCl). In order to understand electrokinetic effects, it is essential to understand the formation of interface layer called electrical double layer (EDL) that arises from the solid-liquid interface. Therefore, formation of EDL is discussed in detail followed by ACEO and DEP phenomena.

**Chapter-III: (Numerical Simulation and results & discussion)**

It introduces the computational study that are being simulated analytically using COMSOL Multiphysics software package. Since the research problem involved interface study, the computational work carried out by simulating electrode-electrolyte interface subjected to the time-varying field. This chapter introduces the modeling of geometry, defining boundary conditions for interface followed by computing the physics of ACEO and DEP. The objective of this chapter is finding "trapping-points" for polarizable molecules by means of force calculations. We may have to include part of results (simulations) in this chapter. This chapter comprising of TWO parts, one is on computational study of Electrokinetic phenomena and the other one is experimental part of electrical responses of DNA molecules suspended in a solution under DC electric field. This part summarizes the analytical simulation results which have been computed using COMSOL Multiphysics software. The simulation results of ACEO & DEP are discussed independently and correlate objective of research problem.

**Chapter- IV: (Fabrication of microelectrodes & I-V characteristics)**

It presents the fabrication process of triangular metal (gold) electrodes using electron beam lithography (EBL). Since the triangular microelectrodes are expected to achieve effective manipulation/trapping of polarizable molecules, this part presents the different processing steps that are involved in fabrication using EBL. The SEM images of fabricated electrodes are presented and also, I-V (current-voltage) characteristics of device with and without keeping sample are discussed. Finally, the future scope of this research work is addressed as a conclusion part of thesis.

# Chapter- 1
# Introduction

## 1.1 Background

Over the past several years, there has been a significant amount of research in manipulating polarizable biomolecules under electrokinetic forces in micro devices as it finds novel applications in LOAC (lab-on-a-chip) technology, microfluidics, and DNA diagnostics etc. [1]. The technological applications have been driven by miniaturization process. In order to improve the miniaturization of devices, components, and integrated systems, it is necessary to think of possibilities and developments in the ability to measure, organizing and manipulating the things at the nanoscale level. There are certain goals to be addressed for modern nanotechnology like fabrication of novel miniaturized, functional structures for applications in microelectronic computing or detecting and bio sensing. It has been realized [2] that the nanostructures using biological molecules is one possible way to miniaturization. They also provide the advantage of self-assembling properties. The DNA is in the nanometer range and exhibits interesting properties of manipulation. In this context, the synthesis of biomolecules and their manipulation represents a key step for developing new miniaturized structures. It is worth mentioning that one of the most important features of biomolecules is their ability to self-assemble into highly ordered structures [2]. The building blocks of biomolecules serve as bottom-up architecture owing to their hybridization structures and certainly paves new dimensions in the rapidly growing research field of bio-nanoelectronics or molecular electronics.

In the area of molecular electronics, especially DNA has attracted main attention from researchers. It is a promising material that not only being its function as a carrier for genetic information, which also exhibits self-assembly and polarizable nature when they are suspended in an aqueous solution. In order to fabricate and investigate the devices based on molecules, it is essential to have a selective controlled way of handling of single or a few molecules. In application perspective of molecular electronics, linearly stretched DNA is quite suitable for the demonstration of different case studies. There is a variety of approaches aiming at stretching and aligning individual DNA molecules which would require a suitable environment for manipulating them [3]. A widely used technique for both moving and separating molecules is Electrokinetics. Electrokinetics technique is of an electric field-based manipulation and separation methods that are highly suitable for integration into microdevices. This technique is the interplay between electric and hydrodynamic forces that would facilitate trapping or

manipulating individual biomolecules like DNA [4]. It is clearly understood that in a suitable condition where DNA molecules are suspended in electrolytic solution would form a strong electric dipole moment [5] and this induced dipole causes electrokinetic effects which would allow trapping or manipulating the DNA molecule when they are placed in between two lithographically patterned micro-electrodes. Therefore, this research work is completely based on electrokinetic phenomena where the effects are due to either by applying DC or AC fields. There has been an extensive research [2-5] on suspended or colloidal particles motion under DC and AC electric fields. In our study we present the motion of suspended DNA molecules subjected to AC electric fields. The motion of the suspended particles arises due to AC Electrokinetic phenomena namely AC Electroosmosis (ACEO) and Dielectrophoresis (DEP). ACEO creates motion in bulk solution (aqueous medium/electrolyte) and DEP is exerted forced on suspended particle that causes particle to move. H.A. Pohl, who intended to use the term DEP with his pioneering in this research field and also, he presented a classical text on DEP [6].

Electric manipulations of polarizable biomolecules like DNA in microfabricated structures based on the induced dipole moment of the molecules have been investigated since last one and half decade [5]. Many reports on electrical manipulations of DNA confirmed that high frequency and field intensity are used for DNA stretching in an aqueous medium to form straight shape and immobilized towards the electrodes. With the effect of high frequency and field intensity, the DNA could align parallel to the field with the help of polarization and electrostatic orientation and results out the straight shape of DNA through stretching [10, 28]. The trapping/manipulation of DNA molecules is possible by having a control over electrical forces that arise due to ACEO and DEP. The DEP motion of DNA molecules may require AC electric field which will suppress the electrophoretic effect of the DNA molecules' net charge [7]. Nevertheless, the motion of the DNA molecules and hence their trapping or manipulation possibilities within a set of microelectrodes will also be countered by the flow of bulk solution (electrolyte) known as ACEO [8]. Therefore, balancing both ACEO and DEP is found to be a promising and non-destructive technique to study non-contact manipulation or trapping of DNA molecules that are suspended in an electrolyte solution and are placed within electrically fed microelectrodes [9].

## 1.2 Objective

The present work aimed to devise a suitable and robust method to trap DNA molecule between two metal electrodes using the fact that DNA molecule exhibits significant induced dipole effects. It is to be noted that motion of DNA molecules (in solution) in an electric field is not only affected by the net charge carried by the molecules but also by the dipole induced in the molecules by the field. The induced dipole would result in a gradient force which would pull molecules towards regions of high field strength. In the current work, this gradient force is exploited to trap DNA molecules in the high field strength regions that occur near the edges of the electrodes. There have been many reports on I-V measurements in both DC and AC out of which electrical measurements through a single DNA molecule trapped and bridged between two with 10 nm triangular metal electrodes was reported by Porath [37], et al. Electrodes were fabricated using ultra-modern electron beam lithography. The work clearly exhibited that the electric field strength which was extremely large at the vertices of the triangular electrodes, coupled with polarization properties of DNA molecules, played a crucial role to guide the flow of molecules in and around the tips of the electrode. Moreover, the triangular shape of the electrode facilitated the chance of a single molecule being bridged between the electrodes. However, this polarization of DNA in an oscillating electric field is highly anisotropic and frequency dependent [10]. Thus, it is apparent that the electrostatic trapping of DNA molecules would also have a bearing on the frequency of the applied electric field.

To understand the entire DNA trapping process, the following steps are proposed:

**a) Theoretical Simulation of AC Electrokinetic phenomena (ACEO & DEP)**

Since DNA molecules present in between the electrodes are in solution, the flow patterns based on electro-osmosis play a critical role in site-specific attachment of molecules with the metal electrodes. As the electric field gets non-uniform at the vicinity of the edges, long molecules approaching this region are likely to be attracted by the electrode and when one end touches, it gets anchored there with the other end perpendicular to the electrode. As long as the size of the DNA is slightly greater than the electrode gap, it is possible to have its free end subsequently getting anchored to the other electrode. However, this process may be facilitated or inhibited by the existing flow pattern due to electro-osmosis. Previous studies [11, 12] have predicted that for nanoscopic objects ac electro-osmosis tunes fluid motion at low frequencies (~ several kHz) whereas, for suspended objects typically of the order of or greater than 1 mm, buoyancy could produce an added effect in the flow pattern. As DNA molecules used in the present study

would have a few hundred base-pairs, which is around 100 nm in length, the afore-mentioned buoyancy-effect may be ignored. However, there seems to exist a lower bound for the frequency for which polarization reaches a saturation giving rise to DNA molecules being aligned perpendicular to the electric field [12]. Hence it is of importance to examine flow pattern in the DNA solution between the electrodes and the range of frequency of applied electric field which would be most appropriate for our purpose of trapping DNA molecules at both ends. Evidently, the shape of the electrodes is likely to have a modifying effect on the electric field in between them. As for example, with triangular electrodes with two vertices facing each other, the field is much stronger around the point. The software COMSOL Multiphysics (MEMs Module) is used, to estimate the electrode geometry and the gap length which would produce an electro-osmosis-driven flow pattern to serve our purpose.

**b) Making of metal electrodes**

Figures 1 (a) & (b) show the device structure for trapping of DNA molecules having different shapes of electrodes, one is plane parallel and other is triangular. The rectangular electrodes will have a dimension 1mm x 1mm which is good enough for electrical probing using wire bonding or Ag paste bonding. For triangular electrodes, (fig.1 (b)) pads of dimensions 1mm x 1mm on its side will be fabricated for electrical contacts. As explained later, fig.1 (b) presents the most suitable arrangement to facilitate trapping of a single DNA molecule. An oxidized un-doped silicon wafer of high resistivity will be the starting material on to which the device will be fabricated. An oxide of a thickness of at least 1000 μm is preferred to prevent pinhole leakages. Photo/Electron-beam lithography would be used to open the "window" between the electrodes. A thin metal is evaporated and subsequently, electrodes are made by using standard lift-off technique. A thin layer of Cr/Ti may be used for improved adhesion of the metal film if required. Enough margins are provided for dicing these DNA chips. The type of metal used for making electrodes will be varied to study its effect on the interaction between DNA and the metal electrode. Au is used for the study. The fabrication process and characterization are discussed in detail in chapter 4.


***Fig. 1:*** *Electrodes geometry (a) Parallel (b) Triangular*

**c) Synthesis of DNA molecules**

The DNA extraction process is carried out with the help of Biological science department, BITS Pilani Hyd. Campus using purification kit. We used λ-DNA in this study.

**d) I-V measurement study**

To perform this study, the fabricated device should have electrical contacts which would establish an external connection between device and I-V measurement instrument. These electrical contacts work completed using a wire-bonder machine with the help of packaging lab, CeNSE, IISc. Later experimentation part i.e. I-V study carried out from University of Hyderabad using semiconductor parameter analyzer. I-V measurement carried out for the triangular EBL patterned microelectrodes at room temperature. This study would help to understand the conductive behavior of trapped DNA molecules.

## 1.3 Motivation

In order to understand the behavior of polarizable biomolecules like DNA, it is essential to think of fabrication aspects since the fabrication process involved many challenges. Therefore, it is worthy to remember that the major challenge in fabrication of smaller devices is to find a robust method and design with the ease of ability to trap and manipulating DNA molecules. In spite of the advanced development of lithographic fabrication techniques that have led to astounding advances in integrated circuits the limits of lithography prevent nanometer-scale electronic devices from being economically manufactured. The inherent limitations of the tool that prevents the fabrication of devices have put forward proposals for alternative nano-manufacturing technologies based on 'bottom-up' chemical self-assembly techniques.

Recent research in nanoelectronics, focusing on the minimization of silicon-based devices, utilized the unique properties of nanostructured materials which differ from their bulk counterpart [13]. Two such properties, namely surface effect, and quantum confinement led to new device applications [14-16]. Nevertheless, most of the "Quantum Devices" fabricated using intricate and expensive top-down approaches lack reproducibility of device characteristics as the functional materials used to tune the device properties get randomly positioned in and around the active area [14, 17]. This results from the fact that conventional synthesis of nanostructures through physical or chemical vapor deposition may at most control size dispersion but deprives of any position control [18]. To this end, scientists have tried scanning probe techniques to manipulate nanostructures especially, quantum dots with limited success [19]. These techniques seem to have a limit for achieving position control in

nanostructures as repetitive manipulation is difficult and time-consuming. However, "bottom-up" approach utilizing the self-assembling properties of nanoscopic objects have revealed that materials having dominant self-assembling qualities promote positioning of them at the desired places with relative ease [20, 21].

Thus, devices made of biomolecules are a suitable alternative to any conventional silicon-based quantum devices. Among the different biomolecules, DNA is an important biological polymer carrying genetic information and therefore it is a viable choice. It is highly interesting as a functional nano-sized material due to its unique features that cannot be found in other polymers. DNA possesses complementarity; a self-assembling ability that always forms hydrogen-bonded base pairs of adenine and thymine and of guanine and cytosine where the base pairs line up one-dimensionally at 0.34-0.36 nm intervals. Due to these self-assembling abilities, DNA can be highly integrated with no need for top-down technique. As a double-stranded DNA, under certain conditions, behaves as a one-dimensional conductor (molecular wire), the self-assembling property may be exploited to develop nanoscale electronic circuits, switches or memory devices. Moreover [5, 10], the mechanical strength and ease of availability of DNA give it an advantage over other bio-molecules.

**1.4 Literature**

Experiments over the past two decades have demonstrated ways to orient, stretch, transport, and trap DNA using non-uniform fields generated in microfabricated devices [22]. First theoretical predictions for trapping of DNA on microelectrodes given by Ajdari and Prost with promising applications, but these predictions did not have experimental confirmation [23]. There have been both the qualitative and quantitative studies of DNA manipulation and trapping over the different microelectrodes by utilizing combined DEP and ACEO effect. To manipulate these bioparticles, whose diameters range from 10 nm to 100 μm, researchers have exploited electrostatic force as it becomes dominant at micrometer scale [23, 24]. The methods include Electrophoresis, Electroosmosis, and Dielectrophoresis. Among these methods, Dielectrophoresis is traditionally recognized as a cell separation technique. The term Dielectrophoresis was first used by H.A. Pohl, which he described as the translational motion of neutral matter caused by polarization effects in a non-uniform electric field [25]. Originally, this term was strictly referred to the phenomena of an induced dipole on particles due to a non-uniform field. However, the term has now been broadening to include other electrokinetic phenomena arises from non-uniform electric fields [26]. In the early stage, Dielectrophoresis was performed using pin-wire electrodes where manipulation is limited to large particles like cells. Using this electrode, Pohl and Hawk have demonstrated the separation of viable and non-

viable yeast cells in 1966. Pohl has then extended the experiments to separate other biological cells, including canine thrombocytes, red blood cells, chloroplasts, mitochondria, and bacteria [6, 22, 24, and 25]. In recent years, microelectrodes with dimension as small as 0.5 μm have been fabricated using photolithography/electron beam lithography techniques. Electrodes are now small enough to generate high electrical field gradients to manipulate sub micrometer particles. Dielectrophoresis can now be used to separate viruses, proteins, and DNA [27].

Washizu and Kurusowa [28] were the first to attempt experimentally, manipulation of kilobase DNA in a microfabricated structure using dielectrophoretic force. They adopted a set of interdigitated sinusoidally corrugated aluminum microelectrodes to experimentally observe site-specific immobilization of double-stranded DNA molecules under AC electric field. They demonstrated a DEP method to stretch DNA along the field lines and positioned it onto electrode edges. Washizu and his coworkers described two effects in their study, one is the dielectrophoretic attraction towards the electrode gaps and the second one is the electrostatic orientation of the DNA along the field lines. They applied a field of $1x10^6$ V/m and a frequency of about 1 MHz between aluminum microelectrodes [10]. This study exhibited that the orientation of DNA molecules depended strongly on the electric field strength. Similar inter-digitated rectangular metal microelectrodes of different dimensions and gap lengths were later investigated, both experimentally and numerically, by several researchers [10] with an aim to understand the movement of DNA molecules within microelectrodes under electro-kinetic effects. Later Asbury and Van den Engh [29], have reported that the trapping of DNA under oscillating electric field using thin gold film stripes. They even showed that it is possible to make trapped DNA molecules to move from one edge to another edge of the thin gold film. This study is quite useful for the manipulation of small quantities of molecules in microdevices.

Therefore, it is clearly understood that the design of the microelectrodes (especially the shape) is of key importance for a well-defined Dielectrophoresis. The influence of the electrode shape on the precision of positioning DNA molecules was demonstrated [30]. The prevalent electrode material is gold, microstructured upon glass or silicon substrates.

Since the manipulation/trapping of polarizable particles like DNA molecules depends strongly on the strength of the applied electric field, it is expected that the sharpness or bends of the electrode edges would influence the overall electro-kinetic process. In this regard, it appears that one might further exploit state-of-art lithographic technique to fabricate smaller electrodes with sharper bends which would intensify the non-uniformity of the electric field and significantly influence DNA manipulation. Nevertheless, from these investigations, it was

not apparent if such geometries of electrodes could serve the purpose of bridging the electrode with a single DNA molecule out of several such species suspended in the solution. This is of paramount interest as it is well established that DNA molecules of some typical length and having specific combinations of base pairs do behave like a metal and once one is bridged between two metal electrodes, it would behave as a molecular wire.

**1.5 Riddles**

It is worth mentioning that seemingly contradicting results on nature of charge transport in double-stranded DNA molecules received serious attention from the scientists all around but most of the work used bundles of DNA between two metal electrodes to study electrical transport through them [31, 32]. Studies on a single DNA molecule, trapped between the metal electrodes have been very few and the very mechanism behind site-specific immobilization has either not been addressed or it remains inconclusive [33]. In many of the dc measurements, contact with metal electrodes was achieved by laying down the molecules directly on the electrodes [34]. Although expedient, this approach has two significant drawbacks. First of all, the process is not strictly site-specific and secondly, it is very difficult to prove that DNA molecule is in direct physical contact with the electrode. Moreover, a recent experiment on octanedithiol has shown that deliberate chemical bonding between the organic molecules and the metal electrodes promotes reproducible conductivity results [35]. The bonds should be strong enough to withstand shear forces in a flow and should survive the measurement process. For an instance, a double-stranded DNA molecule having $OH^-$ and $PO_4^-$ at the ends, it is still unclear how the ends get attached to the metal electrodes forming a bridge structure. Undoubtedly, this information is highly important in the context of DNA being used a molecular wire and to satisfy the desire to use them as the ultimate building blocks of electronic circuits.

In order to overcome the aforementioned drawbacks and to realize the use of single DNA molecules in electronic circuits, firstly a method needs to be developed wherein a site-specific immobilization of a single DNA molecule can be achieved and secondly it must be verified if any chemical interaction has taken place between the metal and the molecules resulting in (strong) bonding when it is in physical contact with the metal electrodes.

Site-specific immobilization of a DNA molecule in a solution can be achieved in two ways [33, 37]:

1) The entire DNA molecule is immobilized along its length using a positively charged substrate and exploiting the fact that DNA molecule is negatively charged due to the

presence of phosphate groups along its length. In this method, not only is the DNA attached at the ends but also at all intermediate points along its length.

2) Trapping of a DNA molecule between the two metal electrodes by application of a bias.

The first method inhibits reading and identification of the DNA sequence after the DNA molecule is immobilized which is a serious drawback in terms of DNA computing. The second method is favorable as it allows DNA molecule to get stretched and attached at their ends only with the electrodes without any attachment at intermediate points. Hence there is no inhibition to the identification of DNA sequences even after trapping. However, in this process there exists a possibility that a DNA molecule may not get attached to the electrodes at both ends and when the electric field is turned off, the DNA stretched by the electric field shrinks back to random-coil conformation with an end fixed at one electrode and the other making Brownian motion [38]. The fluid flow in the medium under the electric field plays a crucial role in facilitating attachment of the DNA molecules to the other electrode as well [10]. This fluid flow under a bias or electroosmosis becomes particularly significant near the edges of the electrodes where the field is very high. To overcome this difficulty, Washizu et al. [10] used floating potential electrodes consisting of two outermost electrodes, and several thin strip electrodes between the gap. The power supply was connected only to the outermost electrodes without any electrical connection to the thin strip electrodes. This method was successful in attaching DNA molecules at both ends but the experiment failed to solve the site-specific immobilization of a single DNA molecule. It had actually led to attachment of a bundle of DNA molecules between the two electrodes.

As mentioned in the above section literature review [22-30], several attempts have been made to trapping DNA molecules using different electrode geometry. Through our work, we will address that the trapping of DNA molecules using triangular electrodes which would generate strong nonuniform electric fields owing to the sharp edges and other parameters of electrode geometry. Our main objective in this research is to enlighten the readers and researchers how the variation of electrode geometry would affect the trapping of DNA molecules under AC-Electrokinetic phenomena such as ACEO and DEP. The knowledge of electrode geometry parameters would help to design and fabricate electrodes to have sharp edges that would facilitate effective trapping with strong nonuniform electric fields.

## References


1. Notomi. T, Okayama. H, Masubuchi. H, Yonekawa. T, Watanabe. K, Amino. N & Hase. T, "Loop-mediated isothermal amplification of DNA", Nucleic Acids Res., 28(12), 63, (2000).
2. N C Seeman: "The use of branched DNA for nanoscale fabrication. Nanotechnology", 2, 149-159, (1991).
3. Bensimon A, Simon A, Chiffaudel A, Croquette V, Heslot F, Bensimon D., "Alignment and sensitive detection of DNA by a moving interface", Science, 265, 2096-2098 (1994)
4. "AC electrokinetics: colloids and nanoparticles", Morgan & Green (2003) Research studies press ltd.
5. Washizu. M & Kurusowa. O, "Electrostatic Manipulation of DNA in microfabricated structures", IEEE Trans. Ind. Appl., 26(6), 1165-1172, (1990).
6. Pohl, Herbert Ackland, "Dielectrophoresis: the behaviour of neutral matter in nonuniform electric fields", Cambridge university press, Cambridge, (1978).
7. Bakewell, D.J. & Morgan, H. "Dielectrophoresis of DNA: time-and frequency-dependent collections on microelectrodes", IEEE Trans. Nanotechnol., 5(1), 1-8, (2006).
8. Loucaides, N.G., Ramos, A. & Georghiou, GE, "Trapping and manipulation of nanoparticles by using jointly dielectrophoresis and AC electroosmosis", J. Phys.: Conf. Series, (100), 052015-052020, (2008).
9. Du, J.R., Juang, Y.J., Wu, J.T. & Wei, H.H, "Long-range and superfast trapping of DNA molecules in an ac electrokinetic funnel", Biomicrofluidics, 2(4), 044103-044106, (2008).
10. Washizu. M, Kurusowa. O, Arai. I, Suzuki. S & Shimamoto. N, "Application of electrostatic stretch and positioning of DNA", IEEE Trans. Ind. Appl., 31, 447-456, (1995).
11. A. Castellanos, A. Ramos, A. Gonzalez, N.G. Green and H. Morgan, "Electrohydrodynamics and Dielectrophoresis in microsystems: scaling laws", J. Phys. D. Appl. Phys. 36 2584, (2003).
12. Diekmann. S, Porschke. D, "Thresholds in field-induced reactions of linear biopolymers. Strong chain-length dependence of field effects in DNA", Biophys. Chem. 16(3),261-7, (1982).
13. S. Sato, S. Nozaki, and H. Morisaki, "Tetragonal germanium films deposited by the cluster-beam evaporation technique", Appl. Phys. Lett. 66, 3176, (1995).
14. Souri Banerjee, S. Huang, T. Yamanaka and S. Oda, "Evidence of storing and erasing of electrons in nanocrystalline-Si based memory device at 77 K", J Vac. Sc. Technol. B 20, 1135, (2002).
15. P. Moreno, M. Richard, M. Rossetti, M. Portella-Oberli, L. H. Li, B. Deveaud-Plédran and A. Fiore, "Intraband Carrier Photoexcitation in Quantum Dot Lasers, *Nano Lett.*, 2008, 8 (3), pp 881–885
16. I. O'Driscoll, M. Hutchings, P. M. Smowton, and P. Blood, Many-body effects in InAs/GaAs quantum dot laser structures", Appl. Phys. Lett. 97, 141102, (2010).

**17.** Yoshishige Tsuchiya, KosukeTakai, Nobuyuki Momo, TasukuNagami, Hiroshi Mizuta, and Shunri Oda, "Nanoelectromechanical nonvolatile memory device incorporating nanocrystalline Si dots", Journal of Applied Physics, 100, 094306, (2006).

**18.** Bruce J. Hinds, Takayuki Yamanaka, and Shunri Oda, "Emission lifetime of polarizable charge stored in nano-crystalline Si-based single-electron memory", Journal of Applied Physics 90, 6402, (2001).

**19.** N. Nilius, T. M. Wallis, W. Ho, "Development of One-Dimensional Band Structure in Artificial Gold Chains", Science, 297, 1853, (2002).

**20.** Kenji Ohmori, Y. L. Foo, Sukwon Hong, J. G. Wen, J. E. Greene, and I. Petrov, "Directed Self-Assembly of Ge Nanostructures on Very High Index, Highly Anisotropic Si(hkl) Surfaces", *Nano Lett.*, 5 (2), 369–372, (2005).

**21.** C Schneider, A Huggenberger, T Sünner, T Heindel, M Straub, S Göpfert, P Weinmann, S Reitzenstein, L Worschech, M Kamp, S Höfling and A Forchel, "Single site-controlled In(Ga)As/GaAs quantum dots: growth, properties and device integration", Nanotechnology 20, 434012, (2009).

**22.** David. J. Bakewell, Haywel Morgan, "Dielectrophoresis of DNA: time and frequency dependent collections on microelectrodes", IEEE Trns. On nanobioscience, 5, 1-9, (2006).

**23.** Ajdari. A, Prost. J, "Free flow electrophoresis with trapping by transverse inhomogeneous field", PNAS, USA, 88, 4468-4471, (1991).

**24.** David J. Bakewell, Nuria V Irigaray, David Holmes, "DEP of biomolecules", JSM Nanotechnology & Nanomedcince, 1:1003, 1-14, (2013).

**25.** Zhang. C, Khoshmanesh. K, Mitchell. A, Kalantar-Zadesh. K, "DEP for manipulation of micro/nano particles in microfluidic system", Anal Bioanal Chem., 2012, 369, 401-420 and Herbert A. Pohl, Joe S Crane, "DEP of cells", Biophysical, Journal, 11: 711-727, (1971).

**26.** Martin Z. Bazant, Todd M. Squires, "Induced charge electrokinetic phenomena", COCIS, 15, 203-213, (2010).

**27.** Khoshmanesh K., Zhang C., Tovar-Lopez F.J., Nahavandi S., Baratchi S., Kalantar-zadeh K., Mitchell A. "Dielectrophoretic manipulation and separation of microparticles using curved Microelectrodes" Electrophoresis, 30: 3707–3717, (2009).

**28.** M.Washizu and O. Krurusowa, "Electrostatic Manipulation of DNA in microfabricated structures", IEEE trans. On Industry Applications, 6, 26, (1990).

**29.** Asbury, G.V. d. Engh, "Trapping of DNA in nonuniform oscillating electric fields", Biophysical J. 74, 1024, (1998).

**30.** F. Dewarrat, M. Calame, and C. Schonenberger. "Orientation and positioning of DNA molecules with an electric field technique", Single Molecules, 3, 189-193, (2002).

**31.** P. J. de Pablo, F. Moreno-Herrero, J. Colchero, J. Gomez Herrero, P. Herrero, A. M. Baro, Pablo Ordejon, Jose M. Soler, and Emilio Artacho, "Absence of dc-Conductivity in λ-DNA", Phys. Rev. lett. 85, 4992, (2000).

**32.** Y. Zhang, R. H. Austin, J. Kraeft, E. C. Cox, and N. P. Ong, "Insulating Behaviour of λ-DNA on the Micron Scale", Phys. Rev. lett., 89, 198102, (2002).

**33.** Hezy Cohen, Claude Nogues, Ron Naaman and Danny Porath, "Direct measurement of electrical transport through single DNA molecules of complex sequence", PNAS, 102 (33), 11589-11593, (2005).

**34.** A. Rakitin, P. Aich, C. Papadopoulos, Yu. Kobzar, A. S. Vedeneev, J. S. Lee, and J. M. Xu, "Metallic Conduction through Engineered DNA: DNA Nanoelectronic Building Blocks", Phys. Rev. Lett. 86, 3670, (2001).

**35.** Cui XD, Primak A, Zarate X, Tomfohr J, Sankey OF, Moore AL, Moore TA, Gust D, Harris G, Lindsay SM, "Reproducible measurement of single-molecule conductivity", Science. 19; 294(5542):571-4, (2001).

**36.** Danny Porath, Alexey Bezryadin, Simon de Vries and Cees Dekker, "Direct measurement of electrical transport through DNA molecules", Nature volume, 403, 635–638, (2000).

**37.** Masao Washizu, Seiichi Suzuki, Osamu Kurosawa, Takeshi Nishizaka, and Tusuneo Shinohara, "Molecular Dielectrophoresis of Biopolymers", IEEE Trans. On Industry Appl., Vol. 30, NO. 4, 835, (1994).

# Chapter-2
# AC-Electrokinetics

*Electrokinetic phenomena have been judiciously utilized to manipulate the movement of polarizable particles like DNA that are suspended in aqueous medium and placed between electrically fed microelectrodes. Electrokinetic devices are used to move or separate the particles under the influence of electric fields. This chapter enables to understand the physics behind the motion of the suspended polarizable particles and the forces that are acting at the interface of liquid-solid.*

## 2.1 Introduction

There are many methods that can be used for manipulating/trapping or sorting particles, either singly or bunch when the particles are suspended in an aqueous medium. A widely used technique for both moving and separating the suspended particles is electric field-based manipulation which is highly suitable for integration into microdevices. In electric field manipulation, both the AC and DC voltages can be used to move suspended particles and bulk liquid. Therefore, the interaction between electric fields and the suspended particles in an aqueous medium can be referred to Electrokinetics. The Electrokinetic effects are widely used in micro- and nanoscale fluid mechanics. The devices that are fabricated at Micro- and nanoscale finds intensive applications for chemical and particulate separation and analysis, biological characterization, sensors, cell capture and counting, micropumps, and actuators etc., [1]. The Electrokinetic phenomena are considered to be the transportation of both suspended particles and bulk liquid. Electrokinetic transport referred to the combination of Electroosmosis and Electrophoresis [2]. Electroosmosis refers to the motion of bulk liquid pasts a stationary solid surface and Electrophoresis describes the motion of charged surface due to the action of an applied electric field. It is to be noted that the Electroosmosis results in a net mass transfer of the aqueous solution whilst the electrophoresis causes movement of charged particles or molecules through the solution. Therefore, Electrokinetics refers to the study of the motion of bulk fluids or selected particles that are embedded in fluids under the influence of electric fields. Electrokinetics provides effective manipulation techniques in the micro and nano regime where the biological particles meet the length scales. The ease of ability to manipulate particles down to molecular level explores incredible applications in biological science and technology [3].

Electrokinetics phenomena arise from the fact that the relative motion between charged surface and electrolyte subjected to electric fields and it leads to the formation of a thin layer called Electrical Double Layer (EDL). And there are different types of phenomena out of which considerable interest in Electroosmosis (EO) and Electrophoresis (EP). AC Electrokinetics is much more concerned with the study of the effect of AC electric fields on particles that are suspended in bulk fluid. The application of an AC electric field to a system of suspended particles can move both the particles and fluid in different ways. The electrical forces can act both on particles and suspending fluid and the major forces are EP and/or Dielectrophoresis (DEP). EP acts on the fixed, net charge of the particle while DEP only acts when there are induced charges, and only results in motion in a non-uniform field. The applied electric field produces a force on suspending medium if there is charge density gradient in the fluid. EO originates from the bulk fluid motion due to the interaction between applied filed and free charge in EDL [4].

The AC electrokinetic manipulation of particles has become a major area of research and it finds intensive applications in biotechnology filed like Lab-On-A-Chip (LOC) where different micro devices are integrated onto a single chip. And it is also employed in the fabrication and characterization of MEMS (Micro Electro Mechanical Systems) and NEMS (Nano Electro Mechanical Systems) devices [5-7]. Many researchers have been investigated trapping and manipulation of biomolecules that are embedded in the fluid by microelectrodes of different shapes and geometries using electrokinetic effects subjected to inhomogeneous electric fields. Ramos et al. discovered AC Electroosmosis (ACEO) over the surface of microelectrodes [8]. Later Ajdari described exploitation of ACEO effect using asymmetric arrays of inter-digitated microelectrodes [9]. The above breakthroughs, supported by the several experiments of Green et al, Brown et al, Studer et al, and others, focused attention on nonlinear AC Electrokinetics and opened up avenues for new advances [4, 10].

## 2.2 Electrical Double Layer (EDL)

The accumulation of charges takes place over the surface of the electrode due to the application of potential which results in a field. This causes charges movement and change in charge density. Thus, formed thin layer of potential is often called as Electrical Double Layer (EDL). In order to understand the liquid flow, particle movement and induced potential, the knowledge of the spatial distribution of the free charges and their mobility are essential which forms the foundation in Electrokinetics [11].

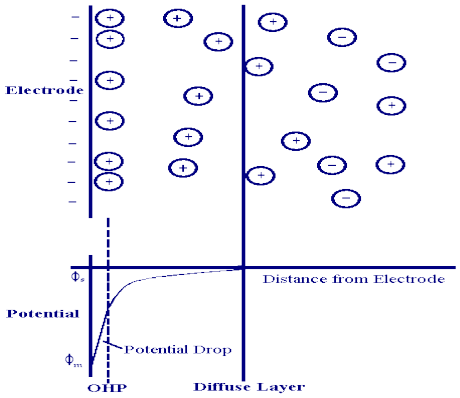


***Fig 2.1:*** *Schematic representation of EDL (Adopted from Cambridge university press)*

In general, a surface of the metal electrode carries a net charge which comes about either through dissociation of chemical groups on the surface or by adsorption of the ions or molecules from solution onto the surface. This accumulation of charge creates an electrostatic surface potential local to the interface. And it can be referred to surface charge polarization phenomenon due to Van der walls forces. When the surface of the electrode is immersed in an electrolyte solution, the accumulated surface charge is balanced by an equal (and opposite) amount of excess charge in the EDL forms electrostatic potential at the surface of the electrode. The electrostatic potential attracts ions of opposite charge (counter ions) from the electrolyte solution and repels the ions with like charges (co-ions).

The region of liquid near to the interface has a higher density of counter ions and lower density of co-ions than the bulk solution. This region is referred to as the diffusive region of the EDL and carries a net charge due to counter ions. Above this region liquid (bulk) is electrically neutral. The EDL is of two regions; one is an immobilized layer (Stern layer) at the surface of the electrode and the other is a diffusive layer which is an electrically neutral layer in bulk solution. And the EDL can be characterized by its length called Debye's length represented by $\lambda_{DL}$. It is a measure of the EDL thickness and it is typically a few nm.

$$\lambda_{DL} = \sqrt{\frac{\varepsilon K_B T}{2 N_A e^2 C}} \tag{1}$$

Where ε is permittivity, $K_B$ is Boltzmann constant, T is room temperature (298$^o$ K), $N_A$ is Avogadro number, e be the charge of an electron, C is a concentration of one ion at infinite dilution in the medium calculated using the following equation.

$$C = \frac{\sigma}{\lambda_\infty} \tag{2}$$

Where σ is the conductivity and $\lambda_\infty$ is Molar conductivity of KCl at infinite dilution at room temperature.

EDL is effectively a capacitor skin at the interface (solid-liquid). The variation of potential in EDL is assumed to be falling linearly in the region of surface charge (electrostatic charge surface-Stern layer) whilst decays exponentially in the region of diffusive charge (net charge density) layer with a characteristic distance given by the Debye length and goes zero in the bulk where the net charge is zero. When an electric field is applied externally, the components of the electrical potential normal to the electrode surface induce the charge in the EDL, while the tangential component produces a body force on the induced charge, thus the net charge in the EDL drag the bulk fluid over the electrode surface. Because the electrodes are applied with AC signals, the EDL charges change their polarities periodically and so does the tangential electric field, as a result, steady fluid motion arises instead of oscillatory flow. Therefore, understanding the potential variation in EDL, the motion of induced charges and motion of bulk solution is a crucial aspect of Electrokinetics phenomena. The induced charges movement can be referred to electrophoretic force and the motion of bulk solution is referred to Electroosmosis.

Understanding the behavior of the system of electrode-electrolyte is analogous to capacitors and resistors in an electrical circuit. The capacitance of the EDL can be thought of as a resistance in series with the suspending medium impedance.

$$\frac{1}{i\omega C_{DL}} \tag{3}$$

($C_{DL}$ capacitance per unit area of the EDL which is proportional to the permittivity $\varepsilon_r$ of the suspending medium)

$$C_{DL} = \frac{\varepsilon_0 \varepsilon_r}{\lambda_{DL}} \tag{4}$$

From Eq. (3) if $\omega \to 0$, the reactance value tends to infinity then the voltage across the suspending medium goes to zero. The capacitance of EDL is estimated using the linear RC circuit model for the system as in Debye-Huckel theory [1, 4]. Also, the velocity profiles of fluid flow can be examined by solving Navier-Stokes (N-S) equation and the potential of EDL can be measured by solving Poisson's equation with Debye-Huckel approximations [1, 11 & 12].

### 2.3 AC-Electroosmosis (ACEO)

When a potential is applied to the system of electrode that is being immersed in an electrolyte solution, the field causes charges to accumulate over the surface of the electrode, which changes the charge density near the surface and forms a layer called electrical double layer (EDL), it can also be referred to Electrode Polarization. Since the applied field is oscillatory the EDL interacts with only the tangential component of the electric field and a net force is generated on the EDL, which causes fluid motion. In an alternating electric field, both the sign of the charges in EDL and the direction of the tangential component of the electric field changes. Since the electric field has a tangential component due to the planar electrode geometry, the counter ions are pulled along the tangential component of the applied electric field (from the edge to the middle of the electrode). The direction of movement does not change with the polarity change of the AC voltage because the polarity of the induced counter ions is switched as well. The motion of the ions drags the bulk fluid along the surface. That fluid motion is known as AC electroosmosis (ACEO) [4, 10].

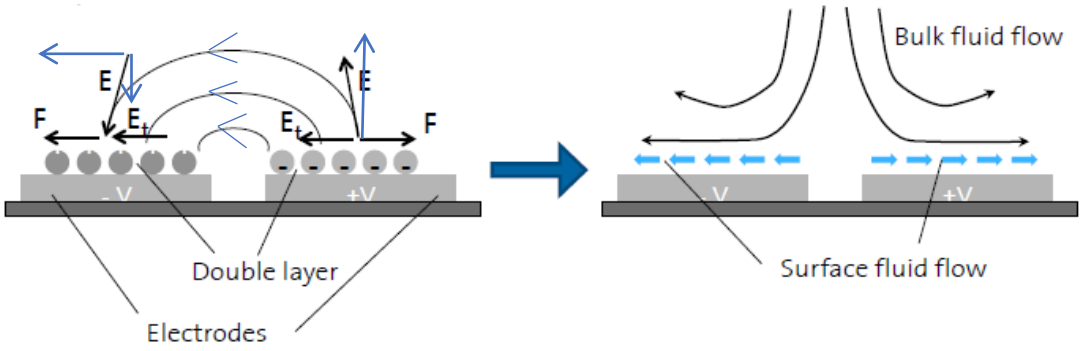


*(a) Filed lines* *(b) Fluid flow*

***Fig 2.2:*** *Field lines & ACEO flow over the surface of electrodes. (Adopted from Morgan & Green "ACEK") [4]*

The schematic representation of the system of ACEO mechanism is shown in the above fig where $E_t$ is the tangential component of the electric field that causes charges to move along and results in motion in bulk fluid. Electrode polarization mechanism is a central aspect to understanding the ACEO phenomenon. The force F experienced by the induced charge is due to the action of $E_t$ which results in fluid flow. Fig. 2.2 (A) represents the system for one half-cycle of applied AC field/potential. In the other half-cycle potential, both the direction of $E_t$ and sign of induced charge are opposite. Therefore, the direction of the force vector unchanged gives rise to a non-zero time-averaged force and steady-state fluid flow occurs as shown in fig. 2.2 (B) over the surface of the electrodes. There had been both theoretical and experimental work with different microelectrodes have shown that the alternating fields can generate local

fluid motion related to the charging of DL and demonstrated the flow using simple parallel finger microelectrodes under AC fields. Since the applied electric field is non-uniform there would be a non-zero time-averaged flow which will not occur in a uniform AC field [13, 14].

The ACEO fluid flow is governed by the charge induced by $E_t$ of the applied electric field near the electrode-electrolyte interface. Since the applied potential is frequency dependent so does the charge. Therefore, the magnitude of ACEO flow is also frequency dependent. At lower frequencies (no field in bulk solution) both the potential across suspending medium and $E_t$ are zero results, the magnitude of ACEO flow tends to zero. And ACEO flow magnitude again tends to zero at higher frequencies for having both the potential across the DL & induced charge are zero (inadequate time for the induced charge to form in the DL). N.G. Green et.al carried out experimental results for velocity profile of electrolytes on coplanar plate microelectrodes subjected to an AC electrified. These measurements carried out as a function of applied signal potential, frequency, the conductivity of electrolyte and position of the electrode. It has been noticed that the velocity at any position on the electrode surface is zero at low and high-frequency limits and maximum at an intermediate characteristic frequency that depends on the conductivity of electrolyte [4, 15].

A systematic study of ACEO behavior is analyzed as a part of work under low AC bias for a wide range of frequency (1Hz-100 kHz) with different geometries of microelectrodes and for different conductivities & viscosities of the electrolytes. Firstly, comparative study is carried out to verify the present numerical method by considering Green's et.al work for simplest model of coplanar plate microelectrodes with electrolyte (KCl is taken as typical electrolyte). And later it is extended to coplanar triangular microelectrodes as this geometry would increase the intensity of electric field in the gap between the electrodes which may affect the flow pattern between the electrodes. Fluid velocities are calculated as a function of increasing frequencies exhibited the flow reversal at high frequencies irrespective of electrode geometries which are explained in the framework of a linear model [Green et.al]. Moreover, this study also presents how fluid velocities vary with frequency and electrode geometries as the viscosities and conductivities of the electrolytes are changed which are discussed in more detail in Results & Discussions.

When the system of electrodes being immersed in an electrolyte (KCl) subjected to AC voltage, the surface of each electrode attracts ions of opposite charge. The applied electric field exerts an electric force on these accumulated ions which point in opposite directions on both the electrodes. This electrical force drags the ions which in turn produces stress on the surrounding fluid which thus moves from the gap between the two electrodes onto the surface

of the electrode on either side. The schematic of the system explaining the mechanism of AC Electro-osmosis (ACEO) is shown in Fig. 3 where the x-component of the electric field and the direction of resultant Coulombic force are shown clearly. If one considers a set of symmetric rectangular parallel electrodes like that used by Green et al [16] then for the frequency of applied voltage at 500 Hz, a typical plot of electric potential and ACEO flow, generated numerically using COMSOL Multiphysics could be realized as depicted in figures 2.3 and 2.4 respectively. It is to be noted that coplanar parallel electrodes (CPE) are placed in a closed glass chamber. It is customary to exploit the symmetry of the system and only one electrode is used for simulation. The schematic of the simulation region (top view) is shown in fig. 2.5. For this typical electrode having a width of 100 μm, the plane Y= 0 is the plane of symmetry. The distance of the electrode from the plane of symmetry is 12.5 μm. This geometry is also used by Green et al [16] as it can be observed from the fig. 2.4. It is to be noted that the COMSOL Multiphysics software is based on finite element method (FEM) where a mesh consists of triangular elements for the two-dimensional parallel electrodes. Finer meshing might be more appropriate if an electrode has a bend or sharp edges due to the discontinuity of electric field at edges.

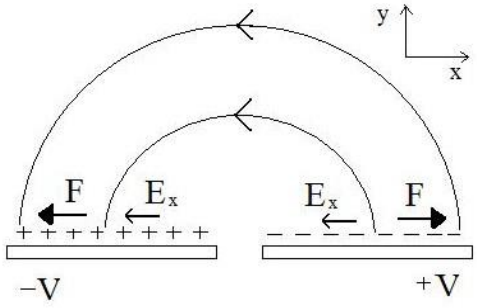


***Fig. 2.3:*** *Schematic of ACEO mechanism*

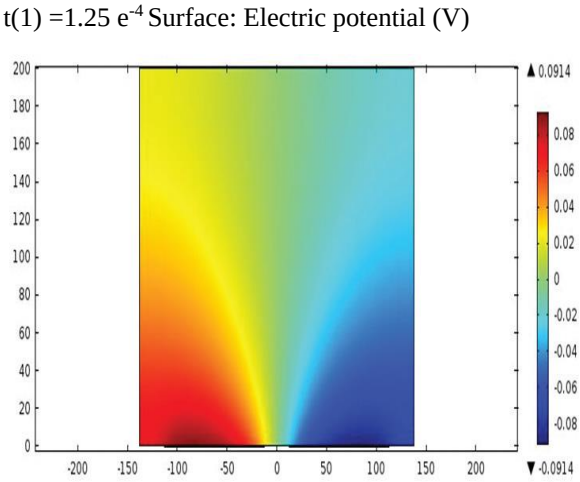


***Fig. 2.4:*** *Electric potential at 500 Hz*

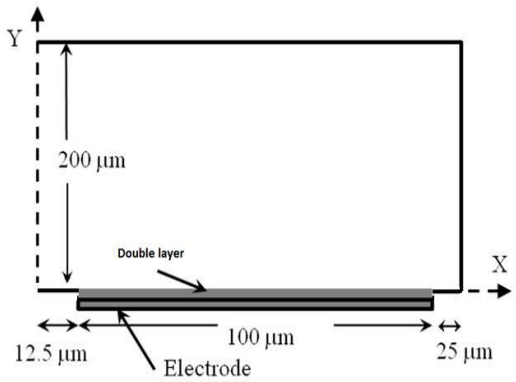


***Fig. 2.5:*** *Schematic of problem space showing a cross-sectional view*

The above electrode geometry, in general, termed as 'the coplanar parallel electrode (CPE) geometry'. It is a simplified linear model to understand the qualitative framework which has been proposed by Green et al. [17-20]. The EDL thickness formed over the surface of electrodes is measured using Eq. (1) & (2) the Debye length approximation. The charge density in the bulk region is considered to be negligible by giving potential V and it is governed by the Laplace's equation;

$$\nabla^2 V = 0 \tag{5}$$

And the following boundary condition is incorporated at the top of EDL,

$$n.J = i\omega C_{DL}(V - V_{ref}) \tag{6}$$

$$V_{ref} = V_0 \sin(\omega t) \tag{7}$$

Where ***n.J*** picks out the normal component of current density, $C_{DL}$ represents the capacitance per unit area of the EDL and $V_{ref}$ is the potential applied to the electrodes which are sinusoidal in nature. The capacitance of EDL is estimated using the linear RC circuit model for the system. [14].

From fig 5, the potential at the image plane is to be taken as zero. Primarily the electric potential is solved and then the coupled time-dependent Navier-Stokes (N-S) equation is solved for fluid flow by considering the fluid to be incompressible.

$$\rho \frac{\partial \vec{u}}{\partial t} + \rho(\vec{u}.\vec{\nabla})\vec{u} = \vec{\nabla}.[-p\vec{I} + \eta(\vec{\nabla}u + \overrightarrow{(\nabla u)^T}] + \vec{F} \tag{8}$$

$$\rho\vec{\nabla}.\vec{u} = 0 \tag{9}$$

Where ρ is mass density of the fluid, taken to be mass density of water, 1000 kg/m$^3$, p refers to pressure, I represent Identity matrix. F refers to the external force on the fluid, electrical force in this context that arises out of potential applied to the electrodes. The region of interest is the bulk region where the charge density is negligible, allows one to assume, F = 0 for simulation purposes. As Reynolds number for microelectrodes is less than $10^{-2}$, the inertial term (second term on the left-hand side of the equation) is neglected in the eq. (8). The walls and electrodes are assumed impervious and therefore have no normal component of the fluid velocity at their surface. On the top of the EDL, horizontal fluid velocity is given by Helmholtz-Smoluchowski formula for electro-osmotic velocity. [18].

$$\vec{u} = \frac{-\varepsilon_0 \varepsilon_r \Lambda \xi E_t}{\eta} \tag{10}$$

Where $\xi = V_{ref} - V$, and this is the potential difference between the outer and inner sides of the diffuse layer, ∧ is the ratio of potential drop across diffusive layer and potential drop across EDL. $E_t$ is the tangential component of the electric field just outside the EDL, η is the

viscosity of the medium. Owing to symmetry, at the image plane, normal component of velocity as well as the sheer stress is zero. As the ACEO flow is unidirectional with respect to the AC voltage, for experimental purposes, time-averaged velocity is usually taken by averaging out the equations (8),(9) & (10), which then become,

$$\vec{\nabla}.\left[-p_{avg}\vec{I}+\eta\left(\vec{\nabla}u_{avg}+\left(\vec{\nabla}u_{avg}\right)^{T}\right]=0\right.$$

$$\rho\vec{\nabla}.\vec{u}_{avg}=0$$

$\vec{u}_{avg}=\frac{\varepsilon_0\varepsilon_r}{2\eta}Re\left(\xi\vec{E}_t\right)^*$ Where * denotes the complex conjugate.

**2.4 Dielectrophoresis (DEP)**

A phenomenon in which manipulation and characterization of particles at the nanoscale and also it employs electric field gradients. Generally, it is the induced motion of a particle when it is placed in an electric field gradient. The term Dielectrophoresis (DEP) first coined by H.A. Pohl, and it is an effect where a particle is carried as a result of its dielectric properties. Pohl defined this effect *as "The motion of suspensoid particles relative to that of the solvent resulting from polarization forces produced by an inhomogeneous electric field"* [7, 21]. The DEP phenomenon refers to the Coulombic response of an electrically polarized particle (assumed to be spherical) in a nonuniform electric field. In the context of uniform field particle gets polarized on either side of the sphere with equal and opposite charge, then the net Coulombic force acting on the sphere is zero whilst in the nonuniform field, one side of the sphere gets the larger electric field and the other side feels opposite which results out gradient in an electric field. This electric field gradient would exhibit an effect on the Coulombic force which makes the particle to move depending upon the dielectric properties of the particle and its surroundings [1].

DEP has become a most powerful technique for manipulation of particles at the nanoscale such as conductor, semiconductor, DNA molecules, nanowires, and graphene. And in the last few decades, there has been a great interest specifically manipulation of materials at nanoscale based on DEP owing to the facilitation of nondestructive and noncontact manipulation method using different microelectrodes which would employ electric field gradients subjected to inhomogeneous electric field [7, 22]. DEP can be referred to electrical forces that would facilitate manipulation of biological matter like cells at micro and nanoscale. In general, electrical forces for manipulating cells and other bio-soft matter include Electrophoresis (EP) and Dielectrophoresis (DEP). EP force ($F_{EP}$) is due to the interaction

between cell's charge and an electric field whilst DEP force ($F_{DEP}$) is due to cell's polarizability. Both the $F_{EP}$ and $F_{DEP}$ can be used to develop microsystems for separating, sorting, positioning, trapping biological molecules such as cells, bacteria, virus, DNA and proteins [10, 23, & 24]. It is worthy to be noted that the fabrication of devices is key of interest to generate electric field gradients which would facilitate effective trapping of polarizable particles like DNA using microelectrodes of different geometries. In recent times, there is a significant growth in the area of feasible lithography fabrication of metal and /or insulator structures that can generate electric field gradients.

Washizu's group performed an extensive research work on DEP of DNA numerically and experimentally since 1990's using Fluid Integrated Circuit (FIC) models [25-27]. They used a set of interdigitated sinusoidally corrugated aluminum microelectrodes to experimentally observe site-specific immobilization of double-stranded DNA (ds DNA) molecules subjected to AC electric field. From their experimental observations, the orientation of DNA molecules is strongly dependent on the electric field strength. Later, several attempts made to understand the movement of DNA molecules within microelectrodes under Electrokinetic effects using interdigitated rectangular metal electrodes of different dimensions and gap lengths [28]. From these reports, it appears that one might further exploit state-of-art lithographic technique to fabricate smaller electrodes with sharper bends which would intensify the non-uniformity of the electric field and significantly influence DNA manipulation. To this end, use of triangular shaped electrodes has recently been very popular [29, 30]. Porath, et al, reported the first experimental evidence of trapping of a single, ds DNA molecule between the two vertices of a set of triangular electrodes where a few nanometers were apart. [29]. From this work, it clearly revealed that the electric field strength which was extremely large at the vertices of the triangular electrode, coupled with polarization properties, played an important role in guiding the flow of DNA molecules in and around the tips. However, the most modern lithographic technique has its limitation to reproduce the bends or sharpness of the electrodes [30]. Thus it is interesting to study how small variations in electrode configurations would affect the nature of immobilization of the suspended DNA molecules confined between them. In results and discussions chapter, a systematic analysis of the effect of the curvature of the electrode tips on the localization of insoluble particles is present and also tried to assess how the convexity of the electrodes could influence the localization process [31, 32].

### 2.4.1 Principle & Theory

The word Dielectrophoresis (DEP) is the conjunction of two parts: dielectro- refers to the motion that depends on dielectric properties of the particle and phoresis- refers to motion. DEP is different from EP since EP requires a net charge on the body for Coulombic interaction subjected to externally applied, spatially uniform electric field. However, DEP does not require a particle to carry a net electrical charge and it can be used to move and manipulate very small biomolecules like DNA under nonuniform electric fields. This makes DEP very popular and relatively easier method of controlling the motion of biomolecules particularly under low voltages. This has been utilized effectively in a micro-device environment such as LOAC or μTAS applications [Ref].

The DNA molecule suspended in an electrolyte solution will develop a strong electric dipole moment under suitable condition as explained by Washizu et al [33]. This induced dipole would facilitate trapping and manipulation of the molecule with the field gradients when placed within microelectrodes. In the presence of an AC electric field, a polarizable particle like a DNA will experience an induced dipole and it will result in a net translational force on the particle as the force on either side of the pole is not equal. The resulting force on the particle is termed the dielectrophoretic force ($F_{DEP}$) and the motion due to this force is known as Dielectrophoresis [34]. The schematic representation of DEP principle is illustrated in the following fig 2.6.

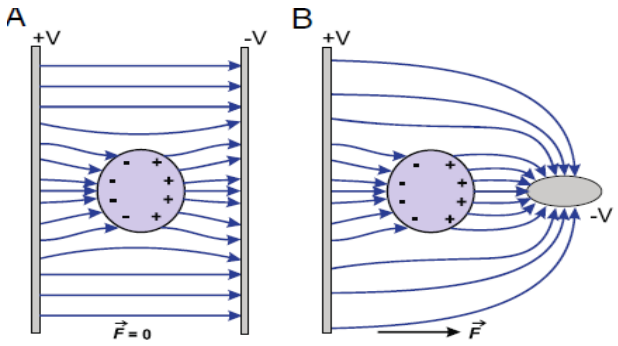


***Fig 2.6:*** *(a) uniform geometry (b) non-uniform geometry*
*(Adopted from Anton Kuzyk Review article [22])*

Surface charges of polarizable DNA molecule are induced in the electric field, positive on one side of the molecule and negative (of the same magnitude) on the other side. Then there will be a Coulombic interaction between the induced surface charges and the applied electric field. In a uniform field, the net force due to the Coulombic interaction is zero, as shown in fig 2.6 (a). Whereas in a non-uniform field, as shown in fig. 2.6 (b), the electric field density is higher on the right side of the molecule, then, there is a net force acting on the molecule in the direction

of the higher field strength. This is a simplified explanation of the DEP force where the effect of a surrounding medium was neglected.

In general, the polarization of the surrounding medium should also be considered. Since the application of electric field will cause charges to accumulate at either side of the interface between molecule and its surrounding medium, the degree of charge building up depends on the polarizability of the medium, which is essentially a measure of both the ability of molecule to respond to the applied field (conductive response) and the ability to produce charges at an interface (dielectric response). Under this situation, the polarizable molecule does not remain stationary since one side of the molecule feels s stronger pull by the electric field gradient than the other side. Based on this response of the particle, DEP classified into positive DEP (p DEP) and negative DEP (n DEP). In positive DEP showed in fig 2.7 (a), due to having higher polarizability than the surrounding medium, the molecule is pushed towards the region of the higher electric field. If the molecule has the polarizability smaller than the surrounding medium, then it is pushed towards the region of the weaker electric field, and it is called negative DEP showed in fig 2.7 (b). The schematic illustration of DEP classification showed in the following figure 2.7. If the molecule has greater polarizability ($\varepsilon_p$) than the surrounding medium polarizability ($\varepsilon_m$), then there will be a large amount of charges accumulation on the particle side of the particle-medium interface which gives rise to develop an induced dipole across the particle, and it is aligned with the electric field. If the molecule has a lower polarizability than the suspending medium, then there will be a larger amount of charges accumulation on the medium side of the particle-medium interface which gives rise to develop an induced dipole across the particle, which is aligned opposite to the electric field. If both the molecule and medium are equally polarizable, then there will be no induced dipole which usually happens under uniform electric field [4]. Therefore, if the applied electric field is uniform, then induced dipole will have an equal and opposing force on each pole which results out no net motion of the molecule. If the field is non-uniform, then one side of the molecule will experience a larger force than the other side, then there will be a net translational motion which is termed dielectrophoretic motion, the di referring to the dipole. And this DEP can exist for both the DC and AC electric fields, the only requirement for DEP is spatially non-uniform electric fields [4]. If the molecule is more polarizable than the medium, the electric field within the molecule is nearly zero, then the external field lines will bend towards the molecule and it pushes the molecule towards the region of maximum electric field (i.e. electrode edges), this can be referred to p-DEP, showed in fig 2.7 (b). If the molecule is less polarizable than the medium, the electric field within the molecule is high, then the external field lines will bend

around the molecule as if it was an insulator and it pushes the molecule towards the region of minimum electric field, this can be referred to n-DEP, showed in fig 2.7 (b).

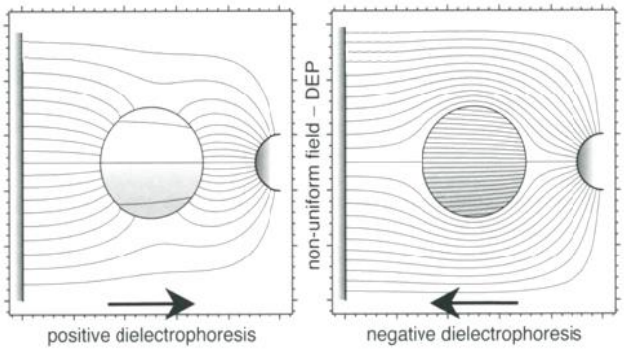


***Fig. 2.7:*** *(a) p-DEP ($\varepsilon_p > \varepsilon_m$)* *(b) n-DEP ($\varepsilon_p < \varepsilon_m$)*
*(Adopted from Morgan and Green "ACEK" [4])*

DEP depends on the fact that the molecule is electrically polarized in the form of the electric dipole with the dipole moment **p** when it is exposed to the electric field. The usual way of representation of dipole moment is, $p = Qd$ (+Q & -Q) equal and opposite charges accumulate on opposite sides of the molecule and d- diameter of the induced dipole). And the force experienced by the molecule is $F = QE$. The polarized molecule will experience a torque and align induced dipoles with the field. In the context of electric field gradient, the two poles (+Q & -Q) of **p** will not experience the same force hence the molecule will move. The induced motion for which $F_{DEP}$ is responsible and acts on a dipole moment **p** subjected to inhomogeneous electric field E i.e. field with a non-zero gradient $\nabla E$, is given by:

$$F_{DEP} = (p.\nabla)E \tag{11}$$

The average dipole moment of the molecules is directly proportional to the magnitude of the electric field,

$$p_{avg} \propto E \Rightarrow p_{avg} = \alpha E \tag{12}$$

Where α is polarizability/polarization factor and it is a measure of the response of the dielectric to applied electric field E. (Units: F-m$^2$).

On solving the potential distributions inside the particle (assumed to be spherical) and medium using Laplace's equation $\nabla^2 \phi = 0$, the induced dipole moment of the dielectric sphere;

$$p = 4\pi\varepsilon_p \left( \frac{\varepsilon_p^* - \varepsilon_m^*}{\varepsilon_p^* + 2\varepsilon_m^*} \right) r^3 E \tag{13}$$

E is oscillatory $e^{\pm i\omega t}$, $r^3$ is the volume of particle and $\left(\frac{\varepsilon_p^* - \varepsilon_m^*}{\varepsilon_p^* + 2\varepsilon_m^*}\right)$ is the real part of Clausius-Mossotti (*Re{$f_{CM}$}*) factor which is the difference in permittivities of particle and its surrounding medium. Where $\varepsilon^*$ is complex permittivity and it is related to the conductivity σ and the angular frequency ω of the applied field through the equation;

$$\varepsilon^* = \varepsilon - i\left(\frac{\sigma}{\omega}\right) \tag{14}$$

On substituting Eq. 13 in Eq. 11 then the DEP force expression turned out to be:

$$F_{DEP} = 4\pi\varepsilon_p\left(\frac{\varepsilon_p^* - \varepsilon_m^*}{\varepsilon_p^* + 2\varepsilon_m^*}\right)r^3(E.\nabla)E \Rightarrow 4\pi\varepsilon_p \,\mathrm{Re}(\{f_{CM}\})r^3\frac{\nabla E^2}{2}$$

Where $(E.\nabla)E = \frac{\nabla E^2}{2}$ from the following vector identities and considering electric field to be irrational $(\nabla \times E = 0) and A = B = E$

$$\nabla(A.B) = (A.\nabla)B + (B.\nabla)A + B\times(\nabla\times A) + A\times(\nabla\times B) and$$
$$\nabla\times(A\times B) = (B.\nabla)A - (A.\nabla)B + (\nabla.B)A - (\nabla.A)B$$

Now, $$\boxed{F_{DEP} = 2\pi\varepsilon_p \,\mathrm{Re}(\{f_{CM}\})r^3\nabla E^2_{rms}} \tag{15}$$

$E_{rms}$ is the *rms* value of the applied field and the direction of DEP force is governed by the direction of the gradient of the square of the electric field. Since E only appears as $E^2$ the sign of the DEP force is independent of the sign of E but is given by the sign of the *Re ({$f_{CM}$}). Re ({$f_{CM}$}) > 0* which means positive when $\varepsilon_p^* > \varepsilon_m^*$ then the particle will experience p-DEP and *Re ({$f_{CM}$}) < 0* which means negative when $\varepsilon_p^* < \varepsilon_m^*$ then the particle will experience n-DEP. If this factor is zero then there is no DEP force.

### 2.4.2 Experimental observations on Manipulation of polarizable molecules

It has been realized that, in order to manipulate such small biomolecules like DNA by DEP technique, it is necessary to have well-defined electrode geometries which would generate high electric field strengths. Since DEP is based on non-uniform electric field, it is very important to figure out the design of electrode structures that are capable of generating optimum nonuniform fields for molecule manipulation. Washizu and Kurosawa s' work was the first experimental observation on electrostatic orientation of DEP of λ-phage DNA (λ-DNA) molecules under high intensity electric field produced in a microfabricated electrode system of two types: One parallel strip electrode with a spacing of 60 μm and the other right-

angle edge-to-strip electrode having a minimum spacing of 70 μm [33]. The fluorescence technique was adopted to visualize the orientation process. It was observed that the orientation of DNA molecules in the form of a number of thin filament-like agglomeration, parallel to the field took place under a field strength of $10^6$ V/m and the frequency around 1 MHz for parallel electrodes. They thoroughly investigated the frequency dependence of the orientation of the DNA molecules wherein they concluded that for the frequency range between 0.1 MHz and 1 MHz, the orientation took place parallel to the electrode.

This work by Washizu and Kurosawa paved the way to novel applications in genetic engineering. Methods were developed to immobilize stretched DNA onto a substrate, including

(a) Immobilization onto conducting substrate for observation with scanning tunneling microscope and

(b) Anchoring onto a substrate only at both ends of DNA using special electrode configuration.

To achieve site-specific immobilization of DNA molecules, Washizu, et al. fabricated an electrode configuration as shown in fig 2.8 which was less likely to induce flow of the medium than a simple parallel strip [27].

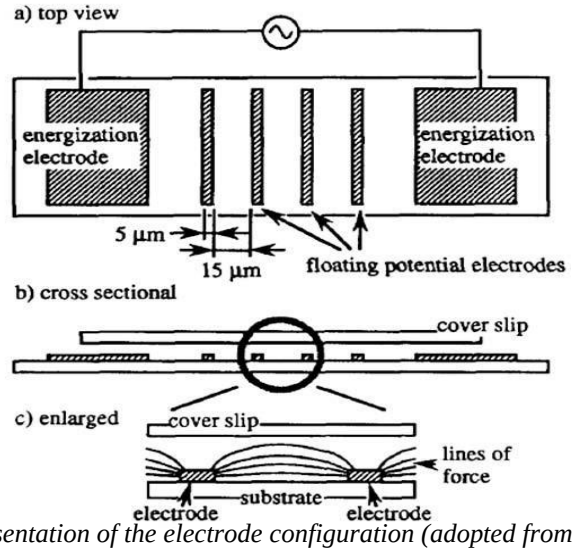


***Fig. 2.8:*** *Schematic representation of the electrode configuration (adopted from Washizu, et al.) [27].*

In a simple parallel strip electrode configuration, the flow pattern in the gap started from the electrode edges towards the center of the gap and went apart from the plane of the electrodes and circulated back. One end of the DNA molecule pulled into the region of the high electric field that might be fixed to an edge, but the other end of DNA molecule was prevented from approaching to the other electrode due to the flow. The electrode set up fabricated by Washizu, et al. consisted of two outermost electrodes and several strip electrodes between the gap [27]. The power supply was connected only to the outermost electrodes and the thin strip electrodes

have no electrical connections giving rise to 'floating potential electrode geometry'. This electrode configuration did not reduce the electric field induced flow at the edge of the energized outermost electrodes, but the flow at the edge of the floating electrodes was substantially suppressed. With this field geometry, DNA was found to get anchored at both ends, bridging over the two-adjacent floating potential electrodes [35].

Asbury and van den Engh s' work showed that the DNA molecules could be manipulated in an aqueous solution in a manner analogous to optical trapping [36]. Their experimental work exhibited that the DNA molecules were locally trapped in an oscillating field using strips of very thin gold film, fabricated using the standard photolithographic technique, to generate strong electric fields with a steep gradient. And they suggested that the spatial control over the trapped molecules was possible because they were confined to a width of about 5 μm along the edges of the gold-film strips [37]. Bakewell and Morgan reported that the measurements that are characterized the collection of DNA onto interdigitated microelectrodes employ high-frequency Dielectrophoresis. The standard photolithographic technique is used to fabricate electrodes from Gold with a Tiunder layer having 10 μm wide with a 10 μm gap. The use of Ti was to improve adhesion of gold on to the substrate [38].

Zheng, et al. used gold electrodes lithographically fabricated quadrupole geometries to manipulate DNA, protein, and nanoparticles for potential circuit assembly. The gap between the electrodes ranged between 3-100 μm and field strengths were typically $10^6$ V/m. They used λ-phage DNA for the experiment (48.5 kbp). Through fluorescence technique, they observed that DNA at chosen experimental condition underwent positive DEP for a range of frequencies between 10 kHz and 30 MHz. The images of the fluorescently labeled DNA are shown in fig 2.9. [39].

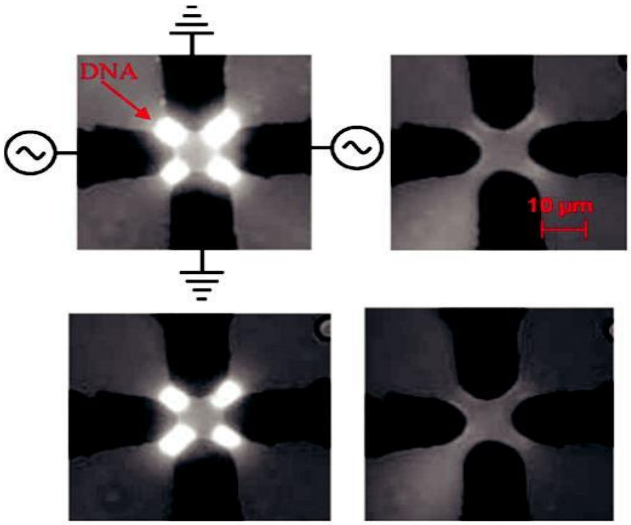


***Fig. 2.9:*** *Images of fluorescently labeled DNA take in on/off sequence*

The above four images were taken in on/off/on/off sequence in a time span of about 30 seconds (f= 1 MHz and applied voltage = 8 V) (Adopted from Zheng, et al.) [39].

Porath, et al work reported the electrical measurements through a single DNA molecule trapped and bridged between two with 10 nm triangular metal electrodes. These electrodes were fabricated using electron beam lithography (EBL). This work clearly exhibited that the electric field strength which was extremely large at the vertices of the triangular electrodes and it couples with polarization properties of DNA molecules, which is a crucial role to guide the flow of molecules in and around the tips. Moreover, this triangular shape of the electrode facilitated the ease of a single molecule being bridged between the electrodes [29]. And recently, Vahidi, et al. confirmed that the triangular metal electrodes were the most suitable form of electrode configuration which would result in attachment of DNA molecules at the electrodes with high aspect ratio. Fig. 2.10 shows SEM images of λ-DNA being bridged between two metal electrodes [40].

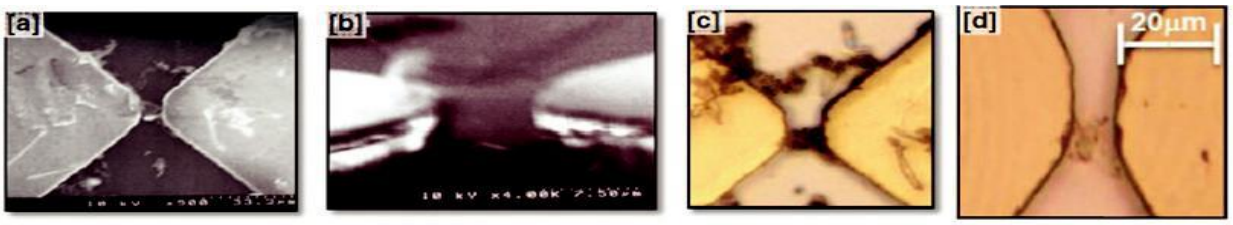


***Fig. 2.10:*** *SEM images of the λ-DNA (Adopted from Vahidi, et al. [40])*

Nevertheless, there is an interesting point to ponder. Though the modern lithography technique electron beam lithography (EBL) is successfully used to pattern nanometer gap electrodes, still there is an inherent limit of accuracy with the instrument. That is to say, bends and sharpness of the electrodes may not be as designed as standard development and lift-off processes. Now, with the sharp and blunt edges, non-uniformity of the electric field would vary, which in turn should affect the combined effect of ACEO and DEP. As a result, the positions, as well as the strengths of the trapping points in the electrolyte solution, facilitating stretched DNA molecules to bridge across the electrodes, would vary.

## References


1. B J Kirby, (2010), "Micro- and nanoscale fluid mechanics", Cambridge University Press.
2. D Burgreen, F R Nakache, "Electrokinetic Flow in Ultrafine Capillary Slits", J. Phys. Chem., 68 (5), 1084–109, (1964).
3. P K Wong, T H Wang, Joanne H. Deval, and Chin- Ming Ho, "Electrokinetics in Micro Devices for Biotechnology Applications", IEEE/ASME Transactions on Mechatronics, 9(2), (2004).
4. H. Morgan and N. G. Green (2003). AC Electrokinetics: Colloids and Nanoparticles. Research Studies Press Ltd., Williston, VT, USA.
5. R Pethig, Ying Huang, Xiao-bo Wang and J P H Burt, "Positive and negative dielectrophoretic collection of colloidal particles using interdigitated castellated microelectrodes", J. Phys. D, 25, 881-888, (1992).
6. H Morgan, M P Hughes, and N G Green, "Separation of submicron bioparticles by dielectrophoresis", Biophys. J, 77, 516-525, (1999).
7. R Pethig, "Review Article-Dielectrophoresis: Status theory, technology, and applications", Biomicrofluidics, 4(2), 022811, (2010).
8. A Ramos, H Morgan, N G Green, A. Castellanos, "AC- Electric field-induced fluid flow in microelectrodes", J. Colloid Interface Sci., 217, 420-422, (1999).
9. A Ajdari, "AC Pumping of liquids", Phys. Rev., E 61, 45-48, (2000).
10. J Voldman, "Electrical forces for microscale cell manipulation", Annu. Rev. Biomed. Eng., 8, 425-454, (2006).
11. J H Masliyah& S Bhattacharjee, "Electrokinetic and Colloid transport phenomena", (2006), John Wiley &sons.
12. J.N. Isarelachivili, "Intermolecular and surface forces", (2011), Elsevier Academic Press.
13. Ramos A, Morgan H, Green NG, & Castellanos A, "AC Electrokinetics: A review of forces in microelectrode structures", J. Phys. D, 31, 2338-2353, (1998).
14. Ramos A, Morgan H, Green NG, & Castellanos A, "AC electric field induced fluid flow in microelectrodes", J. Colloid and Int. Sci., 217, 420-422, (1999).
15. N.G. Green, A. Ramos, A. Gonzalez, H. Morgan, and A. Castellanos, "Fluid flow induced by non-uniform AC electric fields in electrolytes on microelectrodes: I. Experimental measurements", Phys. Rev. E, 61, 4011-4018, (2000).
16. A Ramos, H Morgan, N G Green, and A Castellanos, "ACEK: a review of force in microelectrode structures", J. Phys. D, 31(18), 2338-2353, (1998).
17. Sethi, A. Study of AC Electroosmosis Flow Pattern using different electrode geometries. BITS-Pilani Hyderabad, India, (2012). (Master's thesis).
18. Gonzalez A. Ramos A, Green N G, Castellanos A. & Morgan H, "Fluid flow induced by non-uniform ac electric field in electrolytes on microelectrodes: A linear double layer analysis", Phys Rev. E, 61, 4019-4028, (2000).

**19.** Lide, D. R. CRC, Handbook of Chemistry and Physics, (1997).

**20.** Sluyters-Rehbach, M., Electro-analytical chemistry, edited by Bard A. J. Dekker, New York, (1970).

**21.** Pohl H.A, "The Motion and Precipitation of Suspensoids in Divergent Electric Fields", J. Appl. Phys., 22, 869-871, (1951).

**22.** Anton Kuzyk, "Review- Dielectrophoresis at the nanoscale", Electrophoresis, 32, 2307-2313, (2011).

**23.** Clague, D.S & Wheeler E.K, "Dielectrophoretic manipulation of macromolecules: The electric field", Phys. Rev. E, Stat nonlinear soft matter Phys., 64, 026605, (2001).

**24.** Gunda, N. S. K, &Mitra, "Modeling of dielectrophoresis for myoglobin molecules in a microchannel with parallel electrodes", ASME Proceedings, IMECE, 10765, 13-19, (2009).

**25.** Washizu M, "Electrostatic manipulation of biological objects", J. Electrostat., 25, 109-123, (1990).

**26.** Washizu M, Kurusowa O, "Electrostatic Manipulation of DNA in microfabricated structures", IEEE Trans. On Industry Applications, 28, 1194-1202, (1990).

**27.** Washizu M, Kurusowa O, Arai Ichiro, Suzuki S, Shimamoto N, "Applications of electrostatic stretch-and-positioning of DNA", IEEE Trans. On Industry Applications, 31, 447-456, (1995).

**28.** Asbury C L, DiercksA H, Van den Engh G, "Trapping of DNA by dielectrophoresis", Electrophoresis, 23, 2658-2666, (2002).

**29.** Porath, D., Bezryadin, A., De Vries, S. and Dekker, C, "Direct Measurement of Electrical Transport through DNA Molecules", Nature, 403, 635-638, (2000).

**30.** Zheng, L.F., Brody, J.P. and Burke, P.J., "Electronic Manipulation of DNA, Proteins, and Nanoparticles for Potential Circuit Assembly", Biosensors and Bioelectronics, 20, 606-619, (, 2004).

**31.** Ghonge S, Prasad D N, Narayan S, Francis H, Sethi A, S Deb, Banerjee S, "Effect of curvature of tip and convexity of electrode on localization of particles", OJFD, 5, 295-301, (2015).

**32.** D N Prasad, S Ghonge, S Banerjee, "Investigation of localization of DNA molecules using triangular metal electrodes with varying separation", AIP conference proceedings, 1724, 020036, (2016).

**33.** Washizu M, Kurusowa O, "Electrostatic Manipulation of DNA in microfabricated structures", IEEE Trans. On Industry Applications, 6, 26, 1166-1172, (1990).

**34.** N. G. Green, A. Ramos, and H. Morgan, "AC electrokinetics: a survey of submicrometer particle dynamics", J. of Physics D, 33(6), 632, (2000).

**35.** S. Ghonge, S. Banerjee, Review Article "Dependence of shape and geometry of microelectrodes in manipulating polarizable particles like DNA through electrokinetic effects", Defence Science Journal, 66, 307-315, (2016).

**36.** Asbury C L, Van den Engh G, "Trapping of DNA in nonuniform oscillating electric fields", Biophysic J, 74(2), 1024-1030, (1998).

**37.** Asbury C L, DiercksA H, Van den Engh G, "Trapping of DNA by dielectrophoresis", Electrophoresis, 23, 2658-2666, (2002).

**38.** Bakewell, D,J. & Morgan, H. Dielectrophoresis of DNA, Time-and frequency-dependent collections on microelectrodes. IEEE Trans. Nanobiosci., 5, 1-8, (2006).

**39.** Zheng, L.; Brody, J.P. & Burke, P.J. Electronic manipulation of DNA, proteins, and nanoparticles for potential circuit assembly. Biosens. Bioelectron.,20(3), 606-619, (2004).

**40.** Vahidi, N.W.; Hirabayashi, M.; Mehta, B.; Rayatparvar, M.; Wibowo, D.; Ramesh, V.; Chi, J.; Calish, J.; Tabarés, M.; Khosla, A. &Mokili, J. Bionanoelectronics platform with DNA molecular wires attached to high aspect-ratio 3D metal microelectrodes. ECS J. Solid State Sci.Technol.,3, 29-36, (2014).

# Chapter-3
# Numerical Simulations

## 3.1 Introduction

The simulation part of AC Electrokinetics is of the key interest to this research study in terms of modeling microelectrode geometry and solving numerical equations. This chapter presents numerical simulations of AC electrokinetic phenomena such as ACEO and DEP using COMSOL Multiphysics software. The ACEO phenomenon studied analytically for the flow pattern of Electrical Double Layer (EDL) and obtained velocity profiles by solving Navier-Stoke (N-S) equation [1]. Later, the strength of the force i.e. $F_{DEP}$ which is experienced by the suspended particle is determined at different points called trapping points. And analytical solutions for AC electrokinetic phenomena are discussed with respect to the geometrical parameters such as the gap between electrodes and convexity of the electrodes that would facilitate effective DNA trapping mechanism [2, 3]. Numerical simulation analysis of model equations for various multiphysical problems can be carried out with the help of commercially available software like COMSOL that is designed to solve a wide range of partial differential equations (PDE) based on finite element method (FEM). This method works by dividing the problem space into a mesh of triangles in 2D and tetrahedral in 3D. COMSOL uses an adaptive refinement mesh to minimize the error in the solution [1]. In the context of multiphysical modeling, a system consisting of microelectrodes of two proposed geometries one is coplanar and other is triangular showed in the 1st chapter figure: 1 (a) & (c) enclosed in a glass chamber which is filled with an electrolyte solution (KCl). The first part of this study is to create the geometry of microelectrodes with its enclosed glass chamber, filled with KCl followed by the material selection that is chosen with their characteristic values such as permittivity and conductivity. Later part is to understand the behavior of the system by defining multiphysical equations like electrostatics, electric polarization and fluid dynamics which are available in COMSOL package. Once the geometry is ready with the appropriate material selection, we fix boundary conditions since the numerical study has to compute interface between electrode/electrolyte and electrolyte/glass followed by plugging in multiphysical equations.

In the whole study, EDL is the most crucial aspect where interfacial charges and ions play an important role to understand the AC electrokinetic effect where both the ACEO and DEP are studied analytically by computing multiphysical equations like electrostatics (Poisson's) and fluid dynamics (Navier-Stokes) [4]. EDL is referring to an interface which is in between solid

surface (polarized electrode) and an electrolyte solution. The numerical simulation of EDL is computed using linear approximation called Debye-Huckel approximation where the variation of potential is measured by considering linear *RC* equivalent circuit model which is shown in fig. 3.1. The bulk electrolyte can be considered to consist of a capacitor *C* and a resistor *R* in parallel. This is in series with the double layer impedance, represented here by resistor $R_{DL}$ and capacitor $C_{DL}$ [4].

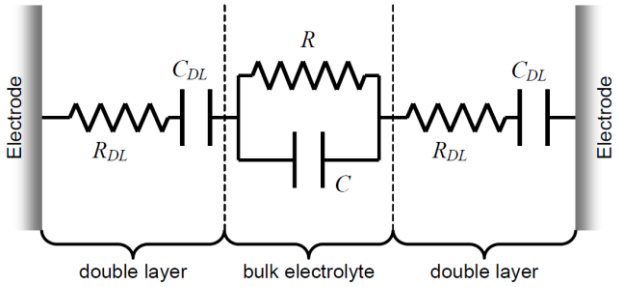


***Fig 3.1****: Schematic representation of linear RC circuit model of EDL (adapted from [3])*

The EDL was represented by a simple capacitor which is generally attributed to Helmholtz model. Later Gouy-Chapman and Stern developed models for potential distribution in EDL where the potential varies exponentially as a function of distance at solid-liquid interface and linearly in bulk region. Debye-Huckel approximation helped to determine the characteristic features of EDL by analytically solving Poisson-Boltzmann equation [1 & 5-7]. The computational work carried out by analyzing the simulation models using COMSOL Multiphysics software that has inbuilt modules electrostatics, microfluidics and etc.

**3.2 Short Introduction to COMSOL**

COMSOL Multiphysics is considered as an interactive environment for both the modeling and solving all kinds of scientific and engineering problems. It provides an integrated desktop environment with a model builder where one can get a full overview of the model and access to all functionality. Using COMSOL one can easily extend conventional models for one type of physics into Multiphysics models that solve coupled physics phenomena simultaneously. It has built-in physics interfaces and also has advanced support for material properties which would help to build models by defining the relevant physical quantities such as material properties, loads, constraints, sources, and fluxes rather than by defining the underlying equations. It is very easy to apply these variables, expressions, or numbers directly to solid and fluid domains, boundaries, edges, and points independently of the computational mesh. COMSOL can be run as a stand-alone platform or together with MATLAB. It can be run in two basic modes of operation, either through the graphical user

interface (GUI) or by running scripts. COMSOL Multiphysics has a flexible graphical user interface (GUI) [1] or by scripts (programming in Java or the MATLAB language). The physics interface allows performing various types of studies including, stationary and time-dependent (transient) studies, linear and nonlinear studies and Eigenfrequency, modal, and frequency response studies. COMSOL Multiphysics uses the proven finite element method (FEM) to solve the models. The software runs based on the finite element analysis together with adaptive meshing (if selected) and error control using a variety of numerical solvers. The major advantage with COMSOL Multiphysics, it creates sequences to record all the steps that create the geometry, mesh, studies and solver settings, visualization and results in the presentation. Partial differential equations (PDEs) form the basis for the laws of science and develop the foundation for modeling a wide range of scientific and engineering phenomena [1].

COMSOL Multiphysics software uses the Finite element analysis. This method works by dividing the problem space into a mesh of triangles in 2D and tetrahedral in 3D in its (COMSOL) default setting. Depending on the physical phenomena taken into consideration and geometry under study, the software allows for different mesh element types to be used. For example, one could also have quadrilateral meshing elements in addition to triangular meshing elements in 2D and elements like hexagons, pyramids, and prisms in addition to tetrahedrons in 3D. The aim of meshing a particular geometrical space (domain) is to solve and analyze the functional physical behavior of problem space that is being modeled. As the number of elements in meshing increased the solution of problem space can be approximated accurately but finer meshing takes more time to solve problem domain owing to more number of elements and it requires a lot of memory to compute. Hence the computational work for this research problem is analyzed by introducing a *plane of symmetry* that minimizes the computational time and memory as well. It reduces the computational complexity by half by simulating only for one electrode and taking the mirror image of a plane of ZERO potential.

**3.3 Simulation Details**

In this research work, a systematic analysis of the behavior of ACEO studied and then DEP studied under low ac bias for a wide range of frequency (1Hz-100 KHz) with different geometries of microelectrodes. Simulation study carried out for different conductivities and viscosities of the electrolyte solution. At first, the ACEO flow with coplanar parallel electrodes is numerically simulated and the results are compared with that observed experimentally by Green *et al* [8] for the same type of electrolyte and similar

geometry of electrodes to verify the present numerical method. Then the study has been extended to coplanar triangular electrodes as this geometry increases the intensity of electric field in the gap between the electrodes which may affect the flow pattern between the electrodes. Fluid velocities are calculated as a function of increasing frequencies exhibited flow reversal at high frequencies for all the geometries of the electrodes which are explained in the framework of a linear model [8-10]. Moreover, this study also presents how fluid velocities vary with frequency and electrode geometries as the viscosities and conductivities of the electrolytes are changed.

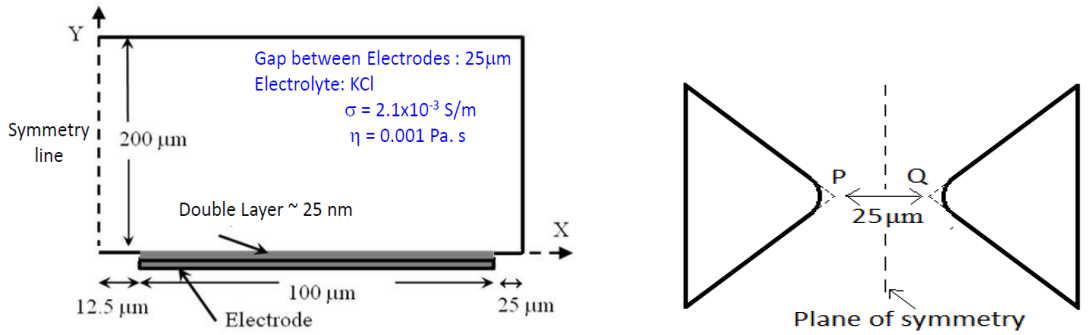


***Fig 3.2**: (a) Cross-sectional view of coplanar electrode (b) Top view of coplanar triangular electrodes (Adopted from Def. Science Journal [3])*

This study consists of two types of electrode geometries: coplanar parallel electrodes and coplanar triangular electrodes. The electrodes are placed in a closed glass chamber. Due to the symmetry of the system, only one electrode is shown and only the shown region is simulated. The schematic of the simulation region is shown in fig 3.2 (b). The plane Y=0 is the plane of symmetry. Fig 3.2 (a) represents the parallel electrode with a width of 100µm. The distance of the electrode from the plane of symmetry is 12.5µm. This geometry is similar to the one used by Green et al [8-10]. Fig 3.2 (b) shows the top view of triangular electrodes. The cross-sectional view is similar to that of parallel electrodes (Fig. 3.2 (a)). Instead of using triangular electrodes with pointed corners, which are hard to fabricate, we use the more realistic triangular electrodes with slightly rounded corners for our simulation. In fig 3.2 (b) the distance of points P and Q from the symmetry line is 12.5µm. Since the electrodes are not pointed, the minimum distance between the triangular electrode and the plane of symmetry is greater than 12.5 µm. We simulate for 2 different radii to fill the corners, 8 and 1µm and study the variation of fluid flow with the changes in the electric field that arise as a result of changing electrode geometry. The electrolyte (KCl) was taken to have conductivity $\sigma$=0.0021 and viscosity $\eta$=0.001. The amplitude of the applied sinusoidal voltage is 0.25V. The

boundary conditions play an important role in numerical simulation study since the problem of space has an interface of solid-liquid and it is represented in the following fig 3.3.

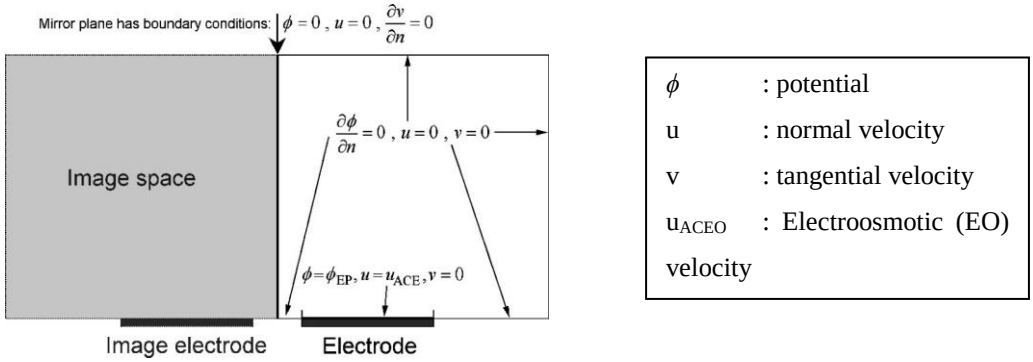


***Fig 3.3:*** *Schematic representation of boundary conditions (Adopted from [8]).*

### 3.4 Simulation procedure

The simulation study using COMSOL Multiphysics involved various steps to build a physical model;

**Physics**

Selecting the physical phenomena to be included

- Modules: AC/DC Electric currents and Microfluidics

**Geometry**

Designing geometries for

- Parallel electrodes and
- Triangular electrodes

**Material**

Selecting material parameters for the geometry under study

- Aluminium for electrodes
- Electrode system being enclosed in a glass chamber
- KCl (electrolyte solution)

**Boundary conditions**

Specifying physical parameters at the interface

- Potentials at the interface (electrode-electrolyte)
- Specifying *plane of symmetry* (mirror image plane)

**Meshing**

Discretizing the geometry for Finite element analysis

- Meshing the electrodes
- Meshing the KCl solution region

**Equations for study**

Initializing the different mathematical equations for simulating the physical phenomena of ACEO and DEP

- Stationary time average Navier-Strokes equation
- Time-Dependent Navier-Strokes equation

} For ACEO

- Dielectrophoretic force for polarizable particles

} For DEP

**Parameters**

Deciding parameters in ACEK phenomena;

For ACEO:

- Electroosmotic (EO) velocity Vs. frequency
- Varying solution conductivity (σ)
- Varying solution viscosity (η)

For DEP:

- Varying apex angle- θ (convexity)
- Varying fillet radii- r (vortex)
- Varying the spacing between electrodes (d)

**Result plots**

Analysis of physical phenomena through different plots obtained

- velocity Vs frequency for different conductivity
- velocity Vs frequency for different solution viscosity

} ACEO study

- Force Vs apex angle (convexity)
- Force Vs fillet radii (vortex)
- Force Vs separation between electrodes

} DEP study

**Structure of problem-solving**

The typical steps used when solving a problem using COMSOL are;

- Define the geometry or domain of the problem
- Define the partial differential equation and boundary conditions to be solved
- Meshing the region of space (domain)
- A solutionto the problem
- Post-processing of the results to generate various graphs

**Study approach**

- The frequency of the applied electric potential 1 Hz to 100 KHz

- Electric field computed using electric currents interface
- Fluid flow was computed using the creeping flow interface which makes use of the time-dependent Navier-Stokes equation
- The Debye layer is modelled as a capacitive boundary condition over the electrode surface
- The EO velocity is computed using the inbuilt equation (Helmholtz-Smoluchowski formula)
- Symmetry of the electrodes only the right half electrode geometry simulated
- The time-averaged velocity is computed at various distances along the electrode surface

**3.5 Numerical model for ACEO**

In this section, the equations that are governing ACEO phenomenon will be described. The most important region of interest to compute in ACEO study is numerically simulating EDL over the surface of the electrode in terms of solving potential distribution across the double layer using Laplace's equation followed by analyzing the capacitance of EDL considering it as linear RC circuit model using Debye-Huckel approximation and then obtaining velocity profiles using Helmholtz-Smoluchowski formula.

As described earlier in the 1st& 2nd chapters, the system consists of two long thin coplanar parallel electrodes over which the surface has a KCl solution and when AC voltage is applied to the system of electrodes, an electrical current is established in the solution. Owing to interfaces glass/electrolyte and metal/electrolyte double there will be the formation of EDL with a typical thickness determined by Debye length formula. We used 25 nm as its length in this simulation work.

$$\lambda_{DL} = \sqrt{\frac{\varepsilon K_B T}{2 N_A e^2 C}} \tag{1}$$

Where ε is permittivity (78.49), $K_B$ is Boltzmann constant, T is room temperature (298$^o$ K), $N_A$ is Avogadro number, e be the charge of an electron, C is a concentration of one ion at infinite dilution in the medium calculated using the following equation.

$$C = \frac{\sigma}{\lambda_\infty} \tag{2}$$

Where σ is the conductivity (0.0021 S/m) and $\lambda_\infty$ is Molar conductivity (149.79 S-m$^2$-mol$^{-1}$) of KCl at infinite dilution at room temperature. And solving the EDL of physical system

numerically is a major part of this problem. It is solved by considering EDL as a capacitive layer and bulk solution as a resistive layer, which results in the potential in bulk solution satisfies Laplace's equation,

$$\nabla^2 V = 0 \tag{3}$$

With the applied boundary condition (metal/electrolyte interface) for electrode surface which is outside EDL is given by

$$\sigma \frac{\partial V}{\partial y} = \frac{\partial q_{EDL}}{\partial t} \tag{4}$$

And the above equation also describes the charging of the EDL due to the bulk current. $\partial q_{EDL}$ is charge per unit area in EDL. Since EDL is considered to be the linear model the charge and voltage relationship can be taken as

$$q_{EDL} = C_{EDL}(V - V_{ref}) \tag{5}$$

The complex amplitude can be taken as follows and is applied as a boundary condition at the top of EDL [8]

$$\sigma \frac{\partial V}{\partial y} = i\omega q_{EDL} = i\omega C_{EDL}(V - V_{ref}) \quad \text{Or} \quad n.J = i\omega C_{DL}(V - V_{ref}) \tag{6}$$

Where $V_{ref}$ is the potential applied to electrodes $V_{ref} = V_0 \sin(\omega t)$ (7)

***n.J*** Picks out the normal component of current density and $C_{EDL}$ is EDL capacitive layer. And the capacitance per unit area in EDL can be estimated using Debye-Huckel theory by considering EDL as a linear resistance layer.

$$C_{EDL} = \frac{\varepsilon}{\lambda_{DL}} \tag{8}$$

Once the potential in EDL is solved, the electro-osmotic (EO) velocity outside the EDL at the surface of the electrodes can be calculated using Helmholtz-Smoluchowski formula and solve coupled time-dependent Navier-Stokes equation.

$$\vec{u} = \frac{-\varepsilon_0 \varepsilon_r \wedge \xi E_t}{\eta} \qquad \text{(Helmholtz-Smoluchowski formula)} \tag{9}$$

Where $\xi = V_{ref} - V$, and this is the potential difference between the outer and inner sides of the diffuse layer, $\wedge$ is the ratio of the potential drop across the diffusive layer and the potential drop across EDL. $E_t$ is the tangential component of the electric field just outside the EDL therefore the above equation gives only the tangential velocity on the electrodes, $\eta$ is the viscosity of the medium. And this velocity value can be used as a boundary condition at the electrode surface to calculate the bulk motion.

In order to obtain the velocity profile in the bulk solution, the Navier-Stokes equations must be solved. For microelectrodes, the Reynolds number is usually very small ($\approx 10^{-2}$), therefore neglect the inertial terms in the N-S equations. The coupled time-dependent Navier-Stokes (N-S) equation is solved for fluid flow by considering the fluid to be incompressible [4, 11].

$$\rho \frac{\partial \vec{u}}{\partial t} + \rho(\vec{u}.\vec{\nabla})\vec{u} = \vec{\nabla}.[-p\vec{I} + \eta(\vec{\nabla}u + \overrightarrow{(\nabla u)^T}] + \vec{F} \quad (10)$$

$$\rho\vec{\nabla}.\vec{u} = 0 \quad (11)$$

Where ρ is mass density of the fluid, taken to be mass density of water, 1000 kg/m$^3$, $p$ refers to pressure, $I$ represent Identity matrix. $F$ refers to the external force on the fluid, electrical force in this context that arises out of potential applied to the electrodes. The region of interest is the bulk region where the charge density is negligible, allows one to assume, $F = 0$ for simulation purposes. As Reynolds number for microelectrodes is less than ($\approx 10^{-2}$), the inertial term (second term on the left-hand side of the equation) is neglected in the eq. (10). The walls and electrodes are assumed impervious and therefore have no normal component of the fluid velocity at their surface. The following boundary conditions are applied to solve & obtain velocity profiles; (1) the tangential ACEO velocity on the electrodes (2) zero tangential velocity on the glass and (3) zero normal velocity on every boundary. As the ACEO flow is unidirectional with respect to the AC voltage and considered linear regime, for experimental purposes, time-averaged velocity is usually taken by averaging out the equations (9), (10) & (11), which then become,

$$\left.\begin{aligned} &\vec{\nabla}.[-p_{avg}\vec{I} + \eta\left(\vec{\nabla}u_{avg} + \left(\vec{\nabla}u_{avg}\right)^T\right] = 0 \\ &\rho\vec{\nabla}.\vec{u}_{avg} = 0 \end{aligned}\right\} \quad (12)$$

$\vec{u}_{avg} = \frac{\varepsilon_0\varepsilon_r}{2\eta} Re\left(\xi\vec{E}_t\right)^*$ Where * denotes the complex conjugate.

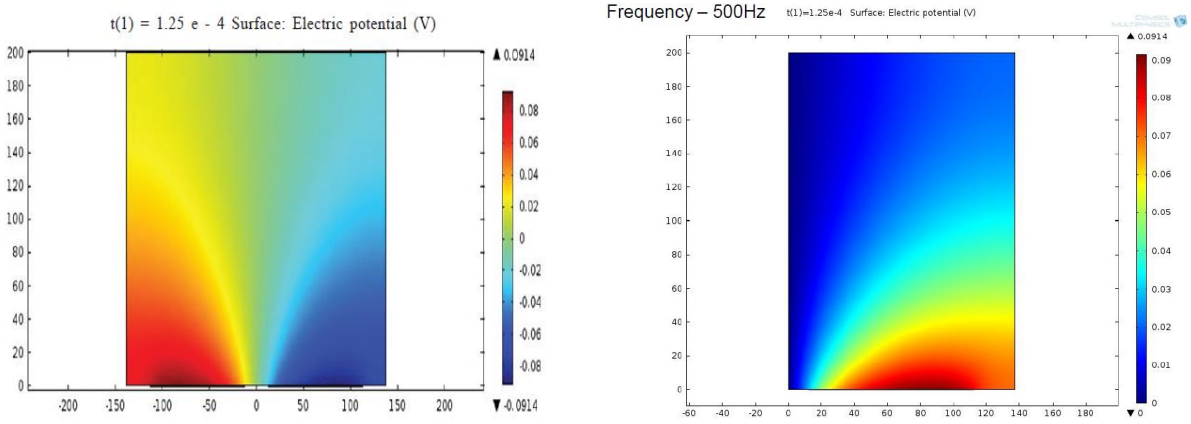


***Fig: 3.4*** *(a) Electric potential at 500 Hz* *(b) Potential simulated for half electrode region*

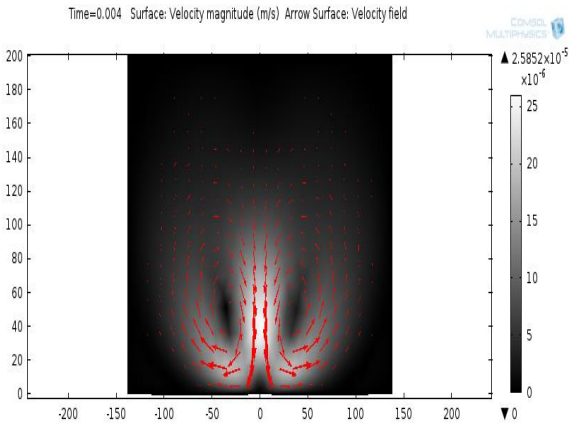


*(c) ACEO flow pattern at 500 Hz*

The velocity profiles are analyzed for different frequencies, conductivities and distance from symmetry line (mirror image PQ line) and discussed in the following section. The motion of the fluid is caused by electrical stresses that are nonzero only in the diffuse double layer owing to the charge density in the bulk region is zero. These stresses cause in the variation of the velocity profile in the diffuse layer, changing from zero at the wall to a finite value just outside the double layer. This finite velocity value can be used as a boundary condition at the electrode surface to calculate the bulk motion.

### 3.6 ACEO simulation results & discussion

In this section, we examined the simulated results for the two forms of N-S equation, stationary and time-dependent. And also, we examined the dependence of flow pattern on conductivity, viscosity and electrode shape.

#### *3.6.1 Coplanar Parallel Electrode Geometry (CPE)*

#### *Verification of simulation*

For an applied potential of peak 0.25 V, conductivity $\sigma$ = .0021S/m and viscosity $\eta$ = .001Pa S, solved the system for electric potential and time-averaged N-S equations (2nd chapter 2.3 section) and compared the results with Green's et al [8, 9]. We used the same equations for the purpose of comparison we take applied potential of 0.25 as taken by Green et al. [8]. Applied potential is written in form of exponential for calculation purposes, $V_{ref} = V_0 e^{i\omega t}$. Fig 3.5 shows the magnitude of electroosmotic velocity generated as a function of frequency. Fig 3.6 is taken from Green et al [8] work. Similarity between the two plots showed in Figures 3.5 and 3.6 verifies our simulation method.

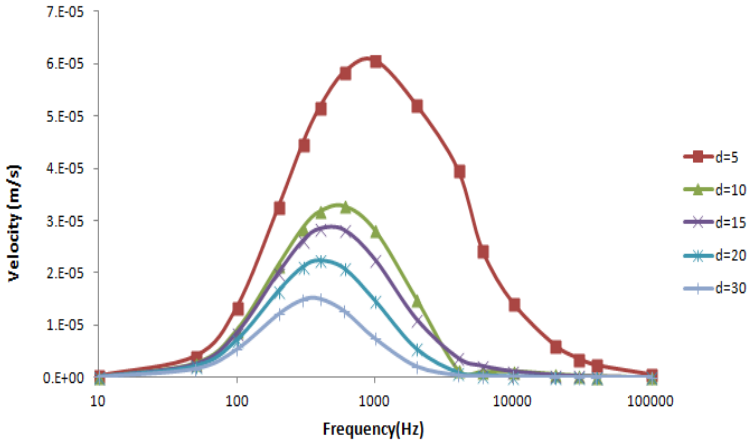


***Fig 3.5:*** *Plot of electroosmotic velocity profile for Parallel electrodes as a function of frequency at different distances across electrode surface after solving time-averaged NS equation*

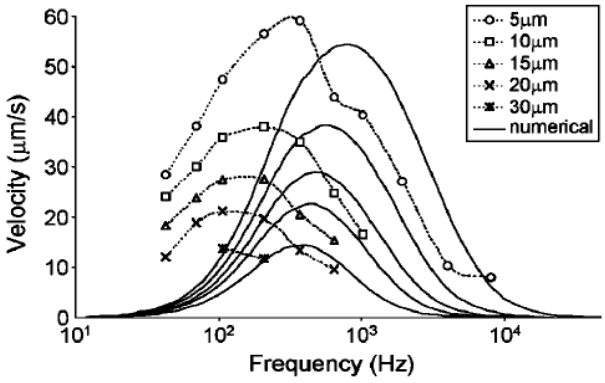


***Fig 3.6:*** *Reference plot for simulation verification (adapted from Green et al.)*

Nevertheless, with the variation in the values of the AC voltage within a time cycle, the value of velocity varies. Therefore, using time-averaged equation is only an approximation method. Having verified the credibility of the simulation method, we attempt to solve the system for time-dependent N-S equation rather than the stationary equation that gives different values of velocity at different time steps within a cycle. After having solved the time-dependent N-S equation ($2^{nd}$ chapter 2.3 section), we calculate the average value of velocity over 1-time cycle and plot that averaged value at different values of frequency. Fig 3.7 shows the plot of time-averaged velocity with varying frequency for an applied potential of .25 V, conductivity $\sigma$ =.0021 S/m and viscosity $\eta$ =.001 Pa S.

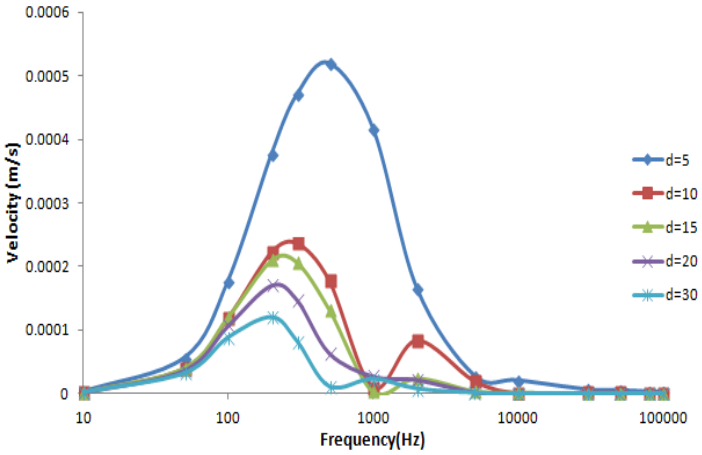


***Fig 3.7:*** *Variation of Electroosmotic Velocity with frequency at different distances across the electrode surface using the time-dependent N-S equation for parallel electrodes*

The shape of the curve remains similar to the fig 3.5 at low frequencies. However, there are two noticeable differences. First, there is a difference in the values of the velocity at all frequencies and second, at higher frequencies, the fluid undergoes flow reversal which was not observed while using the time-averaged equations (2nd chapter 2.3 section). We showed in figure 3.8-3.11 the snapshots of velocity pattern with increase in frequency. As the frequency increases, the flow pattern moves closer to electrode edge. Flow reversal is clearly visible at higher values of frequency.

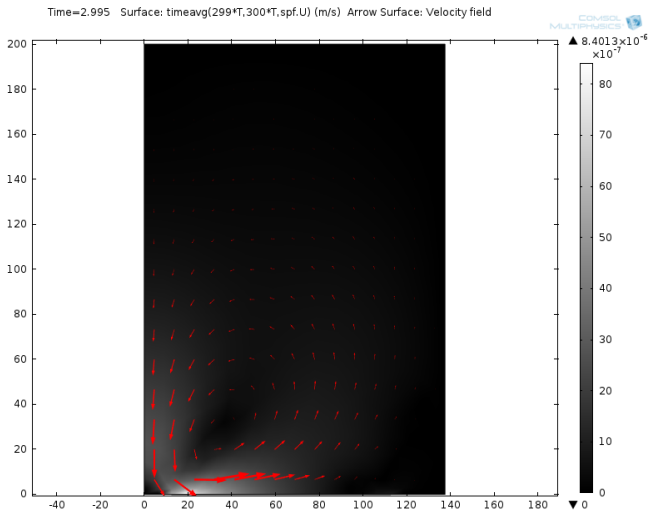


***Fig 3.8:*** *Electroosmotic Velocity flow pattern at 500Hz using parallel electrodes*

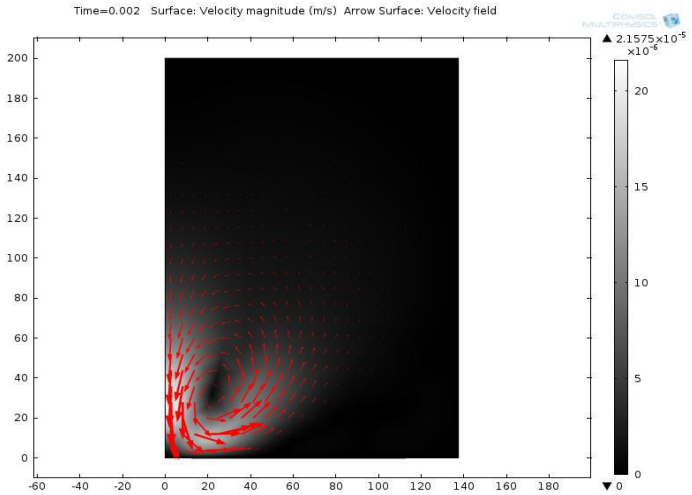


***Fig 3.9:*** *Electroosmotic Velocity flow pattern at 1000Hz using parallel electrodes*

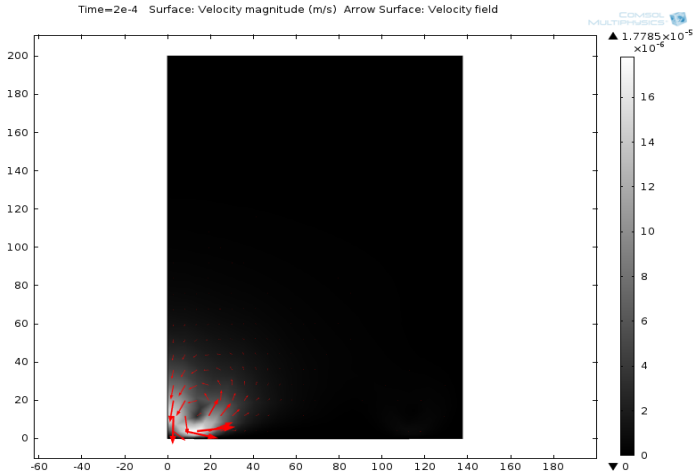


***Fig 3.10:*** *Electroosmotic Velocity flow pattern at 10000Hz using parallel electrodes*

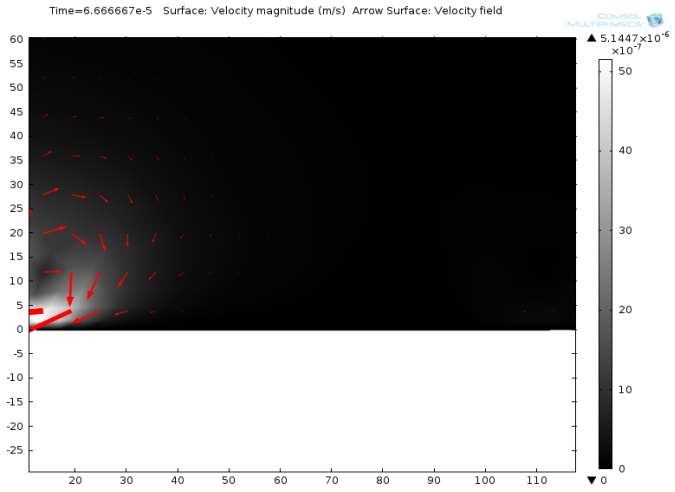


***Fig 3.11:*** *Electroosmotic Velocity flow pattern at 30000Hz using parallel electrodes*

We plot in fig 3.12 the comparison of values of magnitude of electroosmotic velocity simulated by using the two forms of N-S equation at coordinate (17.5, 0.557). The second

peak in magnitude of velocity after solving the time-dependent N-S equation is clearly visible in the figure. Applied potential 0.25 for both cases.

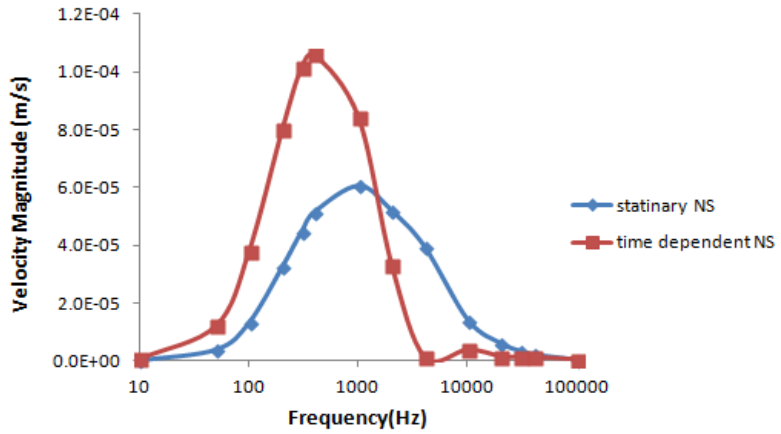


***Fig 3.12:*** *Comparison of magnitude of velocity values obtained from time-averaged N-S equation and the time-dependent N-S equation for parallel electrodes*

We next examine the dependence of ACEO dynamics on the conductivity of the electrolyte with viscosity fixed at $\eta$=.001Pa S. Fig 3.13 shows the velocity Vs frequency plot at three different values of conductivity, $\sigma 1$ = .000513, $\sigma 2$ =.0021 and $\sigma 3$ =.0086 S/m. The results of fig 3.13 are in qualitative agreement with the experimental results of Green et al. [9] according to which at a given point, with the increase in conductivity of the electrolyte, the peak frequency, i.e. the value of frequency at which the value of velocity is maximum hence increases. Thus, the plot shifts to the right at higher values of conductivity.

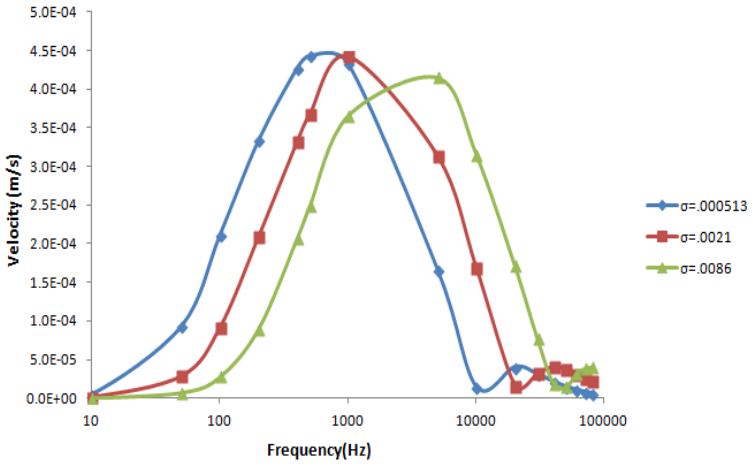


***Fig 3.13:*** *Magnitude of velocity as a function of frequency at point (13, 0) at 3 different values of conductivity, $\sigma 1$ = .000513, $\sigma 2$=.0021 and $\sigma 3$=.0086 S/m using parallel electrodes*

We next simulate the dependence of ACEO on the viscosity of the fluid for three different viscosity values, $\eta 1$=.00025, $\eta 2$=.001 and $\eta 3$=.004 Pa S. Plotting the time-averaged values of velocity over a time cycle at different frequencies at a conductivity $\sigma$ =.0021S/m, we obtain fig 3.14. From fig 3.14 as viscosity increases, the values of velocity at a particular frequency

decrease. This is expected as according to Helmholtz expression, ***u*** varies inversely as viscosity. This observation is also in agreement with the results of Green et al. [9]. Also, since all the values of velocity at a particular viscosity differ by the same factor from velocity at a different viscosity, the peak frequency remains unchanged.

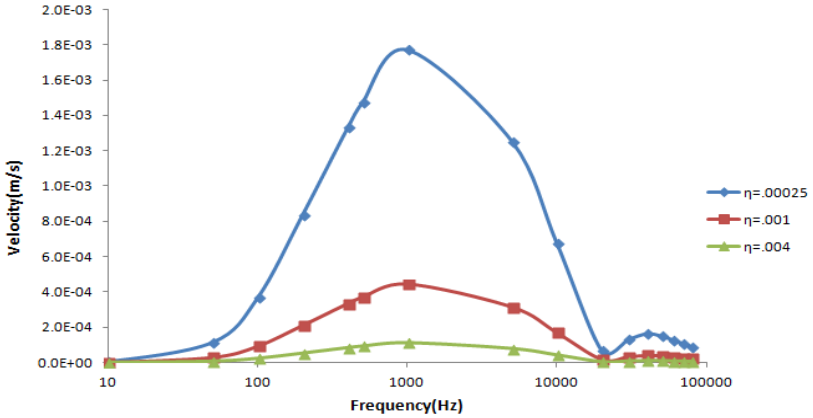


***Fig 3.14:*** *Magnitude of velocity as a function of frequency at point (13, 0) at 3 different values of viscosity, η1=.00025, η2=.001 and η3=.004 Pa S using parallel electrodes*

It is to be noted that from the above plots, there is another peak which is smaller by one order of magnitude was observed at higher frequencies. The second peak persists even with changing conductivity and viscosity.

### *3.6.2 Coplanar Triangular Electrode Geometry (CTE)*

We now extend our study of ACEO to triangular electrode geometry. We study two variants of triangular geometry, one with a fillet radius of 8 μm and other with fillet radius 1 μm. The peak voltage is fixed at 0.25 V and the conductivity and viscosity values at 0.0021S/m and 0.001 PaS respectively. Fig 3.15 and fig 3.16 show velocity pattern with respect to frequency for fillet radius r1=8 μm and 1 μm, respectively. The qualitative nature of the graph remains the same as for the case of the parallel electrode with the velocity being maximum at a particular frequency and lower on either side of that frequency.

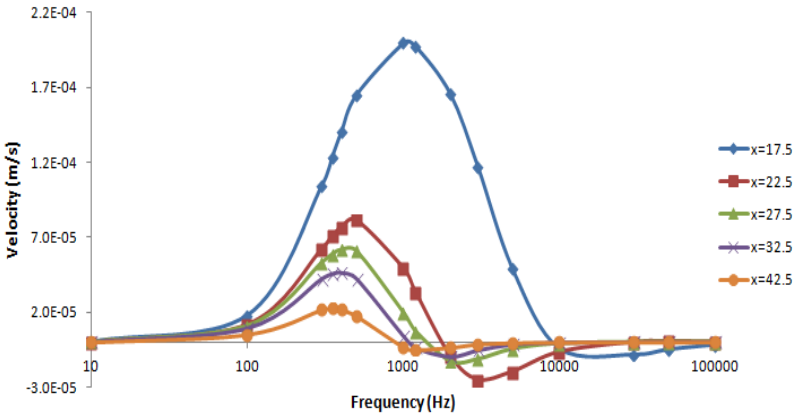

***Fig 3.15:*** *Electroosmotic velocity(x-component) as a function of frequency using triangular electrodes with fillet radius=8 μm*

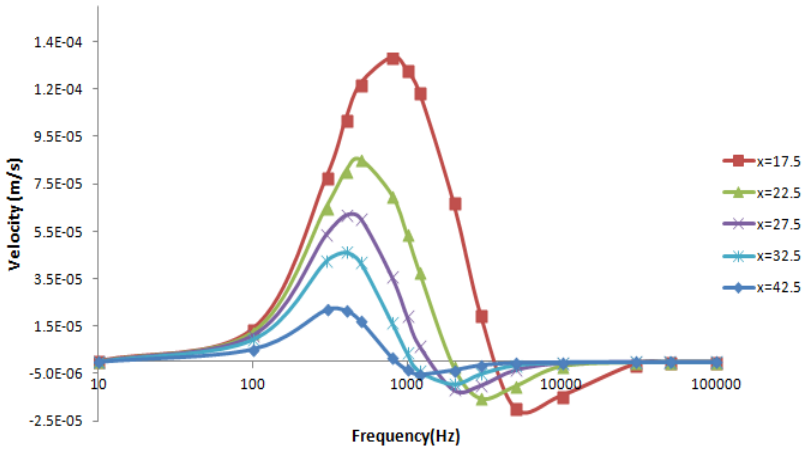


***Fig 3.16:*** *Electroosmotic velocity (x-component) as a function of frequency using triangular electrodes with fillet radius=1 μm*

In order to understand the dependence of flow pattern on fillet radius of triangular electrodes, we plot the velocity values as a function of frequency for the two cases of the radius in fig 3.17. For the purpose of comparison, we plot the values at approximately the same distance, 5 μm from the maximum curvature for both triangular shapes. Therefore, for the radius=1 μm, coordinate chosen for plotting figure corresponds to x~17.5 μm, y=0 and for radius=8 μm, coordinate is x~20 μm, y=0.

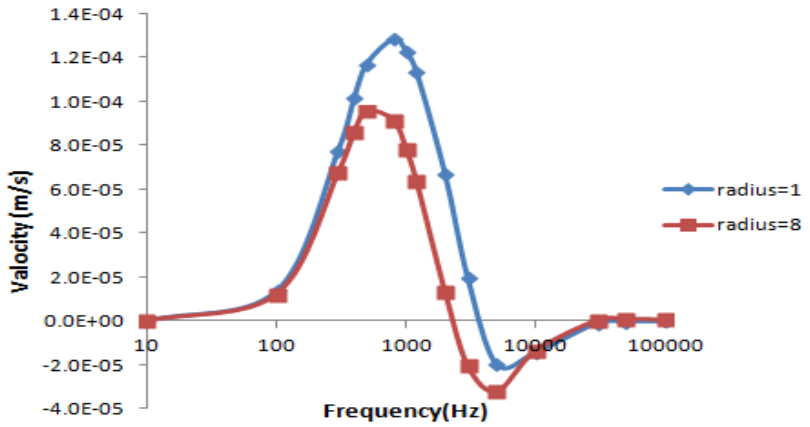


***Fig 3.17:*** *Electroosmotic velocity as a function of frequency using triangular electrodes with fillet radius= 8 μm and 1 μm*

In fig 3.17, the values of the x component of velocity are higher for radius=1 μm than for the radius=8 μm. As the fillet radius decreases, the intensity of electric field should increase. The plot in fig 3.17 is consistent with this expected theory.

**Conclusions**

A symmetric CPE geometry filled with an electrolyte was subjected to an alternating potential. The difference in using the N-S equation in two forms, solving the time-averaged N-S equation and solving a time-dependent N-S equation and then averaging the velocity values, has been successfully examined. While solving the time-dependent N-S equation, a reversed tangential flow of the electrolyte close to the surface between the two edges of the electrode at high frequencies (above 10 kHz) has been found. Although smaller by an order of magnitude, there is an appearance of the second peak in the velocity spectrum. Such a reversed flow confirms the onset of formation of a complex diffused layer. It also suggests that the dynamics of the fluid at higher frequencies of the applied potential become noticeably different. The dependence of ACEO has been successfully examined with varying parameters like conductivity and viscosity and electrode shape [12].

**3.7 Numerical model for DEP**

DEP facilitates trapping and manipulation of biological molecules subjected to nonuniform electric fields. DEP phenomenon is all about determining the exerting force i.e. dielectrophoretic force ($F_{DEP}$) on a polarizable particle like DNA molecules when they are suspended in an electrolytic solution. In order to understand DEP phenomenon, it is necessary to know the dielectric properties of both the particle & the suspending media (surrounding) and the geometry of device that is used to facilitate effective manipulation/trapping process. In this section, the governing equation of DEP and its numerical simulation approach will be described followed by the idea of proposing our geometry of microelectrodes. And the general introduction of DEP phenomenon is discussed in detail in chapter 2, section 2.4.1. DEP simulation carried out by calculating $F_{DEP}$ on a polarizable particle (assumed to be spherical) under nonuniform electric field (AC field applied in our study).

When a polarizable particle is aligned with the uniform electric field, the induced charge distribution experience the same magnitude of Coulombic force but it is in opposite directions. Therefore, the net electric force on the particles is zero. Whilst in the context of the nonuniform electric field, the net force is nonzero, which means induced dipole moment is established. This induced dipole moment causes the particle to move by exerting a force on the polarizable particle and this force can be referred to $F_{DEP}$. Depending on the magnitude of the particle polarizability with respect to the surrounding, a DEP process is named as 'positive DEP' or 'negative DEP' [13, 14].

The mathematical expression for $F_{DEP}$ on a polarizable particle is the following [4, 13].

$$F_{DEP} = 4\pi\varepsilon_0\varepsilon_m \,\mathrm{Re}(\{f_{CM}\})r^3(E.\nabla)E \quad (13)$$

Simulation work done using these values; particle is assumed to be spherical r = 2~4 μm, ω = 5000 Hz, $\varepsilon_m = 4/\varepsilon_0$, $\sigma_m$=2.4 S/m, $f_{CM}$=0.999~1.3345 X $10^{-7}$.

- $(E.\nabla)E$ is interpreted as the scalar (or dot) product of the vector E and the vector $\nabla E$ which means $F_{DEP}$ acts along the direction of $\nabla E$. $F_{DEP}$ is zero when the field is uniform i.e. $\nabla E = 0$. And the term $(E.\nabla)E$ is most important one since electrode geometry is also involved. This is the field factor to design electrode geometry and its magnitude can be increased by a suitable scaling down of the electrode dimensions. [ $(E.\nabla)E$ dimensions: $V^2/m^3$ ]
- $f_{CM}$ is Clausius-Mossotti (C-M) factor; the polarity of $F_{DEP}$ is determined by the particle's polarizability relative to its surrounding media. The $F_{DEP}$ of a particle would be different for different media owing to the dielectric properties. If $F_{DEP}$ is positive, particle polarizability is more polarizable than surrounding medium, the force is directed the particle along a path leading to a filed maximum (field can be maximum only at an electrode edge, never in free space) and it can be referred to positive DEP (pDEP). On the other hand, $F_{DEP}$ is negative, the particle is less polarizable than surrounding medium, the force is directed the particle away from an electrode towards a minimum field and it can be referred to negative DEP (nDEP). And the expression for $f_{CM}$ is given by

$$f_{\mathrm{CM}} = \left( \frac{\varepsilon_p^* - \varepsilon_m^*}{\varepsilon_p^* + 2\varepsilon_m^*} \right) \quad (14)$$

- Where r is the particle radius, the dependence of $r^3$ shows that the larger the particle volume the greater is the $F_{DEP}$ acting on it. And $\varepsilon_m^*$ & $\varepsilon_p^*$ are the complex permittivities of the medium and the particle respectively which are related to the conductivity σ and the angular frequency ω of the applied field through the following equation:

$$\varepsilon^* = \varepsilon - i\left(\frac{\sigma}{\omega}\right) \quad (15)$$

The eq.13 has also an alternative expression; time-averaged $F_{DEP}$ taking the AC field to be sinusoidal and of magnitude given by its root mean square (*rms*) value.

$$\langle F_{DEP} \rangle = 2\pi\varepsilon_0\varepsilon_m \,\mathrm{Re}(\{f_{CM}\})r^3\nabla E_{rms}^2 \quad (16)$$

$\{\because 2(E.\nabla)E = \nabla E^2$ From sec 2.4.1 eq.15$\}$

- $(E.\nabla)E$ the field factor term, shown to relate to the square of applied voltage. Therefore, DEP is independent of the polarity of the applied field direction. In Eq.16, $F_{DEP}$ depends on the square of applied field magnitude, indicating that DEP can be observed under both DC & AC. Reversing the polarity of the applied voltage to an electrode does not reverse the direction of $F_{DEP}$. An AC current is one in which the flow of charge periodically reverses direction, whilst in DC flow consistently in one direction.
- The particle r does not depend on the field frequency and even the suspending medium permittivity. The only term that can change with frequency is $f_{CM}$.

From the literature [15] that has been addressed in earlier chapters, it is important to realize that, the idea of designing geometry of microelectrodes which would establish high electric field strengths to achieve firm trapping/manipulation of polarizable particles like DNA. And it is strongly believed that the sharp edge or pointed tip electrodes would facilitate effective manipulation/trapping. But, in practice, despite having successfully used electron beam lithography (EBL) patterned electrodes to nanometer gap, fabricating such sharp edges/point tip electrodes are limited by the inherent precision of the instrument. This means the sharpness and bends of electrodes may not be as designed after lift-off process. This difference from designing to practicality would vary the nonuniformity of electric field which in turn should affect the electrokinetic effect. That result in the positions, as well as the strengths of the trapping points in the electrolyte solution, facilitating stretched DNA molecules to bridge across the electrodes, would vary.

Through our simulation study, we have shown how those minute bends of the electrodes and sharpness of the edges could affect the sites of the trapping points as well as its strength [2, 16]. The proposed electrode geometry is shown in the following fig 3.18.

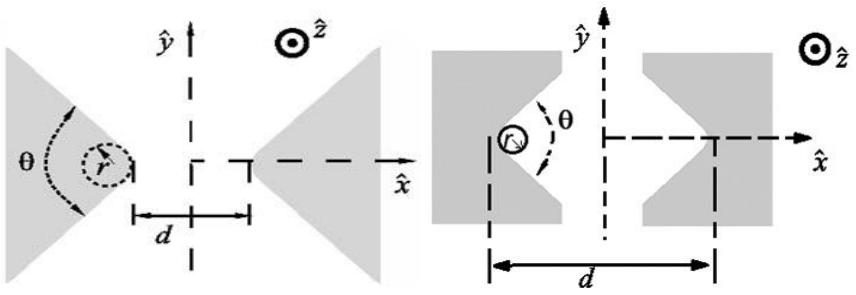


***Fig 3.18:****(a) Convex geometry (b) Concave geometry*
*(Schematic representation of the top view of the electrodes geometry (adopted from OJFD [2]))*

COMSOL Multiphysics is used to simulate to systematically study the behavior of the system by varying three parameters:

(i) The apex angle θ which governs the notion of convexity,

(ii) The fillet radius *r* which governs the notion of sharpness of the rounded tip and

(iii) The electrode separation *d*.

An increase in θ while keeping the other two parameters constant would cause a decrease in convexity. Similarly, an increase in *r* causes a decrease in sharpness. Numerical studies were done using mirror image symmetry as mentioned in the text before, by varying each parameter while keeping the other two fixed to explore the possibility of obtaining trapping points and to analyze the strength of these trapping points as a function of these parameters. Decreasing the apex angle leads to increasing an electric field density near the tip. The presence of a tip causes a sudden rise and fall in the value of the electric field – this causes the formation of trapping points as is observed in the plot of the *x* component of the net force plotted against the *x* coordinate. And more simulation study results are discussed in detail in chapter 5 results and discussion.

### 3.7.1 DEP simulation procedure

Following points are outline of DEP simulation work;

1. Simulated the electrode-electrolyte interface with a time-varying electric field. The aim of the exercise is to seek "*trapping points*" for a polarizable particle.
2. In our case, simulated the Physics generated by two Physical Phenomena: ACEO and DEP.
3. Since we wanted to focus on nonuniform electric fields, we modeled our electrodes to be triangular (convex and concave).
4. Our simulation incorporates the idea of the method of images and reduces the computational complexity by half by simulating only for one electrode and taking the mirror image of a plane of ZERO potential.
5. The methodology for determining a trapping point is as follows;
   a. Simulate the physics for the DEP and determine the Electric Field at every point in the volume.
   b. Simulate ACEO and determine the velocity field of the fluid flow at every point in the volume.
   c. Use the above two fields (Electric field for $F_{DEP}$ and Velocity Field for $F_{ACEO}$) and other quantities such as polarizability of the particle to determine the Force at each point.

**d.** Note that nowhere in the simulation, have we actually inserted a particle in the system. We are assuming the particle is very insignificant in size to drastically influence the bulk system flow.

**e.** Seek a region where the Force is "stabilizing" i.e. if particle happens to venture into this region, it would get stabilized there.

**f.** This is done by looking for regions in the Force v/s coordinate graphs which exhibit like Harmonic Oscillator like force behaviour i.e. F = kx.

**g.** The point where the Force is zero and its vicinity stabilizing is a trapping point.

**6.** We have done the simulations by varying different parameters of the electrodes;

**a.** Fillet Radius of the tips of the electrodes facing each other. (Let's call this as vertex V)

**b.** The sharpness of the angle at vertex V

**c.** The distance between the tips of the electrodes

**7.** Our results indicate the following

**a.** Trapping point stability increases for decreasing fillet radius

**b.** Trapping point stability increases with increasing sharpness of the electrodes

**c.** Trapping point stability increases for decreasing distance b/w the tips of the electrodes

### 3.7.2 DEP simulation results & discussion

DEP results obtained by using mirror image symmetry as mentioned in the 2nd chapter, by varying each parameter while keeping the other two fixed to explore the possibility of obtaining trapping points and to analyze the strength of these trapping points as a function of these parameters. The electrode geometry used is as shown in figure 3.19.

Three important parameters in this study are the following.

(i) The apex angle θ which governs the electrode edge,

(ii) The fillet radius *r* which governs the notion of sharpness of the rounded tip and

(iii) The electrode separation *d*.

We have carried out the simulations keeping separation d fixed by varying r & θ and also the behavior of the trapping points as a function of electrode separation, having a fixed convexity and properly scaled sharpness of tips are presented.

***(A) Case-I (keeping d fixed and varying r & θ)***

It is observed that decreasing the apex angle leads to increasing an electric field density near the tip. The presence of a tip causes a sudden rise and fall in the value of the electric field,

this causes the formation of trapping points as is observed in the plot of the *x* component of the net force plotted against the *x* coordinate. Fig 3.19 shows a typical variation.

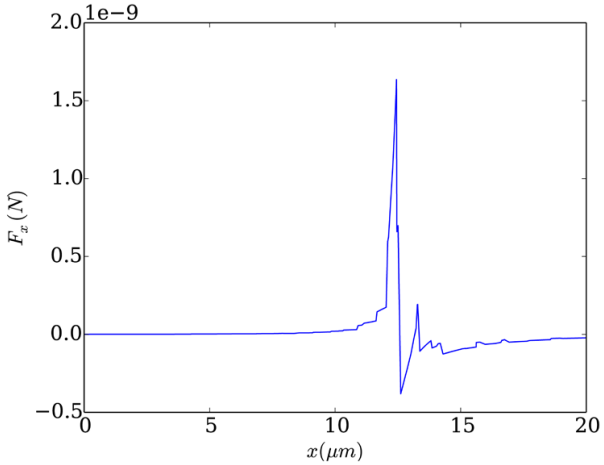


***Fig 3.19:*** *Variation of the x-component of the force on a stretched DNA molecule along the x-axis. The specific parameters used are d = 25 μm, r = 0.5 μm, θ =102°*

We used a particle size of $R$ = 4 μm to study the feasibility of polarized and stretched DNA molecules forming a bridge across electrodes. The forces on the stretched DNA molecule are the DEP force (calculated from the computed electric fields) and the drag force (calculated from Stoke's law). Fig 3.19 shows the variation of the *x*-component of the force on a stretched DNA molecule along *x*-axis for an electrode system having typical parameters $d$ = 25 μm, $r$ = 0.5 μm, and θ= 102°. It is important to point out that at any point in time the electrodes under the application of an alternating voltage have opposite polarities. The symmetry of the electrode configuration and the simultaneous antisymmetric of the electric potential exists for all ranges of parameters $r$, $d$, and θ. The range of parameters examined to show the same nature of the x-component of the force. Here we present only a typical plot of the force for $d$ = 25 μm, $r$ = 0.5 μm, θ = 102°. Therefore, fig 3.19 is representative of any electrode configuration defined by the parameters $d$, $r$, and θ. It is worth noting from the plot that the force has a positive and a negative value on either side of a point where the force vanishes. Such a force can represent only a vortex. The suspended particles in the electrolyte upon entering the vortex get trapped in it due to the torque set up by the vortex. The results show that the vortex is located near the edge of the electrode and therefore the insoluble particles in the vortex will have a higher probability of bridging the gap between the electrodes. This also requires that the torque on the trapped particles should not be too great to prohibit it from exiting the vortex.

### *Variation of Apex Angle (θ)*

A variation of $\theta$ for a fixed $r$ and electrode separation leads to increasing electric field density with decreasing $\theta$. Quickly varying electric field densities indicate the existence of strong vortices with a short span along the $x$-axis, as envisaged from fig 3.19 as well. We test it for four different angles keeping $r$ = 0.5 μm and $d$ = 25 μm. Fig 3.19 shows the variation of the slope (stiffness) of the $x$ component of the force as a function of $\theta$ for the convex (dashed curve) and the concave (solid curve) electrodes where the magnitude of the slope is taken as a measure of the stiffness. The plot clearly shows a systematic increase in the stiffness of the force with increasing $\theta$ for the set of concave electrodes. We have plotted the slope of the x-component of the force for the two cases namely, convex and concave electrodes. It is worthwhile to mention that angle in the plot is the acute angle between the edges of the electrode. Hence, the angle measured for the concave electrode, if measured on the same side of the electrode edge as for the convex electrode, would be are flex angle, and therefore, the two plots in fig 3.20 are consistent with each other. Smaller slope (stiffness) at larger $\theta$ indicates that electrodes with less convexity are likely to generate vortex sites of weaker trapping capacity. This prompts us to further investigate the scenario with electrodes having moderate convexity but with varying apex radius as it would address a more practical issue. It is well accepted that lithographically fabricated micro/nanoelectrodes would yield rounded tips of different curvature due to the resolution limit of the respective lithographic tool used [17, 18].

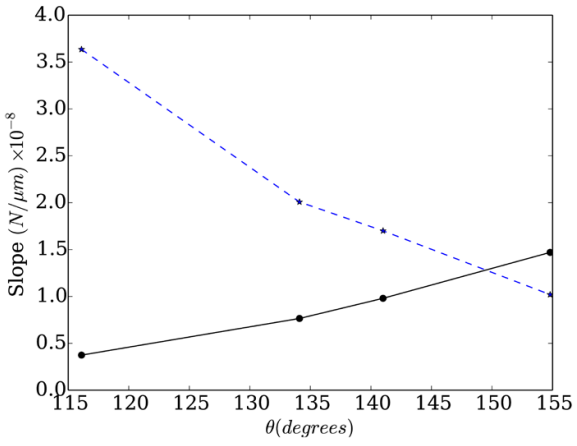


***Fig 3.20:*** *Variation of the slope of the x-component of the force as a function of the apex angle θ for the concave (solid curve) and convex (dashed curve) electrodes*

### *Variation of Apex Radius(r)*

A variation of the fillet radius $r$ changes the electric field density around the tip of the electrodes. A sharper electrode tip produces a stronger electric field and strengthens the DEP force. Thus, the net force across the vortex is expected to change faster for sharper electrodes.

We test this by plotting the variation of *x*-component of the force $F_x$ as a function of the fillet radius *r* at the center of the vortex keeping electrode separation $d$ = 25 μm and apex angle $\theta$ = 102°. Fig 3.21 shows the variation of the slope of the *x*-component of the force as a function of *r* for the convex (*dashed curve*) and the concave (*solid curve*) electrodes. Specifically, the slope was calculated by taking a linear approximation of the curve between the two points where the force reaches its extremal values. $F_x$ varied at a rate of 0.48×10−10 N μm for flat electrodes ($r \to \infty$). The decrease of the stiffness of the force with the fillet radius occurs for all angles checked in the range of 116.1° to 154.8°. The plot (fig 3.21 (a)) suggests that electrodes with smaller *r* (*i.e.* having sharper tip) would produce stronger vortices within the electrolyte. Keeping in mind non-ideal fabrication issues, the strength and the span of the vortex are of interest to us. We calculate the field strength by taking the average of the magnitude of the extremal values of $F_x$ and the span is calculated by finding the spacing between the locations where $F_x$ takes the extremal values. Fig 3.21 (b) and (c) represent the variation of the strength of the field and span respectively as a function of fillet radius. From the plots, it is clear that the strength decreases and the span increases as the electrode tips become more and more blunt.

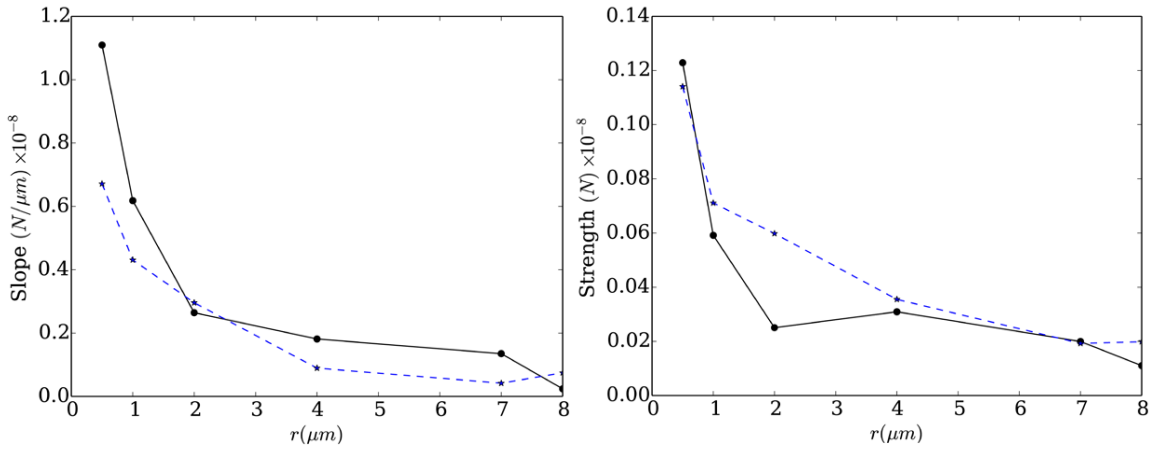


(a) (b)

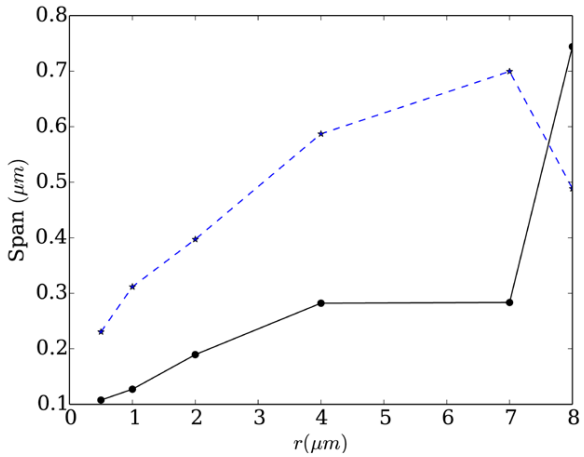


(c)

***Fig 3.21:*** *Variation of the (a) slope, (b) strength and (c) span of the x -component of the force as a function of the fillet radius r for the concave (solid curve) and convex (dashed curve) electrodes*

## Conclusions

We have systematically analyzed two of the three parameters (*the fillet radius and the apex angle)* that may be tuned to have a localizing region for suspended DNA molecules in electrolytes. It is found that stiffness of the force decreases with the increase of the apex angle, indicating weaker trapping sites in the electrolyte as the convexity of the electrode increases. In this context, we tried to address a practical situation where electrodes of fixed and moderate convexity but having different curvature of the tips were considered. Our study reveals that the strength of the vortex gets weaker and its span becomes wider as the tip gets more and more rounded. It also provides an intuitive insight that, if polarization of DNA molecules has any role to facilitate the DNA attachment process, it is desirable to have vortex of moderate strength and span around the edge of the electrode such that the molecules are localized (rather than being strongly trapped) in the vortex facilitating polarization to complete the bridging process. Therefore, it is suggested that a set of electrodes with fixed convexity but having rounded tips may better serve the purpose of bridging electrodes by DNA molecules [2, 16].

***(B) Case-II (Varying d and keeping r & θ unchanged)***

Here we present a systematic analysis of the nature of the trapping points as the separation between the tip of the electrode is reduced from several micrometers to a few nanometers, keeping electrode convexity and properly fixed sharpness unchanged. We studied the feasibility of polarized and stretched DNA molecules forming a bridge across the electrodes. The forces on the molecule are the DEP force and drag force are calculated from the

equations which are discussed in simulations chapter. Fig 3.22 (a) and (b) show a variation of the *x*-component of the net force as a function of *x* for the convex and concave electrode cases respectively. The typical values of $\theta$, *r*, and *d* used are 102°, 0.05 $\mu m$, and 1.25 $\mu m$ respectively. A similar variation exists in the *y*-direction. The plot shows a sharp peak followed by a sudden drop which extends to the other side of the *x*-axis. This maxima-minima pair is modeled linearly corresponds to a stable equilibrium point. It is important to note that fig 3.22 (a) and (b) are representative for all values of *d* at a defined convexity indicating the possibility of producing vortex states or in other words, trapping points for both convex and concave electrode geometries.

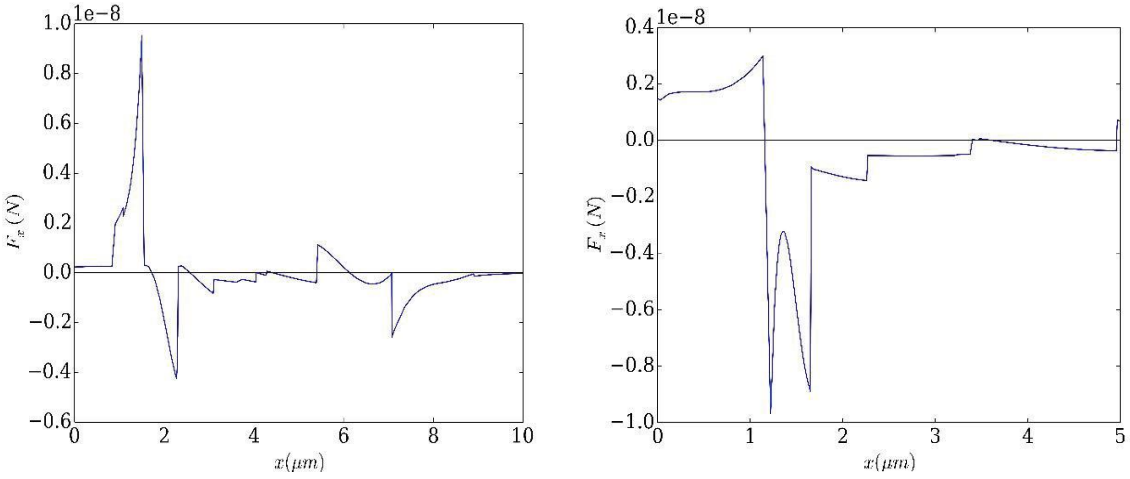


(a) (b)

***Fig 3.22:*** *Variation of the x-component of the force on a stretched DNA molecule along the x-axis for the caseof (a) convex and (b) concave electrodes when separated by 1.25 μm*

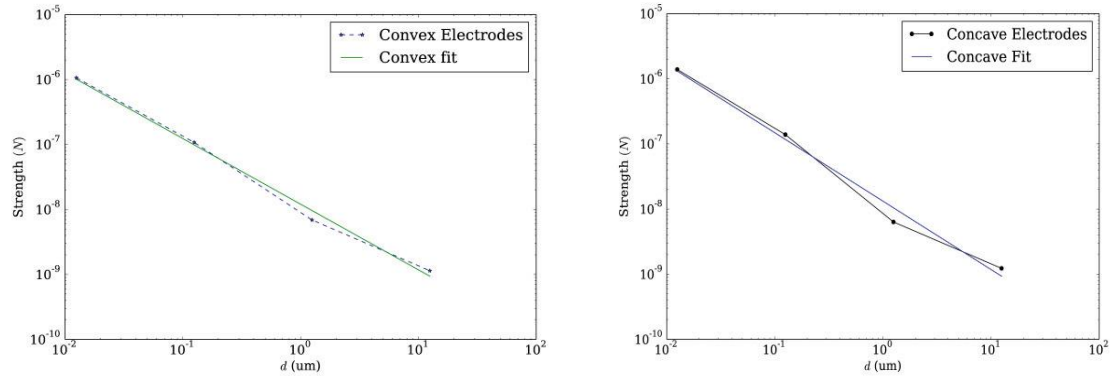


(a) (b)

***Fig 3.23:*** *Variation of the strength of the x-component of the force on a DNA molecule as a function of the separation between the electrodes, d for the (a) convex and (b) concave electrodes. The dotted line shows the simulated points and the continuous line is the fitted line following equation.*

The above plots represent the strength of the *x*-component of the force on a DNA molecule as a function of the parameter *d* for the convex electrode (a) and concave electrode (b),

respectively. The convexity of the electrodes is maintained at a value of θ equal to 102° and its sharpness is kept constant by scaling down the size of the entire system for a decrease in *d*. The *strength*, *S* of the force is calculated by taking the average of the magnitude of the extremal values of $F_x$. From the above two plots, it is clear that the magnitude of force increases with a decrease in distance *d* between the electrodes. We have also calculated the localization points in the plane of the electrodes where the net force is vanishing for different convexity of electrodes. It is found that the localization points become more stable with the decrease of the radius of the vertex tip. Further, we have tried to fit the simulated points in the *Strength* versus *d* plot which suggests an inverse power law relationship with the value of the slopes of the linear fit of the log-log graphs being -1.00 and -1.05 respectively, for convex and concave electrodes. It could be put forward as an equation given by [16],

$$S\alpha\frac{1}{d}$$

**Conclusions**

We have investigated presence the localization/trapping points of DNA molecules suspended in a solution between two metal electrodes (having convex and concave geometries) under electrokinetic effects. The electrode separation is varied from micrometer down to nano-meters which encompasses practical situations. The trapping points are realized within the electrodes and their strength is found to obey an inverse power law with the electrode separation [2, 16].

## References


1. COMSOL Multiphysics Manual
2. Ghonge S, Prasad D N, Narayan S, Francis H, Sethi A, S Deb, Banerjee S, "Effect of curvature of tip and convexity of electrode on localization of particles", OJFD, 5, 295-301, (2015).
3. S. Ghonge, S. Banerjee, Review Article "Dependence of shape and geometry of microelectrodes in manipulating polarizable particles like DNA through Electrokinetic effects", Defence Science Journal, 66, 307-315, (2016).
4. H. Morgan and N. G. Green (2003). AC Electrokinetics: Colloids and Nanoparticles. Research Studies Press Ltd., Williston, VT, USA.
5. Overbeek , JTG 1952, in colloidal science Vol.1, edited by H.R Kruyt (Elsevier, Amsterdam),
6. K. H. Bhatt, S. Grego, and O. D. Velev, "An AC Electrokinetic technique for collection and concentration of particles and cells on patterned electrodes," Langmuir 21(14), 6603–6612, (2005).
7. Hunter R.J, 1981, zeta potential in colloidal science: principles and applications (academic press, London)
8. N. G. Green, A. Ramos, A. Gonzlez, H. Morgan, and A. Castellanos, "Fluid flow induced by nonuniform ac electric fields in electrolytes on microelectrodes. III. Observation of streamlines and numerical simulation", Phys. Rev. E Vol 66, p. 026305, (2002).
9. N.G. Green, A. Ramos, A. Gonzalez, H. Morgan, and A. Castellanos, "Fluid flow induced by nonuniform AC electric fields in electrolytes on microelectrodes: I. Experimental measurements", Phys. Rev. E, 61, 4011-4018, (2000).
10. Gonzalez A. Ramos A, Green N G, Castellanos A. & Morgan H, "Fluid flow induced by non-uniform ac electric field in electrolytes on microelectrodes: A linear double layer analysis", Phys Rev. E, 61, 4019-4028, (2000).
11. B J Kirby, (2010), "Micro- and nanoscale fluid mechanics", Cambridge University Press.
12. A Sethi, P Parikh, S Benedict, S Deb and S Banerjee, "Multi-peaked velocity spectrum of a AC-electric-field-induced electrolytic flow with microelectrodes", Applied Mechanics and Materials, 229, 957-960, (2012)
13. Ronald Pethig, Dielectrophoresis: Theory, Methodology and Biological Applications, John Wiley & Sons, (2017)
14. Pohl, Herbert Ackland. Dielectrophoresis: the behaviour of neutral matter in nonuniform electric fields. Cambridge university press, Cambridge, (1978).
15. F. Dewarrat, M. Calame,and C. Schonenberger. "Orientation and positioning of DNA molecules with an electric field technique", Single Molecules, 3, 189-193, (2002).

**16.** D N Prasad, S Ghonge, S Banerjee, "Investigation of localization of DNA molecules using triangular metal electrodes with varying separation", AIP conference proceedings, 1724, 020036, (2016).

**17.** Porath D, Bezryadin A, De Vries S and Dekker C, "Direct Measurement of Electrical Transport through DNA Molecules", Nature, 403, 635-638, (2000).

**18.** Vahidi, N.W.; Hirabayashi, M.; Mehta, B.; Rayatparvar, M.; Wibowo, D.; Ramesh, V.; Chi, J.; Calish, J.; Tabarés, M.; Khosla, A. &Mokili, J. Bionanoelectronics platform with DNA molecular wires attached to high aspect-ratio 3D metal microelectrodes. ECS J. Solid State Sci.Technol.,3, 29-36, (2014).

# Chapter- 4
# Microelectrodes: Fabrication, Characterization & Electrical Contacts

## 4.1 Introduction

The aim of this chapter is the idea of proposing microelectrodes design and fabrication that would facilitate effective trapping/manipulation of DNA molecules under balanced electrokinetic phenomena (ACEO & DEP). From H. A. Pohl's research work on DEP, he proposed that metal wires and thin sheet electrodes employed nonuniform fields [1, 2]. It has been realized that the field control term in $F_{DEP}(E.\nabla)E$ expression has units of $V^2$-$m^{-3}$ and this provide the clue that, by miniaturizing the electrodes, they are being able to use much smaller applied voltages hence able to establish high electric field strengths and also thermal effects could be avoided [3]. It has been addressed some of the proposed electrode geometries like interdigitated, castellated and quadrupole to achieve effective DEP in the earlier chapters [4]. A significant development has been introduced in terms of new material and new methods for fabricating microelectrode DEP devices. The DEP technology development has always been driven by both curiosity and consistent search for potential applications.

Efforts towards achieving electrical contact to nanostructures have been active for over a decade. Electron beam lithography, with its incredible accuracy and patterning precision, is at the forefront of nanotechnology and nano-gap fabrication. Nano-gaps hold promise for a variety of reasons [5]. Nano-gaps could also be used for better DNA detection and research in molecular electronics. Since the manipulation or trapping of polarizable particles like DNA molecules depends strongly on the strength of the applied electric field, it is expected that the sharpness or bends of the electrode edges would influence the overall electro-kinetic process. In this regard, it appears that one might further exploit state-of-art lithographic technique to fabricate smaller electrodes with sharper bends which would intensify the non-uniformity of the electric field and significantly influence DNA manipulation. Electrical measurements through a single DNA molecule trapped and bridged between two EBL fabricated electrodes were reported by Porath *et al*. [6]. The work clearly exhibited that the electric field strength which was extremely large at the vertices of the triangular electrodes, coupled with polarization properties of DNA molecules, played a crucial role to guide the flow of molecules in and around the tips. Moreover, the triangular shape of the electrode facilitated the chance of a single molecule being bridged between the electrodes. Recently, Vahidi*et al.* confirmed that triangular metal electrodes were the most

suitable form of electrode configuration which would result in attachment of DNA molecules at the electrodes with high aspect ratio [7].

However, there is an interesting point to ponder. Though electron beam lithography is successfully used to pattern nanometer gap electrodes, there is an inherent limit of accuracy with the instrument. That is to say, bends and sharpness of the electrodes may not be as designed after standard development and lift-off processes. Now, with sharp and blunt edges, non-uniformity of the electric field would vary, which in turn should affect the combined effect of ACEO and DEP [4, 8]. As a result, the positions, as well as the strengths of the trapping points in the electrolyte solution, facilitating stretched DNA molecules to bridge across the electrodes, would vary. Recently we studied in detail, through simulations how those minute bends of the electrodes and sharpness of the edges could affect the sites of the trapping points as well as its strength [8, 9]. In this chapter, we present fabrication process of nanogaps between electrodes directly with electron beam lithography (EBL) and external connections for the fabricated device using wire bonding machine. The fabrication and characterization of electrode devices work could carry out with the help assisted by CeNSE department IISc, Bengaluru and CEN department IIT-Bombay, Mumbai.

In this chapter, we report a method for fabricating nanogaps directly with electron beam lithography (EBL). The primary resolution-limit of EBL, electron back-scattering is reduced by using a lower accelerating voltage and slightly thick resist bilayers [10, 11]. To fabricate we used a recipe in which doped silicon (Si+) wafers with highly polished, 1000 nm-thick silicon dioxide layers are grown. We performed the EBL on this with a field emission JOEL 6400 and Raith 150 Two scanning electron microscope (SEM) operating an accelerating voltage of 15 kV. The electron beam (smallest attainable aperture ~ 7.5 μm) was controlled with a Raith writing program. A single layer of PMMA (4% 950 K PMMA layer) was spin-cast on the silicon dioxide. Nanogaps were written using a 60 μm aperture electron beam in the EBL chamber with pressure below $10^{-6}$ Torr. The resist was exposed at a magnification of 500X, corresponding to a write field of (400 μm), to beam doses ranging from 90 to 100 $\mu C/cm^2$, depending on the desired size and geometry of the nanogap. The device was then developed in MIBK: IPA (3:1 volume ratio) for the desired time and loaded into the low-pressure environment of a thermal evaporator. For metallization, several nanometres of chromium (5 to 10 nm) were evaporated first to act as an adhesion layer between the gold and the substrate, followed by 40 nm of gold. After metallization lift was done to get the smaller dimension electrodes. For lift we put the sample into acetone for 30 minutes then after sonication, we got the smaller dimension electrodes. Larger features were then written into

the resist with the help of DSA for the purpose of connecting the nanogaps to large contact pads. The device was then developed in the developer (3:1 volume ratio) for the desired time and loaded into the low-pressure environment of a thermal evaporator again. For metallization, several nanometres of chromium (5 to 10 nm) were evaporated first to act as an adhesion layer between the gold and the substrate, followed by 40 nm of gold. The wafers were put into acetone at room temperature in order to achieve lift-off. The gaps were then imaged with SEM attachment of Raith 150 Two.

**4.2 Electron Beam Lithography (EBL)**

EBL is a fundamental technique of nanofabrication, allowing not only the direct writing of structures down to sub-10 nm dimensions but also enabling high volume nanoscale patterning technologies such as (DUV and EUV) optical lithography and nanoimprint lithography through the formation of masks and templates. With its ability to form arbitrary two-dimensional patterns down to the nanometre scale, EBL is one of the most important techniques in nanofabrication. In short, it involves the exposure by a highly focused electron beam to modify the solubility of a resist material during a subsequent development step. The key objectives of EBL writing are to achieve arbitrary patterns in the resist with high resolution, high density, high sensitivity and high reliability [12]. These characteristics are interrelated in a complex fashion. The key determinants will be the quality of the electron optics (e.g., the ability to create a finely focused spot), the choice of resist, substrate, and developer, and the process conditions: electron beam energy and dose, and development time and temperature. Factors that complicate these objectives are delocalization of electrons due to forward and backscattering (proximity effects), the collapse of the pattern due to swelling and capillarity forces, and fluctuations in the sizes of features (line edge roughness). EBL consists of shooting a narrow, concentrated beam of electrons onto a resist-coated substrate. Electrons can induce the deposition of substances onto a surface (additive) or etch away at the surface (subtractive).

EBL is particularly important in microelectronics, which require extremely precise placement of micro-sized circuit elements. EBL allows scientists to design and place elements at the smallest possible scale. Also, electrons can be used to etch a “mask” whose patterns can be later transferred onto a substance using other techniques. However, with such precision, components can only be made very slowly and only one at a time, greatly increasing the time and cost and prohibiting mass commercial acceptance. Also, because electrons are charged particles, it is necessary to perform EBL inside a vacuum, further complicating the required equipment and process. There are different scanning methods in

which e-beam lays the desired pattern, we used raster scan method to achieve our proposed design. The e-beam is swept across the entire surface, pixel by pixel, with the beam being turned on and off according to the desired pattern. This method is easy to design and calibrate, however, because the beam is scanned across the entire surface, sparse patterns take the same amount of time to write as dense patterns, making this method inefficient for certain types of patterns as shown in figure 4.1.

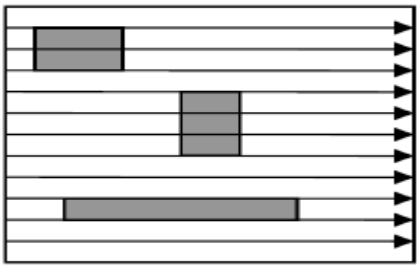

***Fig 4.1:*** *Schematic representation of raster scan*

### 4.3 Process flow for microelectrodes

This work is involved fabrication of nanometre gap electrodes. Firstly, we attempt the fabrication of 500 nm gap electrode and then the gap is reduced to 100 nm. The device is as shown below. The device is fabricated in this manner to enable the trapping of the DNA molecule efficiently between the gap. The first configuration as shown in figure 4.2 (a) is fabricated for the uniform electric field to see how the field enables the trapping of the molecule. In the second configuration as shown in figure 4.2 (b), the field is nonuniform, the reason for fabricating this device is the requirement of the nonuniform field which gives rise to DEP enabling the DNA trapping process and also since the aim is to trap a single or a few DNA molecules with the pointed configuration.

***Fig. 4.2:*** *(a) Uniform field configuration* *(b) nonuniform field configuration*

- Start with oxidized Si wafer
- Deposit $SiO_2$ layer of thickness at least 1μm to avoid pinhole leakage. The value of this thickness is only customary. Any value is fine as long as there is no pinhole.
- Spin coat EB resist (positive - PMMA Polymethyl Methacrylate)
- Use EB direct writing to make the pattern on top of the resist.

  The pattern is made in two steps:

- ✓ In step 1, 500µm X 500µm square; large beam current. This will be used for metal pads.

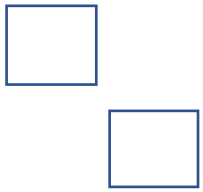

***Fig. 4.3:*** *(a) larger pads*

- ✓ In step 2, use the smallest beam diameter available with the EB system (small beam current) to write smaller square on the larger squares one as shown.

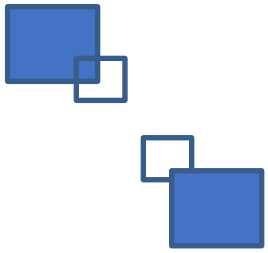

***Fig. 4.3:*** *(b) both smaller & larger*

- Take the sample out of EB system and then develop. As positive resist is used after development, resist remains only in the region where there is no pattern. Figure 4.4 below shows the pattern.

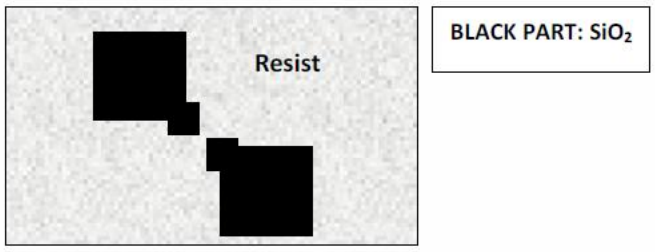


***Fig. 4.4:*** *with photoresist*

- Evaporate metal. First, a thin layer of Ti/Cr (5-10 nm) and then Au (25-35 nm) is deposited. Cr or Ti will improve adhesion quality. After one set with Au, we repeat the process with Al.
- Final Step: Liftoff to achieve the pattern.

### 4.4 Experimental Procedure

- A silicon wafer (either p or n-type) is taken and the oxide is grown to a thickness of around 1μm. The method used for oxidation is Wet oxidation and the oxidation process is carried out for 3 Hr 14 min at a temperature of 1100$^{o}$C.
- Resist spinning: For electrodes which have a gap of 500 nm the resist thickness is 500 nm and for the electrodes, with 100 nm gap, the resist thickness is 100 nm. The resist used is PMMA (Polymethylmethacrylate) which is a positive resist and has good adhesion properties. The resist is spun at a given speed to obtain the thickness of 500 nm and 100 nm in a spinner.
- The wafer with the resist coated is then made to undergo E-beam exposure to writing the desired pattern. Since very pointed features are desired the pads of different sizes are written at different currents. The bigger pads are written at a current of around 250 pA at 30 kV and the smaller pads are written at around 50 pA at 30 kV. The exposure process is optimized by varying the different parameters. The wafer is then developed in 1:3 MIBK/IPA developer for around 40 secs to 1 min depending on the development rate.
- After development, the wafer is coated with metal (Aluminium or Gold) using 4 target E-beam evaporation at a current of giving a deposition rate of 0.4 $A^0$ for 40-45 seconds for Titanium giving a thickness of 5 nm and 0.5 $A^0$ for 5 minutes for Aluminium giving a thickness of 25 nm.
- After metallization, the sample then undergoes a process of lift-off by immersing the sample in Acetone for about 30 min and sonicating for 2 sec to 5 sec if necessary.

Different configurations were processed in order to come up with the pattern that gives the best EBL writing efficiency giving the best gap and most suitable for lift-off process. The two configurations are shown in figure 4.5.

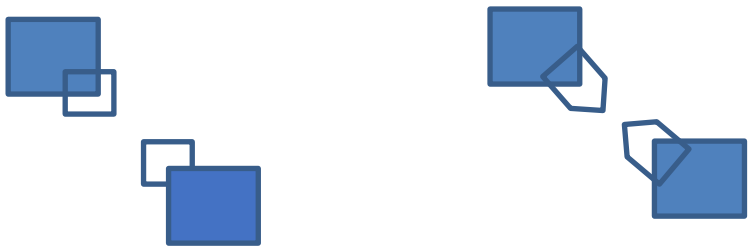

***Fig. 4.5:*** *nonuniform field configurations*

The resist materials used and the spin speed and thickness used for initial runs were:

a) 8% 950K PMMA in Anisole at a spin speed of 4000 rpm to get a thickness of 600 nm.

b) 4% 950K PMMA in Anisole at a spin speed of 1000 rpm to get a thickness of 500 nm.

c) 4% 950K PMMA in Anisole at a spin speed of 2000 rpm to get a thickness of 500 nm.

The exposure parameters tried on JEOL 6400 SEM/EBL for initial runs were:

Big pads:

a) Dose = 90 μC/m$^2$, Current = 250 pA, Step size = 30 nm
b) Dose = 90 μC/m$^2$, Current = 250 pA, Step size = 20 nm
c) Dose = 180 μC/m$^2$, Current = 250 pA, Step size = 20 nm

Small pads:

a) Dose = 90 μC/m$^2$, Current = 50 pA, Step size = 30 nm
b) Dose = 90 μC/m$^2$, Current = 30 pA, Step size = 30 nm
c) Dose = 90 μC/m$^2$, Current = 30 pA, Step size = 20 nm

**4.5 EBL Writing process**

*Process followed for fabrication of 500 nm gap electrodes*

- PMMA 950 K in Anisole was used as the resist. Different percentages of PMMA was used and spun at different spin speed to get thickness around 500nm. The thickness was measured using ellipsometer.
  - ✓ 950 K 8% PMMA @ 4000 rpm thickness obtained 550 nm
  - ✓ 950 K 4% PMMA @ 1000 rpm thickness obtained was 534 nm
  - ✓ 950 K 4% PMMA @ 1600 rpm thickness obtained was 300 nm
  - ✓ Bilayer resist of 495 K 4% PMMA @ 4000 rpm thickness obtained 300 nm and 950 K 4% PMMA @ 2000 rpm thickness obtained 200 nm. A post bake of 1 min 30 sec was done after each spin.
- Resist used was 950 K 4% PMMA @ 1000 rpm to get 500 nm thickness. The smaller structures of different configuration and sizes were written as the optimization of these smaller structures was most important.
- The developer used was 1:3 MIBK/IPA for the required duration and a rinse in IPA for 15-20 sec to reduce scumming terminating the development process.
- The configurations used were:

  Square pads: 10 μm X 10 μm
  15 μm X 15 μm
  20 μm X 20 μm

  Fingertip pattern: Triangle base: 7.14 μm, height: 7.14 μm, square: 7.14 μm X 7.14 μm

Triangle base: 7.14 μm, height: 7.14 μm, square: 14.28 μm X 14.28 μm (triangle at the center)

Triangle base: 14.28 μm, height: 14.28 μm, square: 14.28 μm X 14.28 μm

The trials for optimization were done on JEOL 6400 EBL. The final EBL was done on Raith 150 two. The current and dose for the smaller patterns were optimized as 30 pA and area dose of 90 $\mu C/m^2$ at 30 kV. Both the 500 nm thick and 300 nm thick resist were used. After metallization during lift off it was found that the 500 nm thick resist was better as it would provide a better undercut. The current and dose for the bigger patterns were optimized as 250 pA and area dose of 180 $\mu C/m^2$ at 30 kV. While writing the bigger patterns it was necessary to keep the step size as 20 nm for a current of 250 pA otherwise the writing would happen in strips.

When both the patterns were combined it was found that the smaller pads did not develop well the reason might be the high aspect ratio and low density of the structures. In order to get sharp features which are well aligned the writing was done on Raith 150 two keeping the field size of 200 μm and magnification of 500X. The smaller patterns were written at a current aperture of 7.5 μm to get a current of 24 pA at accelerating voltage of 20 kV and a dose of 80 $\mu C/m^2$. The bigger pads were written at a current aperture of 30 μm to get a current of 281pA and dose of 160 $\mu C/m^2$. The dose of both patterns was kept lower as the writing happened at accelerating voltage of 20 kV(dose reduces with a reduction in accelerating voltage). The dose of the bigger patterns was kept large to ensure that they would develop first when compared to the smaller patterns. However, the edges of the smaller patterns did not develop well giving a gap of 2.7 μm.

After metallization and lift off, it was observed that the smaller patterns were not there, the reason might be low undercut provided by the resist due to which the smaller patterns were also lifted off. In order to overcome this bilayer resist was used with different development rate. However, the development rate difference was kept low to prevent the resist in the gap from developing. The total resists thickness was 500 nm which consisted of 300 nm of 495K 4% PMMA and 200 nm of 950 K 4% PMMA. The thickness of 495 K 4% PMMA was kept large to prevent excessive development as the development rate is higher than 950 K 4% PMMA and this might develop resist in the gap if developed longer. The next step was to optimize the dose. A dose matrix was run for a dose of 110 $\mu C/m^2$ for the larger patterns and doses of 100 $\mu C/m^2$ and 120 $\mu C/m^2$ for the smaller patterns. The development time was 2 min 5 sec giving a gap of 501 nm. Followed by a post-development bake at 900 C

for 1 min to harden the resist thereby enabling better lift off i.e. smoothening the edges. The post-development time is kept low in order to prevent the resist from hardening much which might pose a problem during lift-off as the hardened resist may not be removed with acetone. The parallel configuration with a gap of 500 nm was then taken up for optimization. This consisted of 500 μm X 500 μm larger patterns and 10 μm X 10 μm smaller patterns.

First, the configuration consisted of only two larger patterns 500 μm X 500 μm separated by a gap of 500 nm. Since current was already optimized for the patterns the same was used. It was found that the patterns merge due to large aperture of the current and also as the dose went higher the patterns merged. Hence in order to overcome this, the configuration was modified to consist of 500 μm X 500 μm larger patterns and 10 μm X 10 μm smaller patterns. The current used was still the same. However, the dose required for development differs, so a dose matrix was run between 60 $\mu C/m^2$ and 120 $\mu C/m^2$ and the optimum dose was found as 95 $\mu C/m^2$ for both the structures. However, the dose of the larger patterns was increased so that they develop faster compared to the smaller patterns. The optimum dose was found as 100 $\mu C/m^2$ for the larger patterns and 95 $\mu C/m^2$ for the smaller patterns with a development time of 55 sec.

The next step was to optimize the 100 nm gap configuration. The resist used was a bilayer resist consisting of 495 K 4% PMMA spun at 6000 rpm in 3 steps, the time for each step being 20 sec spread cycle at 800 rpm followed by 1 min spinning at 6000 rpm and then a ramp down for 15 sec. This was followed by a bake at 1800$^{o}$C for 1 min 30 sec. Then 950 K 2% PMMA was spun at 3000 rpm in 3 steps, 8 sec spread cycle followed by spinning at 3000 rpm for 45 secs and then ramp down for 5 secs followed by a bake at 1800$^{o}$C for 1 min 30 sec. The dose of the two patterns was then optimized by running a dose matrix. The optimum dose was found as 100 $\mu C/m^2$ for the smaller patterns and 90 $\mu C/m^2$ for the larger patterns with a development time of 2 min 10 sec.

In all the cases the smaller patterns were written first as the precision was very important for the smaller patterns hence focusing was done initially using a current aperture required for the smaller patterns and then without changing the focusing the larger patterns were written at larger aperture since the focusing change would not create a measurable error as they are very large. SEM imaging of the samples was done. It was found that due to back scattering (due to higher accelerating voltage) the gap was reduced to 60 nm for the 100 nm configuration, 344 nm for the 500 nm parallel configuration and 410 nm for the 500 nm configuration. Hence the next steps involve reduce the back scattering and thereby keeping at gap as desired. The length of the 500 nm parallel configuration was 500 μm due to which the

amount of back scattering it receives is higher when compared to the 500nm diagonal configuration. The length was then reduced to 50 μm. However, the back scattering is also affected by the accelerating voltage and the resist thickness. The accelerating voltage was then reduced to 10 kV. Dose matrix was again run for the three configurations and the optimum dose was found as follows:

- ✓ 500 nm configuration: 100μC/$m^2$ for the larger patterns and 90 μC/$m^2$ for the smaller patterns
- ✓ 500 nm parallel configuration: 100 μC/$m^2$ for the larger patterns and 85 μC/$m^2$ for the smaller patterns
- ✓ 100nm configuration: 100 μC/$m^2$ for the larger patterns and 80 μC/$m^2$ for the smaller patterns

The dose of the larger pads is kept larger patterns so that the development of the larger patterns takes place faster than the smaller patterns so as to not to hamper the development of the smaller patterns. In this case,back scattering was reduced but was still there another try to reduce the back scattering was to increase the resist thickness. The total bilayer resists thickness was kept at 585 nm for the 500 nm configurations and 240 nm for the 100 nm configurations. The gap obtained was much closer to the required values. Finally, there was an effort to reduce the writing time. Since the curvature of the larger patterns is not a concern, they were written at a larger current aperture of 60um giving a writing time of 15 min. This did not affect the smaller patterns and hence the current than used was at an aperture of 60 μm.

***The optimized process flow for the configurations is as follows***

### *4.5.1 500nm gap electrode structure*

- Wet oxidation at 1100$^o$C for 3 Hr 15 min to give an oxide thickness of 1200 A$^o$.
- Bilayer resists of 495 K 4% PMMA @ 1000 rpm using the 3-step process of 10 sec spread cycle, 1minute spinning, and 10s ramp down and 950 K 4% PMMA @ 4000 rpm thickness obtained 585 nm. Post bake of 1 min 30 sec after each spin.
- EBL parameters:
  - ✓ Current:

    Smaller patterns: 7.5 μm aperture

    Larger patterns: 60 μm aperture
  - ✓ Dose:

    Smaller patterns: 90 μC/$m^2$

Larger patterns: 100 μC/$m^2$

- ✓ Step size: 20 nm

- Development: 1:3 MIBK/IPA for 2minutes followed by dip in IPA for 15 seconds as shown in figure 4.7 (a).
- Metallization parameters:

  For Cr:

  Current: 0.3 A

  Deposition rate: 0.6 A°/S

  Time: 1minute giving a thickness of 5 nm

  For Au:

  Current: 0.5 A

  Deposition rate: 0.8 A°/S

  Time: 6 min giving a thickness of 25 nm
- Lift off in acetone for 5 min with frequent stirring as shown in figure 4.6 (b).

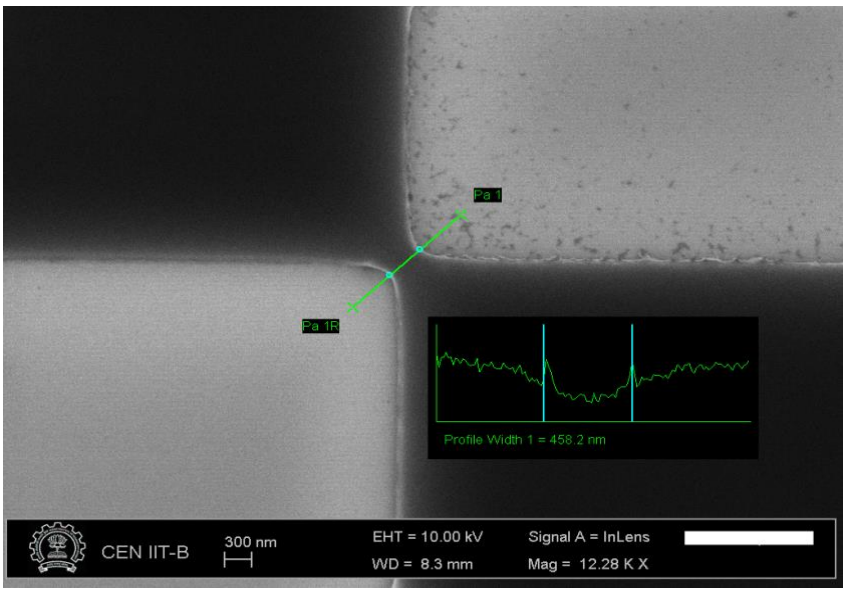


***Fig. 4.6:*** *(a) SEM image of 500nm gap structure after resist development*

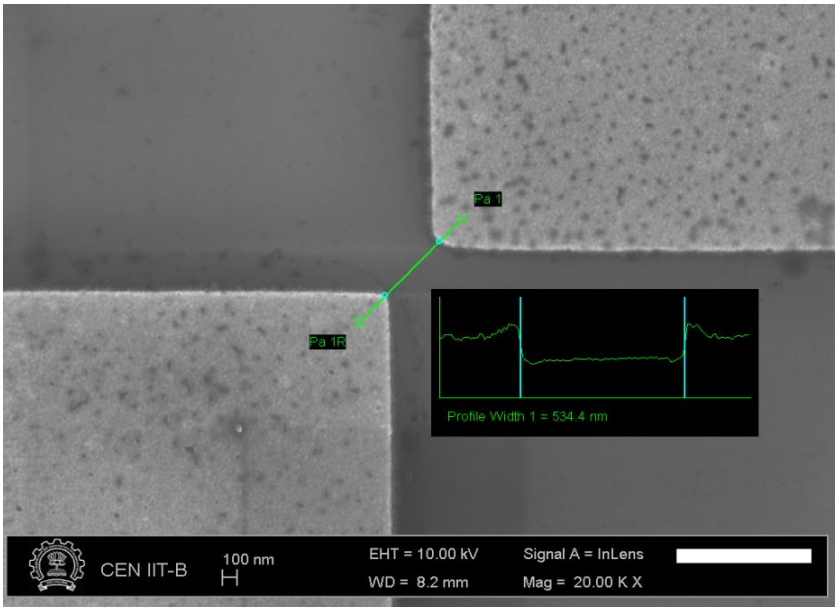


***Fig 4.6:*** *(b) SEM image of 500 nm gap structure after metallization and lift-off*

### *4.5.2 100 nm gap electrode structure*

- Wet oxidation at 1100$^{o}$C for 3 Hr 15 min to give an oxide thickness of 1200 A$^{o}$.
- Bilayer resists of 495 K 4% PMMA @ 6000 rpm using the 3 step process of 20 sec spread cycle, 45sec spinning, and 15 sec ramp down and 950 K 2% PMMA @ 3000 rpm thickness obtained 240 nm. Post bake of 1 min 30 sec after each spin.
- EBL parameters:
  - ✓ Current:

    Smaller patterns: 7.5 μm aperture

    Larger patterns: 60 μm aperture
  - ✓ Dose:

    Smaller patterns: 80 μC/m$^2$

    Larger patterns: 100 μC/m$^2$
  - ✓ Step size: 20 nm
- Development: 1:3 MIBK/IPA for 40 sec followed by a dip in IPA for 15 sec as shown in figure 4.7 (A)
- Metallization parameters:

  For Cr:

  Current: 0.3 A

  Deposition rate: 0.6 A$^{o}$/s

  Time: 1 min giving a thickness of 5 nm

  For Au:

| | |
|---|---|
| Current: | 0.5 A |
| Deposition rate: | 0.8 A°/s |
| Time: | 6 min giving a thickness of 25 nm |

- Lift off in acetone for 5 min with frequent stirring as shown in figure 4.7 (B).

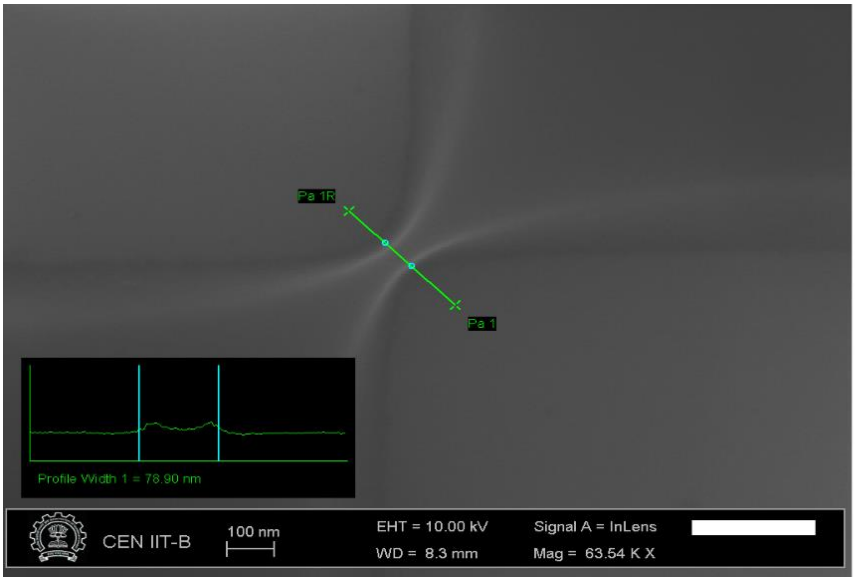


***Fig. 4.7:*** *(a) SEM image of 100 nm gap structure after resist development*

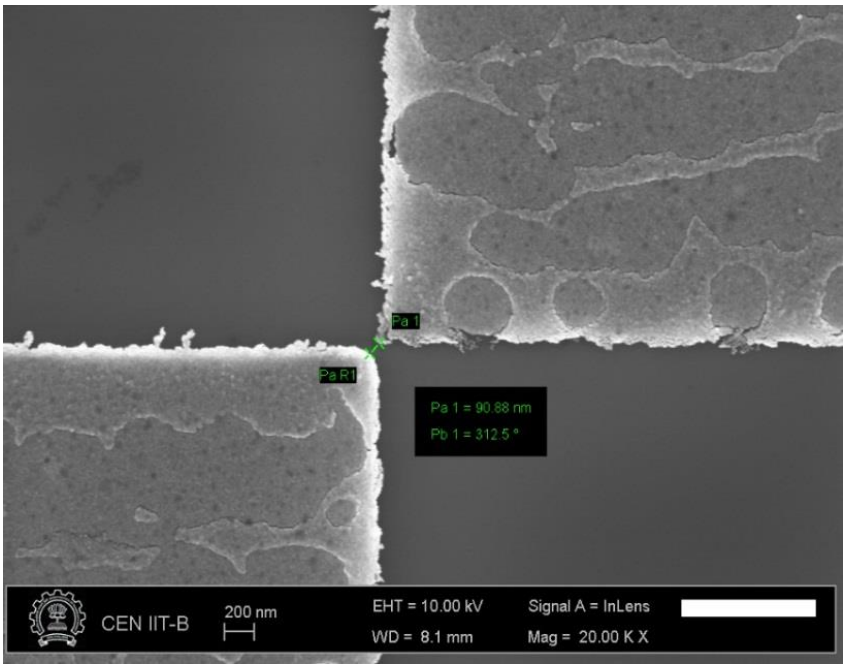


***Fig. 4.7****: (b) SEM image of 100 nm gap structure after metallization and lift-off*

### 4.6 Electrical contacts

Another important step in fabrication and characterization of the device is making electrical contacts. The electrical contacts would facilitate the device for lateral experimentation process by mean of connecting device to an instrument. This contact part could be either 2 probes or 4 probes. In our case, we used 4 probes I-V characteristic instrument. The electrical contacts work carried out with help assisted by CeNSE, IISc from packaging lab using the wire-bonder instrument. Wire bonder establishes connectivity between die and substrate using Au (25 μ)/Cu/ Al (33 μ) wire using Ultrasonic energy, Force and Time. The fabricated device should have minimum bond pad size of 100X100 μm, pad pitch of 150 μm and thickness of 100 nm of material Au/Al with an appropriate seed layer. The 4 probe connections are made for both 100 and 500 nm devices and one of them is shown in figure 4.8 where one can notice two connections for current (I) and remaining two for voltage (V). The connections are established by mounting the device on top of a printed circuit board (PCB) and wire-bonding connections through leads of PCB.

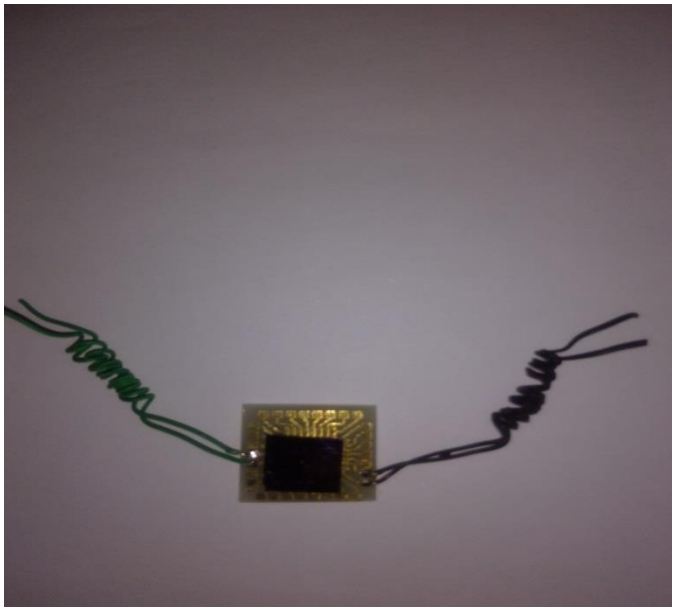

***Fig. 4.8:*** *4- probe electrical contacts to the fabricated device*

Now, this whole setup can be used for lateral experimentation process by connecting it to electrical characterization instrument for I-V characteristics. The I-V characteristics work carried out with the help of University of Hyderabad using semiconductor parameter analyzer (Agilent-B1500A). I-V characteristic work is conducted in two ways. First, studied the electrical behavior of the system taking the onlysetup by connecting it to I-V instrument and second, carried out the electrical behavior of the particles that are placed in between electrodes (within the gap between electrodes).

### 4.7 Current-Voltage (I-V) measurement study

In the last part of the thesis work, we present our findings on the preliminary attempt to trap ds-DNA molecules suspended in KCl solution and placed in between 100 nm gap triangular metal electrodes. The device is fabricated on oxidised Si wafer and patterned using EBL as mentioned in 4$^{th}$ chapter. It is worthwhile to recollect that, to acquire at optimal fabrication parameters such as EBL exposure time, resist thickness, etc., we have fabricated device with 500 nm electrode gap. However, we have not used these devices for the present study as reports indicated that DNA molecules of length more than 150 nm would not show any signature of charge conductance through it [13].

It has been reported by several researchers [14, 15] that a favorable condition for trapping of DNA molecules (suspended in a solution) within patterned nanoelectrodes could only be achieved by tuning the device with an AC source. This is also validated by our simulation results with the frequency of the AC supply may vary up to several hundred KHz. depending on the strength of electric field as well as the dimension of the gap between the patterned electrode [OJFD & AIP]. We have adopted the process mentioned below in our attempt to trap DNA molecules within 100 nm patterned electrodes. First, a few ng/µL DNA molecules (length ∼140 nm which equivalent to ∼ 400 base pairs) suspended in KCl solution of strength [standard solution 0.1 M] dropped using micropipette under an optical microscope in the gap region. The device is then connected to an AC supply of 750 KHz for 2 minutes for molecules to stretch and align themselves along the length of the gap and possibly get attached with the electrode.

Then the AC source is removed and I-V measurements are performed under a DC bias between -1 to +1 V. And all experiments are performed at room temperature and open atmosphere using B 1500-A semiconductor parameter analyser at University of Hyderabad. Fig 5.19 shows I-V characteristics obtained from such a device. The inset (a) and (b) gives the I-V characteristics of the device without the active material and with KCL solution alone present in the gap respectively. The inset (a) helps us rule out any leakage through oxidized wafer, whereas inset (b) gives us a measure of conductance of KCl used matching with standard calibration report [15].

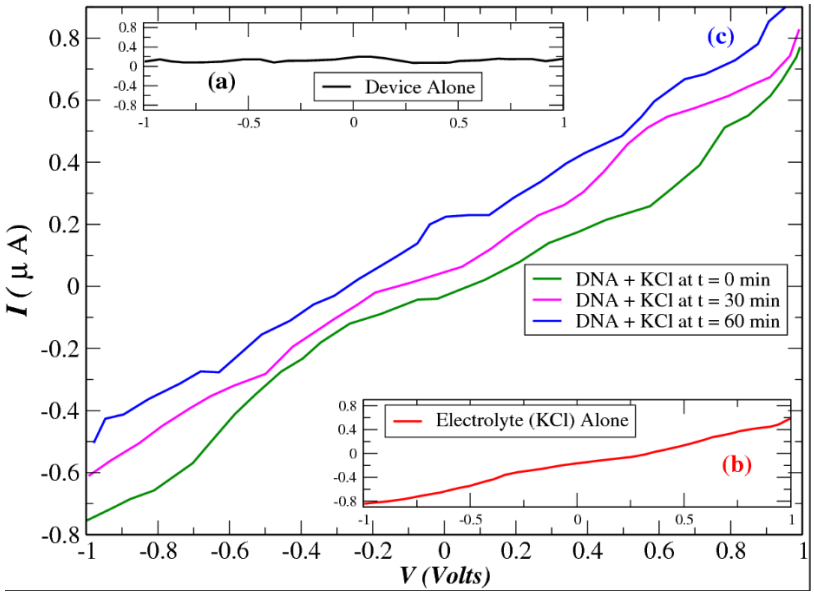


**Fig 4.9:** *I-V characteristics for device (inset black), for KCl (inset red) and for KCL+DNA at different times (t=0, 30 & 60 minutes)*

As the electrical measurements are carried out in open atmosphere, the contamination and humidity are likely to play a role in modifying I-V characteristics of the device [14, 17]. The I-V plots of the sample (suspensoid DNA in KCl solution) measured at t = 0, 30 & 60 minutes are shown by colored lines green, blue and pink respectively labelled as (c). One can observe that the current values have increased as measurements on the same device, are performed at later times. The experimental observations apparently show that open environment could modify I-V characteristics of sample of such nature and it remains inconclusive whether we have been successful in bridging the 100 nm gap with one or more molecules and they have contributed to overall conductance. In this context, it is worthwhile to mention that researchers recently claimed that DNA molecules with thiol at the ends are more probable to get bonded with metal electrodes [7]. However, with the available setup for extraction of DNA molecules, it was not possible to have these thiolated. Therefore, it is likely that when AC voltage is applied, the DNA molecules might have stretched and bridged the gap but fail to get bonded with the electrodes. When the AC source is removed, these returned to their original configuration and barely have contributed to the measured current.

## References


1. Pohl. H.A, The motion, and precipitation of Suspensoids in divergent electric fields, J. Appl. Phys., 22, 869-87, (1951).
2. Pohl, H.A, some effects of nonuniform fields on dielectrics, J. Appl. Phys., 29, 1182-1188, (1951).
3. Mandou, M.J, Fundamentals of microfabrication and nanotechnology, 3rd edition, Vol. 2, CRC Press, Boca Raton, FL.
4. S. Ghonge, S. Banerjee, Review Article "Dependence of shape and geometry of microelectrodes in manipulating polarizable particles like DNA through electrokinetic effects", Defence Science Journal, 66, 307-315, (2016).
5. Ampere A Tseng, Kuan Chen, Chii D Chen and Kung J Ma, "Electron Beam Lithography in Nanoscale Fabrication: Recent Development", IEEE Transactions on Electronics Packaging Manufacturing, Vol.26, No.2, April 2003, 141-150.
6. Porath, D.; Bezryadin, A.; De Vries, S. & Dekker, C. Direct measurement of electrical transport through DNA molecules. Nature, 2000, 403, 635-638.
7. Vahidi, N.W.; Hirabayashi, M.; Mehta, B.; Rayatparvar, M.; Wibowo, D.; Ramesh, V.; Chi, J.; Calish, J.; Tabarés, M.; Khosla, A. & Mokili, J. Bionanoelectronics platform with DNA molecular wires attached to high aspect-ratio 3D metal microelectrodes. ECS J. Solid State Sci. Technol., 2014, 3, 29-36.
8. Ghonge S, Prasad D N, Narayan S, Francis H, Sethi A, S Deb, Banerjee S, "Effect of curvature of tip and convexity of electrode on localization of particles", OJFD, 5, 295-301, (2015).
9. D N Prasad, S Ghonge, S Banerjee, "Investigation of localization of DNA molecules using triangular metal electrodes with varying separation", AIP conference proceedings, 1724, 020036, (2016).
10. M J Rooks, S Wind, P Mc Euen and D E Prober, "Fabrication of 30-nm- scale structures for electron transport studies using a Polymethyl methacrylate bilayer resist", J. Vac. Sci. Technol. B 5(1), 1987, 318-324, (1987).
11. Ampere A Tseng, Kuan Chen, Chii D Chen and Kung J Ma, "Electron Beam Lithography in Nanoscale Fabrication: Recent Development", IEEE Transactions on Electronics Packaging Manufacturing, Vol.26, No.2, 141-150, (2003).
12. B. Hans-Georg, "Electron Beam Lithography", September 22, (2008). Available online. https://www.scribd.com/document/130379018/Electron-Beam-Lithography
13. Y. Zhang, R. H. Austin, J. Kraeft, E. C. Cox, and N. P. Ong, "Insulating behaviour of λ-DNA on the micron scale", Phys. Rev. Lett. 89, 198102, (2002).
14. Washizu. M, Kurusowa. O, Arai. I, Suzuki. S &Shimamoto. N, "Application of electrostatic stretch and positioning of DNA", IEEE Trans. Ind. Appl., 31, 447-456, (1995).

**15.** M.Washizu and O. Krurusowa, "Electrostatic Manipulation of DNA in microfabricated structures", IEEE trans. On Industry Applications, 6, 26, (1990).

**16.** KCl calibration report from standard solutions

**17.** Otsuka, Y., Lee, H. Y., Gu, J. H., Lee, J. O., Yoo, K. H., Tanaka, H., Kawai, T, "Influence of humidity on the electrical conductivity of synthesized DNA film on nanogap electrode", *Japanese J. of Applied Physics*, *41*(2 A), 891-894, (2002)

## Future Scope

This work carried out based on proposing an idea of geometry that could facilitate effective trapping/manipulation of polarizable molecules like DNA. We have examined the pros and the cons of such geometry of the set of the microelectrodes and also tried to provide a solution in terms of shape and sharpness of the electrode that would facilitate DNA molecules to bridge between the electrodes for further application of conducting DNA as a molecular wire. And also examined how polarizable particles like DNA molecules could be electro-kinetically controlled when placed in suspended form in between two micro/nanoelectrodes fed by AC voltage. It opens up a challenge to researchers from theoreticians to experimentalists, from a designer to a fabricator, as it holds high promise to novel applications in applied physics, electrical engineering, and biotechnology. Since the modern electronic industry revolution is driven consistently by miniaturization process, it is expected that further miniaturization is possible in molecular electronics area owing to the fact that remarkable self-assembling and self-organizing properties at molecular unit scale. This study would help to understand the transport/conduction mechanism of biological molecules by means of trapping the molecules electrically using different geometries of electrodes. And this trapping can also be achieved using optical tweezers with lasers and magnetophoresis where magnetic fields are applied. And this study helps to continue research in terms of electrical, physical and mechanical properties of biological molecules.

## List of publications

1) **D. Nagendra Prasad**, S. Ghonge, and S. Banerjee, *'Investigation of localization of DNA molecules using triangular metal electrodes with varying separation'*, AIP proceedings, 1724, 020036, (2016).
2) S. Ghonge, **D.N. Prasad**, S. Narayan, H. Francis, A. Sethi, S. Deb and S. Banerjee, *'Effect of curvature of tip and convexity of electrode on localization of particles'*, Scientific Research Publishers-OJFD, vol-5, 295-301, (2015).

## List of papers presented at conferences

1) S. Narayan, H. Francis, S. Ghonge, **D.N. Prasad**, A. Sethi, S. Banerjee, and S. Kapur, *'AC Electroosmosis and Dielectrophoresis for trapping spherical particles between rectangular and triangular electrodes',* COMSOL proceedings, (2013).

2) P. Parikh, A. Sethi, S. Benedict, **D.N. Prasad**, B. Mallik, S. Kapur, S. Deb and S. Banerjee, *'Effect of conductivity and viscosity in the velocity characteristics of a fluid flow induced by non-uniform AC electric field in electrolytes on microelectrodes'*, COMSOL proceedings, (2012).

## International Conferences

1) Presented paper & poster: *'Investigation of localization of DNA molecules using triangular metal electrodes with varying separation'* at International Conference on Emerging Technologies on Micro & Nano (ETMN-2015) at Manipal University Jaipur, Rajasthan, India.
2) Presented poster: *'A solution to trap DNA molecules under electrokinetic effects in fluids with different electrode geometries'*, at International Conference on MEMS & Sensors (ICMEMSS-2014) at IIT-Madras, Chennai, India.
3) Participated at International Conference on Materials Science Research (IUMRS-ICA-2013) at Indian Institute of Science (IISc-Bangalore), India.
4) Presented at COMSOL conference on Numerical Simulations in the year of 2012 and 2013 in Bangalore, India.

## Training programs/Workshops

**1)** 21-2 May 2014: Indian Nano Users Program (INUP), Familiarization workshop at Centre for Nano Science and Engineering (CeNSE), Indian Institute of Science (IISc), Bengalur, Karnataka, India.

**2)** 19-28 Aug 2014: Indian Nano Users Program (INUP), Hands on Training at Centre for Nano Science and Engineering (CeNSE), Indian Institute of Science (IISc), Bangalore, Karnataka, India. Trained in 100 class clean room environment with hands-on sessions aimed at Micro & Nano Fabrication and Characterization techniques.

## Biography of Student

**Mr. D.N. Prasad** obtained Bachelor degree (B.Sc.) in the year of 2004 from Acharya Nagarjuna University, Guntur, Andhra Pradesh and obtained Master degree (M.Sc. Physics) in the year of 2006 from Bharathidasan University, Trichy, Tamilnadu. He worked as Asst. Prof in various engineering colleges affiliated to JNTU-Hyderabad for about FIVE and half years (2006-2011). He joined as a research scholar in the department of physics, BITS-Pilani Hyderabad campus in the year of 2012 under the supervision of Prof. Souri Banerjee.

## Biography of Supervisor

**Prof. Souri Banerjee** currently working as Professor in the department of physics, BITS Pilani Hyderabad campus. He received his Ph.D. degree from IACS, Jadavpur, West Bengal in the year of 1998. Later he worked as postdoctoral for about 5 years (1998-2003) in Tokyo Institute of Technology and University of Electro-communications, Tokyo. He also served as a guest scientist for JSTC (Japan Science & Technology Corporation) in Tokyo. After his postdoctoral, he joined BITS Pilani (Rajasthan) as a Lecturer in 2004 since then he held various positions in BITS Pilani as a HOD of Physics Dpt., Associate Dean, Faculty affairs & recruitment and etc. He was awarded Japan Society for the Promotion of Science (JSPS) Fellow in the year 2012. He has been engaged in both teaching and research for the past 20 years. He published several prominent research articles in reputed journals and authored a textbook. He guided 1 Ph.D. student and many M.Sc. & M.E. thesis students. He also handled 2 projects from BRNS-DAE in 2011 and CSIR in 2013 and currently co-principal investigator for BRNS-DAE (2018) project.

******THE END******

**THANK YOU**